

A BIOMIMETIC APPROACH TOWARD RED BLOOD CELL SUBSTITUTES BASED ON
PRINT HYDROGELS

Kai Chen

A dissertation submitted to the faculty of the University of North Carolina at Chapel Hill in
partial fulfillment of the requirements for the degree of Doctor of Philosophy in the Department
of Chemistry (Polymers and Materials).

Chapel Hill
2013

Approved by:

Joseph M. DeSimone

Wei You

Sergei Sheiko

Jay S. Raval

Zhen Gu

© 2013
Kai Chen
ALL RIGHTS RESERVED

ABSTRACT

Kai Chen: A Biomimetic Approach toward Red Blood Cell Substitutes Based on PRINT Hydrogels
(Under the direction of Joseph M. DeSimone)

This work utilized PRINT (particle replication in non-wetting templates) technology to fabricate extremely soft, biologically inspired hydrogel particles that mimicked the size, shape and modulus of red blood cells (RBCs). Hemoglobin, the oxygen carrying protein in RBCs, was conjugated into these microparticles without adverse effect on the structure and function of the protein. A prior modification on surface of PRINT particles followed by hemoglobin conjugation enabled the protein-laden microparticles to circulate in blood. The results of this study can potentially lead to a RBC substitute for blood transfusion without causing vasoconstriction, a major hurdle often seen in other hemoglobin-based oxygen carriers (HBOCs).

Vasoconstriction is believed to be inversely proportional to the size of the HBOC. Microparticles with size around or larger than 1 μm may be appropriate as hemoglobin carriers to minimize vasoconstriction, yet they generally do not circulate well in blood vessels due to filtration by small capillaries. Our previous study demonstrated that microparticles with a diameter of 6 μm could still circulate a long time in blood when they were made to be deformable enough.

Retaining the same low modulus, hydrogel particles with diameters ranging from 0.8 to 8.9 μm were studied on their pharmacokinetics and biodistribution in mice. The particles mimicking size of RBCs demonstrated longer circulation times, hence were used as carriers for

hemoglobin in this study. Bovine hemoglobin could be conjugated to the RBC mimicking particles (RBCMs) through reaction between carboxyl groups in the particles and amine groups on hemoglobin.

However, hemoglobin distributed on the surface of the RBCMs made them tend to aggregate in blood and more recognizable by macrophages, resulting in rapid removal from circulation. A strategy was used to synthesize blank RBCMs with such an asymmetric distribution of carboxyl groups that most of them were in the interior with limited exposure on the exterior. After conjugation, hemoglobin could be predominantly confined in the interior of the particles with a neutral surface charge. These particles could circulate in blood with much lower accumulation in the lung than the counterparts with hemoglobin on their surface.

TABLE OF CONTENTS

LIST OF TABLES	viii
LIST OF FIGURES	ix
LIST OF ABBREVIATIONS.....	xviii
CHAPTER 1 BACKGROUND AND SIGNIFICANCE OF RBC SUBSTITUTES	1
1.1 Physiology of Blood and Red Blood Cell	1
1.2 Structure and properties of Hemoglobin	3
1.3 Blood transfusion.....	4
1.4 RBC substitutes	6
1.5 PRINT RBC Mimics	11
1.6 Conclusions	12
1.7 Figures.....	14
1.8 REFERENCES	17
CHAPTER 2 PHARMACOKINETICS AND BIODISRIUTION OF LOW MODULUS HYDROGEL PARTICLES	20
2.1 Introduction	20
2.2 Results and Discussion.....	23
2.2.1 Hydroxyl PEG acrylate Monomers.....	23
2.2.2 Low Modulus HP3A Hydrogels	25
2.2.3 RBC-sized HP3A Particles.....	26
2.2.4 Low Modulus HP3A Particles with Varying Sizes	27
2.2.5 Biodistribution of Soft Hydrogel Particles with Different Sizes.....	28

2.2.6	Pharmacokinetics of Soft Hydrogel Particles with Different Sizes	31
2.3	Conclusions and Future Directions	33
2.4	Materials and Methods	35
2.4.1	Materials	35
2.4.2	Synthesis of Hydroxy PEG Acrylate Monomers	35
2.4.3	Modulus Testing	36
2.4.4	Particle Fabrication	37
2.4.5	Particle Harvesting and Purification	38
2.4.6	Particle Characterization.....	38
2.4.7	Microfluidics	39
2.4.8	In vivo Studies.....	39
2.4.9	Biodistribution.....	40
2.4.10	Pharmacokinetics of Particle Clearance from Blood.....	40
2.4.11	Histology	42
2.5	Figures	43
2.6	REFERENCES	51
CHAPTER 3	RBC MIMICS WITH HIGH LOADING OF HEMOGLOBIN	53
3.1	Introduction	53
3.2	Results and Discussion.....	56
3.2.1	Fabrication and characterization of blank particles	56
3.2.2	Conjugation of Hb into the RBCM particles.....	57
3.2.3	Confocal studies of the Hb-RBCM particles.....	59
3.2.4	Hb loading efficiency of RBCM particles.....	59
3.2.5	CD and UV-vis spectroscopic study.....	62

3.2.6	Oxygen dissociation and NO oxidation kinetics.....	64
3.2.7	Mechanical and fluidic properties of Hb-RBCM particles	65
3.2.8	Cytotoxicity of the RBCM particles	67
3.2.9	Conclusions and Future Work.....	68
3.3	Experimental Section	69
3.3.1	Materials.....	69
3.3.2	Synthesis of dye-labeled Hb.....	69
3.3.3	Synthesis of poly(HP3A-co-CEA)	70
3.3.4	Modulus Testing	70
3.3.5	Particle fabrication and characterization.....	70
3.3.6	Protein Conjugation to particles and polymers	70
3.3.7	CSLM study of model particles.....	71
3.3.8	Reduction of metHb and Hb binding to CO and oxygen.....	72
3.3.9	UV-vis spectroscopy of Hb and Hb-RBCM particles	72
3.3.10	Circular Dichroism (CD) spectroscopy studies	73
3.3.11	Stopped-Flow Spectroscopy.....	73
3.3.12	Microfluidics	74
3.3.13	Rheological measurement	74
3.3.14	Cytotoxicity study.....	75
3.4	Figures.....	77
3.5	REFERENCES	89
CHAPTER 4 MODULATING BIODISTRIBUTION AND EXTENDING CIRCULATION OF HB-LOADED RBC MIMICS		92
4.1	Introduction	92

4.2	Results and Discussions	95
4.2.1	Synthesis of Acid-labile Crosslinker	95
4.2.2	ADA-crosslinked PRINT Particles.....	97
4.2.3	PEGylation of ADA-crosslinked Anionic Particles	98
4.2.4	PEGylation of ADA-crosslinked Cationic Particles.....	99
4.2.5	Quantifying Amine Contents in Particles	101
4.2.6	Succinylation of AEM-particles	102
4.2.7	Conjugation of Hb	103
4.2.8	Particle Interaction with Macrophage.....	104
4.2.9	<i>in vivo</i> Studies.....	104
4.2.10	Conclusions and Future Work.....	107
4.3	Materials and Methods.....	112
4.3.1	Materials.....	112
4.3.2	Synthesis of ADA.....	112
4.3.3	Purification of mPEG-NHS.....	113
4.3.4	Fabrication of Particle A.....	113
4.3.5	Particle characterization.....	114
4.3.6	Particle A Degradation.....	114
4.3.7	PEGylation of Particle A.....	115
4.3.8	Succinylation	115
4.3.9	Hb Conjugation	115
4.3.10	Model Particle PEGylation using Fluorescein-PEG-NHS.....	115
4.3.11	Amine Quantification in Particles	116

4.3.12 Normalizing Particle Numbers	116
4.3.13 Macrophage Interaction Study	117
4.3.14 Intravital Microscopy.....	118
4.3.15 Histology.....	119
4.4 Figures.....	120
4.5 REFERENCES	132
CHAPTER 5 SUMMARY AND FUTURE DIRECTIONS	149
5.1 Summary	135
5.2 Future Directions	137
5.2.1 Effect of ζ -potential on PK and BioD of Soft Particles	137
5.2.2 Nerve Agent Scavenger	138
5.2.3 Nucleic Acid Scavenging.....	139
5.2.4 Other Formulations for Soft Particles.....	140
5.2.5 Nanoparticle Loading.....	141
5.2.6 Hollow RBC Mimic.....	142
5.3 Figures.....	144
5.4 REFERENCES	146

LIST OF TABLES

Table 1.1	PK parameters of RBC mimics found through non-linear regression analysis and fit to a two compartment model for elimination.....	12
Table 2.1	Properties of lightly crosslinked hydrogels composed of different acrylic monomers containing 1% of a 4,000 g/mol PEG diacrylate crosslinker and 1% of HCPK photoinitiator, hydrated for 12 hours in deionized water at room temperature. Monomers are shown with increasing PEG chain length.	24
Table 2.2	Mechanical properties of HP3A hydrogels with varying amounts of PEG4kDA crosslinker and 10% of 2-carboxyethyl acrylate. Swelling ratios were determined from one bulk sample hydrated for 24 hours in PBS. Modulus and strain at break represent an average value determined from three samples cut from the bulk gel, with error representing one standard deviation.	26
Table 2.3	Characterization of particles fabricated for in vivo studies. Particles molded from 1, 2 and 3 μm features were measured by microscopy, with error representing one standard deviation from the mean with $n=50$ for particle diameters. Particles molded at 0.2 μm were measured by dynamic light scattering to determine their hydrodynamic diameter.	28
Table 2.4	Pharmacokinetic parameters for low modulus hydrogel PRINT particles with increasing diameters. Parameters were determined from particle concentration in whole blood at times 0.2 -104 hours post-dose using a standard two-compartment model.	32
Table 4.1	Compositions used to fabricate tightly crosslinked particles. Both AEM and CEA containing particles were fabricated.	98
Table 4.2	ζ -potential of particle B and C when mPEG-NHS with MW of 2k, 5k and 30 k Da were used for the PEGylation for 4h.	100
Table 4.3	Two-compartmental analysis of RBC-sized particles from intravital microscopy experiments. The clearance curve of Particle D cannot be fitted using 2-compartment model.	106

LIST OF FIGURES

Figure 1.1	(A) Tetrameric structure of hemoglobin; (B) Hypothetical oxygen-hemoglobin dissociation curve. Changes in temperature, pH, and organic phosphates like 2,3-DPG directly affect the association of oxygen.....	14
Figure 1.2	Various strategies for modification of the native Hb tetramer (center) intended to avoid renal toxicity, increase circulation time of the free tetramer and, often, to modify the strength of oxygen binding. Counterclockwise from top: 1. The two α or β subunits can be chemically connected to prevent degradation to the toxic $\alpha\beta$ dimer. 2. Otherwise unmodified Hb can be crosslinked to form polyhemoglobin. 3. Genetic modification allows for fusing of subunits as well as tuning of the oxygen binding properties of recombinant Hb. 4. Polymers such as poly(ethylene glycol) or poly saccharides can be chemically attached to the surface of the Hb molecule. 5. Encapsulation in a liposomal carrier or polymeric matrix protects the hemoglobin from degradation.....	15
Figure 1.3	Blank RBC mimics. (A) A graphical depiction of the PRINT process to fabricate RBC mimics. Briefly, from top to bottom, an elastomeric fluoropolymer mold (green) with disc shaped wells was covered by an aliquot of the pre-polymer mixture (red). The mold was passed through a pressured nip (black) covered by a high energy sheet (grey), wicking away excess liquid from the mold surface while filling the wells of the mold. The filled mold was cured photochemically, yielding cross-linked hydrogel particles, which were harvested from the mold by freezing onto a thin film of 1% poly (vinyl alcohol) in water (blue) and peeling away the mold. Melting of this layer resulted in a suspension of red blood cell mimic (RBCM) hydrogel particles. (B-E) Fluorescent images of hydrated RBCMs with varying % crosslinker (B) 10% crosslinked (C) 5% crosslinked (D) 2% crosslinked and (E) 1% crosslinked. Scale bars are 20 μ m.....	16
Figure 2.1	Synthetic scheme for hydroxyl PEG acrylates (HPAs). The structures of the monoacrylated products are shown below the reaction scheme, along with the naming convention.....	43
Figure 2.2	Microscopic images of HP3A particles with 0.25 wt% crosslinker in the mold (A), transferred on to PVOH (B) and suspended in PBS (C); SEM image of dried particles with 1 wt% crosslinker (D). Particles crosslinked with less than 1 wt% PEG4kDA were unable to retain integrity in the dry state that they could not be imaged by SEM.....	44

Figure 2.3	Microfluidic evaluation of HP3A-based RBC mimicking particles. (A) Schematic illustration of the microfluidic device used; (B) An image sequence showing 0.25 wt% crosslinked RBCM particles (5.4 μm in diameter) squeezing through the $3\times 3\ \mu\text{m}$ channels (190 ms between frames).	45
Figure 2.4	Fluorescent images of the particles used for the in vivo studies. The particles have hydrated diameters of (A) 0.78 μm , (B) $3.79 \pm 0.17\ \mu\text{m}$, (C) $6.39 \pm 0.56\ \mu\text{m}$, and (D) $8.88 \pm 0.47\ \mu\text{m}$. Scale bars are 20 μm . The particles were imaged at the DyLight 680 channel.	46
Figure 2.5	Biodistribution of extremely deformable particles of different sizes in mice over the course of 5 days. The total fluorescent signal from the particles in each tissue sampled is shown for particles with diameters of (A) 0.78 μm , (B) 3.8 μm , (C) 6.4 μm and (D) 8.9 μm . Four mice were examined per time-point, with error bars representing one standard deviation.	47
Figure 2.6	Biodistribution of extremely deformable particles of different sizes in mice over the course of 5 days. The percentage of the fluorescent signal recovered from the sampled tissues was adjusted by the weight of the tissue. Data is shown for particles with diameters of (A) 0.78 μm , (B) 3.8 μm , (C) 6.4 μm and (D) 8.9 μm . Four mice were examined per time-point, with error bars representing one standard deviation.	48
Figure 2.7	A plot showing the change in particle concentration in blood over time for deformable hydrogel particles of different sizes. Particles with a diameter of 6.4 μm , similar to that of mouse red blood cells, were cleared more slowly and remained in the circulation to a greater extent than both larger and smaller particles with identical mechanical properties and composition. The largest of these particles, with hydrated diameters of 8.9 μm , were cleared to concentrations in blood below our limits of quantification (indicated by the dashed line). Each data point represents 4 mice, with error bars representing one standard deviation.	49
Figure 2.8	Histological sections of lung, liver and spleen tissue from mice sacrificed 104 hours after dosing with (A) 0.78 μm , (B) 3.79 μm , (C) 6.39 μm , and (D) 8.9 μm particles. Images are an overlay of fluorescence from DAPI staining (blue) and the Dylight 680 dye that is covalently bound to the hydrogel particles (red). Scale bars are 20 μm	50
Figure 3.1	Fluorescent micrograph of polymerized particles (fabricated from 88.85 wt% HP3A, 10 wt% CEA, 0.05 wt% PEG4kDA,	

1 wt% photo-initiator, 0.1 wt% PolyFluor 570) in the mold (A), and fully hydrated particles free of the mold, suspended in PBS (B). Scale bars=20 μm	77
Figure 3.2 Scheme for the conjugation chemistry between carboxyls of particles and lysines of Hb.	78
Figure 3.3 Conjugation of Hb to RBCM particles. Dyeless particles reacted with Fluorescein-tagged Hb (A) and Rhodamine tagged Hb (B). Fluorescein-labeled RBCM particles reacted with Rhodamine-tagged Hb were observed in the (D) Fluorescein, (E) Rhodamine channels of fluorescence; (F) overlay of D and E. Scale bars=20 μm . (G) FTIR spectra of blank particles, Hb, and Hb-RBCM conjugate. The arrow pointing to 1579 cm^{-1} denotes the peak of carboxylate in the particles; the two arrows pointing to 1550 and 1660 cm^{-1} denote the amide groups in Hb.....	79
Figure 3.4 Dyeless particles (A) conjugated with AF488-BSA (B). The green background in B is actually stream of particles flowing during the capturing of the image. For determination of loading ratio, dyeless BSA was conjugated to particles with a feeding ratio of 1 mg particle : 2 mg BSA, and we found that 0.4 mg BSA (using Coomassie's assay and plate reader to determine the difference before and after reaction) became conjugated after reaction for 12h.	80
Figure 3.5 A 3D reconstruction view of fluorescein-Hb-conjugated particles observed using xyz scan mode of the confocal laser scanning microscope, with the inset showing orthogonal cross-section views of a representative particle (indicated by the white arrow). The fluorescent protein seems to be homogenously distributed throughout the hydrogel particle.	81
Figure 3.6 (A) Loading ratio R and the encapsulation efficiency of Hb into the RBCM particles with respect to different starting concentration of Hb for the conjugation while the particle concentration was maintained at 1mg/mL (n = 3). (B) RBCM particle size with respect to different loadings of Hb; the size of the particles were measured by analyzing fluorescent micrographs of the particles (n = 50) which had polymerized Rhodamine dye inside.	82
Figure 3.7 (A) Far-UV circular dichroism spectra of pure Hb, Hb physically mixed with particles (Hb+particles), and Hb conjugated to particles (Hb-c-particles). For Hb-c-particles, the sample was half diluted as Hb-c-particles Diluted to confirm the isodichroic point as denoted by the arrow. The spectra were all measured in 10 mM K ₂ HPO ₄ buffer with a path length of 1 mm.	

(B) Soret CD of the first three samples with Hb concentration of 1 mg/mL in 10 mM K₂HPO₄ buffer. (C) UV-vis spectra of Hb-particles with the hemes of Hb at different binding states. Particle concentration in the sample was 0.05 mg/mL with Hb concentration of 0.14 mg/mL. The as prepared Hb-particles showed a Soret peak at 405 nm, indicating mostly metHb in the particles. When sodium dithionite was added to the particle suspension, metHb was reduced back to deoxyHb, characterized by the Soret peak at 430 nm. Carbon monoxide purged into the suspension converted deoxyHb into CO-Hb as the Soret peak moved to 419 nm. When exposed to light and air, the Soret peak of the suspension moved to 412 nm, indicating formation of oxyHb. (D) MetHb level in polymer-Hb conjugate over time. The polymer was based on a similar formulation as for the particles but without crosslinker. Overall Hb concentration in the conjugate solution was 5 mg/mL. 83

Figure 3.8 Time courses of (A) oxygen dissociation and (B) NO oxidation of oxyHb. Hb concentration was 0.5 μ M after mixing in all the studies with 14 μ M NO solution to ensure pseudo-first-order reaction by large excess of NO. All the measurement carried out at 23 °C. 85

Figure 3.9 (A) Image sequence (top to bottom) showing how a single particle ($R = 2.8$) passed through a constricted pore (from left to right). The time lapse between the frames was 31 ms. (B) Clogged pore entrance by Hb-RBCM particles with $R = 5.1$. (C) and (D) Rheological results showing viscosity and shear stress versus shear rate for blood of two mice and Hb-RBCM suspension ([Hb]= 5.2 g/dL) that had been subjected to a rheometer. The shear rate ranged from 0.1 to 1,000 1/s, covering the possible shear rates in blood flow. (E) Microscopic image showing intact Hb-RBCM particles after being sheared at a constant rate of 1,000 1/s for 10 min. Scale bars = 20 μ m. 86

Figure 3.10 Cytotoxicity of the RBCM particles tested on (A) HUVEC and (B) HeLa cells after 72 h. RBCM particles with 10, 20, and 50 wt% CEA, but unloaded with Hb were studied to assess the biocompatibility of CEA. Hb conjugated particles (10 wt% CEA; $R=2.8$) with metHb reduced were tested with their un-reduced counterparts. Fluorescent micrographs of (C) 20 wt% and (D) 50wt% CEA particles. The size of the particles were 6.5 and 7.5 μ m, and the zeta-potential were -23.5 and -29.9 mV respectively. 87

Figure 3.11 Standard curve of Hb measured by UV-vis spectroscopy, and fitted by linear regression. At 540 nm, the molar absorbance of oxyHb, deoxyHb, and metHb are the same. 88

Figure 4.1 Scheme showing synthetic route from PRINT particles to surface-neutral microgels with charged interiors and functionalization of the microgels (A to E). Control particles with charged surface were produced following route A to H.	120
Figure 4.2 (A) Synthetic scheme for ADA by reacting HEA with 2-methoxypropene in the presence of an organic acid PPTS. (B) NMR spectrum of ADA in CDCl ₃ measured at 25 °C.....	121
Figure 4.3 ADA crosslinked CEA containing particles at different stages. (A) as prepared; (B) after pH=3 treatment for 3 h; (C) PEGylated by mPEG _{5k} -amine using EDC/NHS; (D) pH=3 treatment for 18 h after PEGylation.....	122
Figure 4.4 Fluorescent microscopic image of (A) freshly prepared particle A and (B) swollen particle F after acetal degradation in pH=3 buffer for 2 h. (C) Size increase of particle A overtime in different pHs. Aliquots of particle suspensions were taken out and re-suspended in PBS for sizing by averaging diameter of particles under microscope (n=50).	123
Figure 4.5 Effect of PEGylation on ADA crosslinked AEM-particles. Fluorescent image of acid-treated particle A after PEGylation with unpurified (A) and purified (B) mPEG _{5k} -NHS. Confocal microscopic image of model particles (7×7×3 μm cylinders) after reaction with (C) fluorescein-PEG _{2k} -NHS and (D) fluorescein-NHS.	124
Figure 4.6 Standard curve for fluorescein-PEG _{2k} -NHS regarding fluorescence excited at 492 nm and emitted at 518 nm (3 readings averaged for each concentration). Starting from 1 mg dyeless particle A, the same numbers (5 × 10 ¹¹) of particle C and F were prepared respectively. Both C and F were reacted with 10 mg fluorescein-PEG _{2k} -NHS for 12 h followed by thorough, repeated washing/centrifugation circles. The obtained particle suspensions were re-suspended in PBS to obtain concentration of 1 × 10 ¹¹ particles/mL for both particles. Then starting from this concentration, defined dilutions were made to fit into the linear range of the standard curve. Particle F reacted with mPEG _{2k} -NHS for 6 h (needed time to acquire near-neutral zeta-potential) was also measured for amine content using this method.	125
Figure 4.7 Size and ζ-potential change of particles synthesized following route of (A) particle A to particle E and (B) particle A to particle H.....	126

Figure 4.8	(A) The solutions of 4 mg Hb reacted with 1 mg particles (0.5 mL) of G (left) or D (right) for 6h. The aggregation for G could be avoided when conjugation was carried out at dilute concentrations (0.5 mg/mL particles). For all the <i>in vitro</i> and <i>in vivo</i> studies, the conjugation was carried out at low concentration for both G and D particles. (B) The optical density (720 nm to avoid Hb absorbance) change for hemoglobin loaded particles E and H dispersed in PBS containing 10% fetal bovine serum (900 μ L particle suspension was mixed with 100 μ L fetal bovine serum quickly in the cuvette before reading started). The optical density at 720 nm for the suspensions was read every 1 min over 15-20 h at 23 °C.	127
Figure 4.9	(A) Macrophage interaction with different particles. About 400 particles/cell dosed to a total of 10^5 Raw264.7 cells for each particle type. (B) Cytotoxicity of different particles to Raw264.7 cell line.....	128
Figure 4.10	(A) Intravital microscopy images of mice earlobe blood vasculature imaged at the rhodamine (Rh) channel by injecting dextran _{70k} -rhodamine prior to dosing particles, and imaged at the near-IR (NIR) channel just 100 secs after dosing particles (C , F , H). (B) Decrease in fluorescence of area of interest within 2 h of imaging by IVM (averaged of n=3). For each particle type, 10^7 particles/g body weight were dosed.....	129
Figure 4.11	Fluorescent images of lung with nucleus stained by DAPI for mice injected with different particles (shown in purple from NIR dye) denoted on the right corner of each picture. All scale bars=20 μ m.	130
Figure 4.12	Biodistribution of the different particles into various tissues 2 h postdosing presented by percent fluorescence normalized for tissue weight, with n=3 for each case.	131
Figure 5.1	Fluorescent micrographs of HP3A particles with (A) 20 wt% and (B) 50wt% CEA. The size of the particles were 6.5 and 7.5 μ m, and the zeta-potential were -23.5 and -29.9 mV respectively.	144
Figure 5.2	Cationic hydrogel particles. (A) Particles fluoresce in the green channel due to matrix bound fluorescein dye. (B) Fluorescence in the red channel from adsorbed Cy3 dye-conjugated DNA 20mer. Particles were incubated at 37 °C for one hour with 1 μ M DNA, then washed 3 times to remove unassociated DNA. Scale bars are 20 μ m.....	160

LIST OF ABBREVIATIONS

°C	Degrees C
μm	Micrometer
μM	Micromolar
AEM	2-aminoethyl methacrylate hydrochloride salt
ADA	(propane-2,2-diylbis(oxy))bis(ethane-2,1-diyl) diacrylate
AUC	Area under the curve
BALB/c	A strain of mouse
CEA	2-carboxyethyl acrylate
CLT	Total body clearance
C _p	Concentration of particles in plasma
Cy3	Cyanine dye 3
DEAP	2,2-diethoxyacetophenone
DNA	Deoxyribose nucleic acid
EGDA	Ethyleneglycol diacrylate
FBS	Fetal bovine serum
g/mol	Grams per mole
Hb	Hemoglobin
HBOC	Hemoglobin based oxygen carrier
HCPK	1-hydroxycyclohexyl phenyl ketone
HEA	2-hydroxyethylacrylate
HPA	HydroxyPEG acrylate
IPA	Isopropanol

IR	Infrared
kDa	Kilodalton
kPa	Kilopascal
LbL	Layer-by-layer
miRNA	Micro ribose nucleic acids
mPEG	Methoxy terminated poly(ethylene glycol)
mV	Millivolt
N	Newton
nm	Nanometer
PBS	Phosphate buffered saline
PEG	Poly(ethylene glycol)
PEGDA	Poly(ethylene glycol) diacrylate
PET	Poly(ethylene teraphthalate)
PFPE	Perfluoropolyether
PRINT	Particle replication in non-wetting templates
psi	Pounds per square inch
PVOH	Poly(vinyl alcohol)
RBC	Red blood cell
RBCM	Red blood cell mimicking particle
RNA	Ribose nucleic acid
RNase	Ribonuclease
rpm	Rotations per minute
SEM	Scanning electron microscopy

SU-8	A negative photoresist
$t_{1/2}$	Half-life
TGA	Thermogravimetric analysis
UV	Ultraviolet
V_c	Volume of the central compartment
$V_d\beta$	Volume of distribution in the beta phase
α	Alpha
β	Beta

CHAPTER 1: BACKGROUND AND SIGNIFICANCE OF RBC SUBSTITUTES

1.1 Physiology of Blood and Red Blood Cell

A human can live up to 3 weeks without food, 3 days without water, yet only 3 minutes without oxygen. Blood, responsible for delivering oxygen to tissues and cells, is undoubtedly a vital body fluid. Blood also delivers nutrients to the cells of the body, as well as transports carbon dioxide and other waste products away. It also helps fight infection in the body.¹ Blood undergoes gas exchange in the lung, and is pumped by the heart through a network of arteries and veins. Even the heart cannot survive without blood flowing through the vessels that bring oxygen and nourishment to its muscular walls.

Blood accounts for 7% of the human body weight with roughly 5 liters in volume in average adult. It is composed of blood cells (red blood cells, white cells, platelets) suspended in plasma. Plasma, a yellowish fluid constituting 55% of blood volume, contains 90% water, 8% proteins, and trace amounts of other materials including salts, nutrients, hormones and waste products. The erythrocytes, or red blood cells (RBCs), make up the largest population of blood cells, constituting about 45% of whole blood volume. There are about 1000 times more RBCs than white blood cells. Regarding numbers per μL of blood, there are 4.7 to 6.1 million RBCs in a male, 4.2 to 5.4 million in a female.

RBCs are the gas transporting component in blood. They are originally produced in the bone marrow in a process called erythropoiesis,² which lasts about 7 days. As adults, erythropoiesis is limited to the larger bones while almost every bone produces RBCs during childhood. In adults, approximately 2.4 million new RBCs are produced per second. Mature

RBCs lack a nucleus and mitochondria and are not able to undergo mitosis or cytokinesis (cell division), repair themselves, or generate proteins. They are flexible and have a shape of biconcave disk, with diameter of 6-8 μm , height of 1-2 μm and a volume of 90 fL.³ The unique shape allows RBCs to stack like plates and bend as they flow smoothly through the narrow blood vessels.⁴

RBCs circulate for about 120 days in the body and undergo thousands of trips through the microvascular vessels that are smaller than the RBC diameter, because RBCs are capable of extreme changes in shape, deforming over 100% to navigate the small vasculatures.³ Toward the end of their 120-day journey, catabolic changes occur within RBCs and they lose some of their flexibility and ability to deform.⁵ Clearance of senescent RBCs occurs mainly in the spleen, phagocytically by macrophages in the red pulp of the spleen^{6,7}. Defective RBCs, for example malaria-parasitized RBCs, are also eliminated similarly like senescent RBCs. Changes of RBC mechanical properties have also been observed in stored blood over 3 weeks.⁸ Prolonged storage influences the survival of RBCs after transfusion and probably contributes to transfusion-related side effects such as respiratory distress and systemic sepsis.

Deformability of RBCs can be attributed to the architecture of the RBC membrane.⁹ The membrane is chiefly composed of a phospholipid bilayer with a loose lattice of spectrin and actin attached on the inside surface likely giving the red blood cells their signature shape and mechanical properties. The membrane also possesses several proteins which are considered to be “markers-of-self”; they down-regulate endocytotic pathways and prevent these cells from being cleared by the Mononuclear Phagocyte System (MPS), promoting long circulation times¹⁰.

1.2 Structure and properties of Hemoglobin

Vertebrate RBCs contain Hemoglobin (Hb), an iron-containing protein, which transports oxygen by reversibly binding to oxygen and greatly increasing its concentration in blood.¹¹ In contrast, carbon dioxide, the metabolic waste gas, is dominantly (>90%) transported extracellularly by dissolving in plasma as bicarbonate ion.¹² As the major component of the RBC, there are about 200 million Hb molecules in a single RBC, making up 35% of the total content (water included), and about 97% of the RBC's dry content. As such, RBCs are little more than containers of Hb. The Hb concentration in human blood is around 12-16 g/dL.¹³

The protein Hb is made up of 4 globin subunits, each of which compose of a protein chain tightly associated with a non-protein heme group (**Figure 1.1A**).¹¹ As a tetramer, Hb consists of two α and two β subunits, each made of 141 and 146 amino acid residues respectively, denoted as $\alpha_2\beta_2$. The subunits are structurally similar with a molecular weight of about 16,000 Da, and are connected through Van der Waals forces, hydrogen bond and salt bridges. A heme groups consists of an iron ion centrally held in a porphyrin ring. The iron ion is the exact site of oxygen binding and its binding states dictate the color of blood. Hb also carries carbon dioxide (5-10%), which however, binds to the globin chains rather than iron ion. The iron ion may be either in the Fe^{2+} (ferrous) or in the Fe^{3+} (ferric) state, but ferricHb cannot bind oxygen. FerricHb is specifically termed as metHb (metHb).¹⁴ Within RBCs, there is a complicated machinery involving enzymes like metHb reductase, superoxide dismutase and catalase that work together to ensure no more than 3% metHb is present at any given time.

There is an exquisitely well-adapted mechanism for oxygen coordination and transport by Hb. Dioxygen coordination by Hb is accompanied by minute adjustments of the protein from the tensed (T-form) deoxyHb conformation to the relaxed (R-form) oxyHb conformation in which access to the heme pocket is more open, increasing the affinity to O_2 . Release of O_2 is

accompanied by changes of Hb's conformation back from the R to the T form, reducing its affinity for O₂, facilitating oxygen off-loading. The partial pressure of oxygen (pO₂) affects O₂ affinity, where at high pO₂ (such as those present in the alveoli), the R-form is favored. Inversely, low pO₂ (such as those present in respiring tissues) favors the T-form. As a consequence of this cooperativity, the oxygen binding curve of Hb is sigmoidal, or S-shaped (**Figure 1.1B**), as opposed to the normal hyperbolic curve associated with non-cooperative binding

Hb is also allosteric, meaning it can be regulated by an effector molecule at certain binding site. It has many negative allosteric effectors, especially 2,3-diphosphoglycerate (2,3-DPG) that can stabilize the T-form, causing it to release the carried O₂. Various factors such as low pH, high CO₂ and high 2,3-BPG level of the tissues favor the T-form, which has low oxygen affinity and releases oxygen in the tissues. Conversely, a high pH, low CO₂, or low 2,3-DPG favors the R-form which can better bind oxygen.

Hb's affinity for oxygen, hence its tendency to release or retain the gas, is usually described by the oxygen partial pressure at which 50% of the Hb is saturated (P_{50}). P_{50} is temperature dependent. The capacity of Hb to release oxygen to tissues decreases rapidly when temperature decreases, leading to lower P_{50} . At 37 ° C, P_{50} for purified cell-free human Hb (in the absence of 2,3-DPG) is about 14 Torr, as compared to about 26-28 Torr for Hb in the RBC.

1.3 Blood transfusion

A blood transfusion, nowadays, is generally considered as a safe, common procedure in which people receive blood through an intravenous (IV) line inserted into one of the blood vessels. The purpose of blood transfusion is to replace blood lost during a serious injury or

surgery, and may also be done if the body cannot make blood properly because of an illness. Either whole blood, or blood components, especially RBCs is transfused.

There has been a long and complex history of blood transfusion. It is only after Landsteiner's discovery of the ABO blood group system in 1900 that blood transfusion started to become safe. Blood banking became possible when anti-coagulants were added to collected blood, and now about 107 million blood donations are collected worldwide. The shelf-life of collected blood in fridge is generally regarded as 42 days.

Each year, nearly 85 million units of RBCs are transfused worldwide every year. In the US alone, blood is needed every two seconds and the need for blood donations increases every year.^{15,16} Although an overall annual surplus of RBCs is reported in the U.S., this does not take into account geographic or chronologic variations or the availability of RBCs for patients with special RBC requirements. In fact, 13.2% of hospitals have reported challenges in RBC supply.¹⁷ As such, it appears to be challenging for donor centers to consistently maintain RBC inventories, and these facilities may have difficulty maintaining the optimum three-day supply.

RBC transfusions are under increasing scrutiny regarding efficacy associated with the storage lesion, which refers to the biochemical, biomechanical, and immunologic changes in stored RBCs.^{18,19} Stored RBCs are accompanied by changes of affinity of Hb for oxygen, decrease in pH, hemolysis, changes in RBC deformability, formation of microaggregates, release of vasoactive substances and denaturation of proteins. The concentration of 2,3-DPG in stored RBCs decrease over time and little is left after 2 weeks, making transfusion of stored blood not immediately effective in delivery oxygen. It takes about 24 h for banked RBCs to restore their 2,3-DPG level to about one-half of normal.

RBC transfusions are not without risk: fatal adverse transfusion events can occur, such as transfusion related acute lung injury (TRALI), hemolytic transfusion reactions, or septic transfusion reactions.²⁰ Additionally, there is the risk of receiving RBCs infected with HIV, hepatitis A virus, B19 parvovirus, hepatitis C virus, and infectious prion proteins among other known and emerging pathogens.²¹ Beyond the spread of diseases, if a person has a medical condition that requires repeated RBC transfusions, such as patients with sickle cell disease, they may develop alloantibodies to donor RBC antigens: alloimmunization occurs in about 1 out of 4 people who are afflicted with sickle cell disease.²² Lastly, the safety of the RBC donor cannot be overlooked. Despite the advances in RBC collections, storage, and transfusions, the severe reaction rate associated with donation was 0.09%, and 55 cases of post-donation fatalities have been reported to the U.S. Food and Drug Administration (FDA).²³ The need to develop safe, effective, shelf-stable, and non-immunogenic synthetic blood substitutes is great.

1.4 RBC substitutes

The history of blood substitutes date back to the 1600s when beer, wine and milk were examined as intravenously administered substitutes for blood.²⁴ It is only after WWII, when concern over shortage of blood grew, that research on blood substitutes started to begin, and was boosted by the outbreak of AIDS in the 1980's.

The term “blood substitutes” is a misnomer since the products developed only transport gas and replace lost blood volume, while whole blood clearly carries out more functions. As such, RBC substitutes or oxygen therapeutics would be more proper to describe these products. There are two major types of RBC substitutes: perfluorocarbon (PFC)-based oxygen carriers and Hb-based oxygen carriers (HBOC).

Perfluorocarbons (PFC) are chemically and biologically inert molecules containing primarily, fluorine and carbon atoms.^{25,26} They are capable of dissolving large amounts of many gases, including oxygen. Since PFCs cannot dissolve in water, they are formulated into emulsions containing surfactants, salts and other additives.²⁷ PFCs demonstrate a linear oxygen dissociation curve in contrast to the sigmoid dissociation curve of blood. Hence, elevated arterial partial pressures of oxygen enhance oxygen transport by these molecules. However, this linear relationship can also work as a disadvantage since most of the oxygen is released prior to distribution in the capillary network where the partial pressure of oxygen is lower, and hence the need for oxygen is greater. The first PFC product to be approved by the FDA contained perfluorodecalin and perfluorotripropylamine emulsified with Pluronic F-68 and called Fluosol-DA. But due to marginal efficacy, a short effective half-life, temperature instability, low oxygen-carrying capacity, and adverse effects such as acute complement activation and disruption of pulmonary surfactant, this product has since been withdrawn from the market. A more stable emulsion containing perfluorooctyl bromide and perfluorodecyl bromide emulsified in egg yolk phospholipid (Alliance Pharmaceutical Corporation (California)) was developed. This product called Oxygent is thermally stable and had oxygen carrying capability 4-5 times greater than Fluosol-DA and showed great promise initially. However, phase III trials showed an increased incidence of stroke in treated patients compared to controls and trials have been halted.²⁶

Stroma-free Hb has been investigated as an HOBC since the 1940s, when researchers realized that native Hb is not antigenic and has many advantages over red blood cells, including the ability to withstand sterilization and a shelf life of approximately 2 years at room temperature for some products. Unfortunately, the initial attempts at transfusing stroma-free Hb produced renal dysfunction, coagulopathy, and hypertension. Stroma-Hb is cleared quickly (half-life of

0.5~1.5 h) from the circulation by the kidney due to disassociation into two dimers ($\alpha\beta$), causing severe renal toxicity.¹⁹ Besides, solutions of acellular Hb are not as effective at oxygenation as packed RBCs because of their high affinity for oxygen. Adverse effects were attenuated by various modifications to the Hb molecule to prevent glomerular filtration and to stabilize the molecule to withstand heat and chemical purification during production but even then the hypertension was out of proportion to the volume infused. It is thought to result from Hb binding to nitric oxide, which is a potent vascular endothelial relaxant. Several approaches have been tried to decrease the avidity with which Hb binds to oxygen. These adaptations include the addition of organic phosphate to serve the function of 2,3-BPG and adenosine triphosphate, cross-linking dimers of Hb tetramers and polymerizing the tetramers to decrease oncotic pressure or recombinant Hb where the two alpha subunits are covalently attached, and prevent glomerular filtration (**Figure 1.2**), but hypertension has remained a significant adverse effect of stroma-free Hb.

PolyHeme (Northfield Laboratories Inc., Evanston, Ill) is a first-generation pyridoxylated polymerized Hb made from outdated human blood²⁸. It has a half-life of 24 hours, a shelf life longer than 12 months when refrigerated, and a P_{50} of 28-30 Torr. A 720-patient phase III trial was conducted in trauma patients in which subjects were randomized to receive either PolyHeme or standard of care at the time of injury. Preliminary results indicated that 46 of 349 patients treated with PolyHeme died, whereas 35 of 363 patients in the control group died. FDA denied approval of PolyHeme based on the clinical trial results and Northfield Laboratories suspended operations. Other first-generation polymerized Hb products include HbOC-201 (Hemopure manufactured by Biopure Corporation, Cambridge, Mass) and HemoLink (Hemosol Corporation, Mississauga, Canada). Hemopure is a polymerized form of bovine Hb with a P_{50} of 30 Torr that

is closer to human Hb than stroma-free Hb. It has an intravascular half-life of 8-23 hours and a shelf life of 36 months at room temperature. Hemopure is approved in South Africa for the treatment of adult surgical patients who are acutely anemic with the intention of eliminating or reducing the need for allogenic red blood cell transfusions. In the United States, phase II trials have been put on hold due to safety issues. Biopure filed chapter 11 and was purchased by OPK Biotech.

Hemospan (Sangart Inc., San Diego, Calif), also known as MP4OX, is a PEG-conjugated human Hb currently undergoing clinical trials in the US and Europe²⁹. MP4OX is designed to deliver oxygen in the capillaries, where red blood cells may not naturally reach when the body is suffering from trauma-related ischemia, but is not considered to be a substitute for red blood cells. Adverse effects associated with the vasoactive properties of first-generation blood substitutes are not seen with Hemospan (MP4OX).

As an alternative of modified human or bovine Hb, recombinant Hb has been produced from microorganisms such as E. Coli, hence is free from mammalian infectious agents. Recombinant human Hb was engineered either to have a low oxygen affinity or have the α -globins fused to avoid disassociation³⁰. These recombinant Hb products advanced to clinical trials, but it was stopped due to vasoconstriction and other harmful effects.

For Hb-based oxygen carriers cross-linked with enzymes, there has been an effort to synthesize compounds that not only perform the function of carrying oxygen, as do the molecules mentioned previously, but also harbor some of the enzyme activity that normal red blood cells possess. Polymerized Hb has been cross-linked with catalase (CAT) and superoxide dismutase (SOD) to form a compound that, in animal models can not only carry oxygen but also remove oxygen radicals that are responsible for ischemia reperfusion injuries³¹. PolyHb has also

been cross-linked with tyrosinase to form a soluble complex that can carry oxygen and decrease the systemic levels of tyrosine³². This agent can help increase the efficacy of chemotherapy and radiation therapy in tumor tissue and in a melanoma model has been shown to delay tumor growth without having significant adverse effects.

Efforts have also been made to encapsulate Hb within a lipid-membrane to create a compound capable of carrying oxygen while not being associated with significant vasoconstriction. These liposomes appear to be retained in plasma for a significant period³³. However, they are difficult to produce and can activate the reticuloendothelial system, the complement pathway, and platelets.

The most recent development in blood substitutes is the RBC production from stem cells³⁴. A French research group demonstrated that the cultured RBCs (cRBCs) could complete their maturation when incubated in the necessary *in vivo* conditions, and the cRBCs had a half-life of 26 days after injection into human blood. The lifespan and survival rate of the cRBCs are similar to conventional RBCs, supporting their validity as a possible source of transfusion³⁵. However, scale-up of the production of cRBCs and the overall consumed time and cost remain a formidable hurdle (thousands of dollars per unit).³⁶ Therefore, easy-to-scale-up synthesis of HBOCs is still intensely appealing.

The ultimate RBC substitute would contain not only Hb but also other contents of the RBC encapsulated in an artificial membrane. However, production of such a product would be extremely challenging. Efforts have been made to use synthetic polymer t to create artificial RBCs³⁷. These artificial cells contain Hb along with the RBC enzyme complement including superoxide dismutase, metHb reductase, and catalase.

1.5 PRINT RBC Mimics

Against the history of RBC substitutes, we proposed a fundamentally new approach to the problem of a therapeutically viable RBC substitute. We intended to build truly synthetic RBCs consisting of micron-sized particles with the shape, physical properties resembling true RBCs. This approach has been enabled by recent breakthroughs in the nanotech world that allow us to mold, with nanoscale precision, RBC mimics that are shape-specific, colloiddally stable particles with dimensions and mechanical properties which resemble true RBCs.

We have fabricated RBC-mimicking particles without Hb using the PRINT technology.³⁸⁻⁴⁰ PRINT (particle replication in non-wetting template; **Figure 1.3A**) is a precision-molding technique that can efficiently generate monodispersed particles of desired size, shape, chemistry and surface properties. In PRINT, a photocurable liquid perfluoropolyether (PFPE), is used as a molding material. Master templates are prepared using traditional photolithography techniques with raised features on size scales from ~55 nm to >100 μm . PFPE has an exceptionally low interfacial tension and is able to completely wet such templates, at which time it is photochemically cured to produce a crosslinked elastomeric mold possessing cavities which mirror the raised features of the master template. The low surface energy of the PFPE molds allows the cavities to be filled with a pre-particle solution without wetting the landing area between the individual cavities. In this way, distinct particles can be generated in the absence of a flash (connecting) layer. Particles can then be removed from the mold (harvested) with an adhesive layer such as poly(vinyl alcohol) or polyvinylpyrrolidone. Dissolving of the soluble polymeric excipient layer can lead to dispersed solutions of particles.

Using PRINT, hydrogel particles with similar size, shape, characteristics as RBCs of mouse were fabricated (**Figure 1.3B-E**) with tunable deformability. Bulk hydrogels corresponding to these particles were made with varying crosslinker, and the modulus of them

tested. It was found that these hydrogels particles had dramatically altered behavior *in vivo* in a mouse model due to their different deformability. The pharmacokinetics (PK) parameters of these particles are summarized in **Table 1.1**. Particles made from this hydrogel material with a Young's modulus of 7.8 kPa were eliminated from the circulation over 30 times slower than particles which were only moderately (approximately 8x) stiffer (63.9 kPa). The marked difference in the PK of these particles was presumably due to avoidance of filtration in the capillary beds of the lungs, and to some extent, the spleen for softer particles, as indicated by the fact they were able to deform more than stiffer ones to pass through microfluidic channels that were only as half-wide as the particle diameter¹³. Because even slightly less elastic particles (modulus of 16.9 kPa) had greatly reduced circulation times, a modulus-based threshold for 6 μm diameter particles to avoid filtration *in vivo* was inferred.¹³

Table 1.1 PK parameters of RBC mimics found through non-linear regression analysis and fit to a two compartment model for elimination

% Crosslinker	Modulus of Bulk Material (kPa)	Distribution Half-life (hours)	Elimination Half-life (hours)
10%	63.9 \pm 15.7	0.038 \pm 0.0012	2.88 \pm 0.92
5%	39.6 \pm 10.4	0.066 \pm 0.036	5.12 \pm 2.17
2%	16.9 \pm 1.7	0.15 \pm 0.025	7.12 \pm 0.82
1%	7.8 \pm 1.0	0.35 \pm 0.13	93.29 \pm 31.09

1.6 Conclusions

After more than half-a-century's research for safe, effective RBC substitutes, there is still no FDA approved product to date. Most early generations of RBC substitutes relied heavily on the modification of the protein, yet the intrinsic problem of vasoactivity could not be surmounted. Development in nanotechnology allows nanoparticles to be employed for sustained

circulation of hemoglobin in a way that mimics the cellular structure of RBCs, without the need to modify Hb structure to avoid problems of free Hb. By tuning size and surface chemistry of nanoparticles, circulation time of these oxygen carriers could be extended to increase the efficacy. However, besides liposomes, other nanoparticle based oxygen carriers were not fully explored *in vivo* to fully understand parameters that affect the circulation and biodistribution.

PRINT, by virtue of its ability to control size, shape, chemistry, surface properties and modulus at the same time, enables us to synthesize hydrogel particles, and systematically investigate the effect of one factor on the circulation and biodistribution while retaining other factors constant. Maintaining the size of PRINT hydrogel particles similar to murine RBCs, we discovered that modulus plays an important role governing the circulation and biodistribution of the particles, as softer ones tend to circulate longer than the rigid counterparts as being able to navigate smaller capillaries. This *in vivo* result challenged the long-standing dogma that micron-sized particles would be quickly removed from circulation, and opens new opportunities for using large particles (>1 μm) as possible intravascular delivery system, especially as Hb-based oxygen carriers because larger carriers (>500 nm) may be able to minimize vasoconstriction inherent to smaller carriers.

To begin using the RBC mimics as oxygen carriers by incorporating Hb, it will be interesting and important to study the circulation and biodistribution of hydrogel particles with varying sizes (>500 nm), while retaining similar modulus by using identical compositions. This will provide a complete map that can better guide design for not only oxygen carriers, but also for drug delivery systems. Based on this PK study, we can further extend the mimicry of RBCs by loading Hb into the soft particles with an optimal size, with the potential to control oxygen delivery by improving plasma resident time of confined hemoglobin.

1.7 Figures.

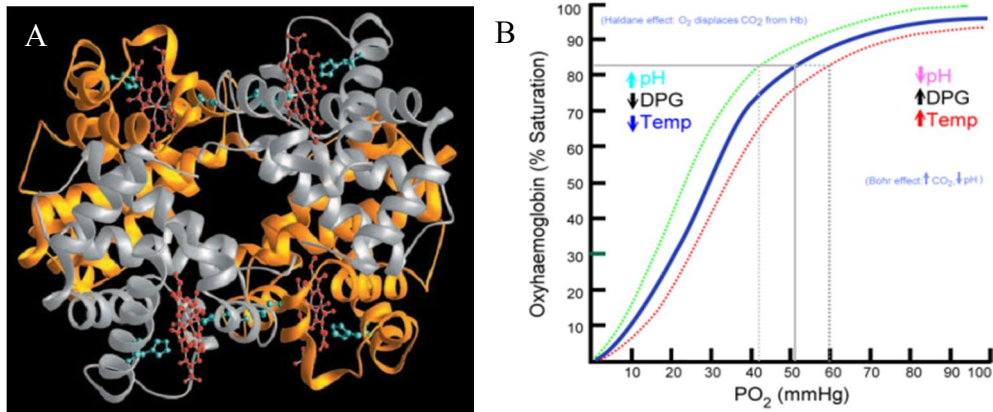


Figure 1.1 (A) Tetrameric structure of hemoglobin; (B) Hypothetical oxygen-hemoglobin dissociation curve. Changes in temperature, pH, and organic phosphates like 2,3-DPG directly affect the dissociation of oxygen.

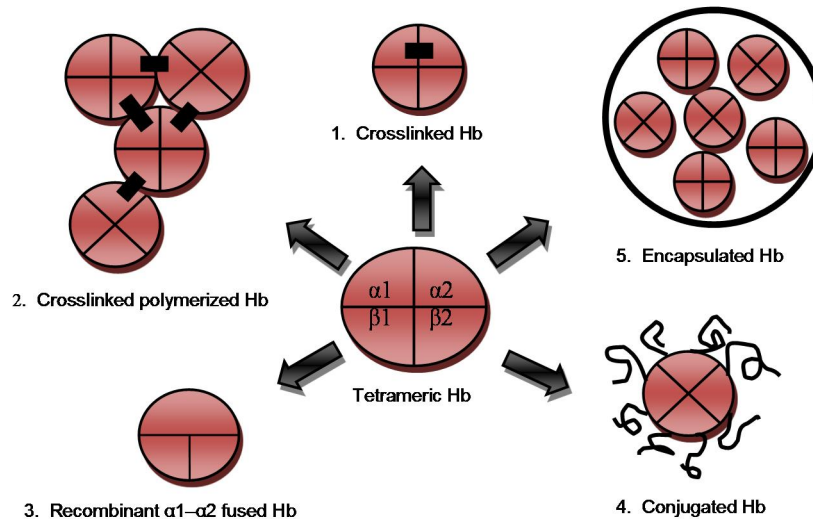


Figure 1.2 Various strategies for modification of the native Hb tetramer (center) intended to avoid renal toxicity, increase circulation time of the free tetramer and, often, to modify the strength of oxygen binding. Counterclockwise from top: 1. The two α or β subunits can be chemically connected to prevent degradation to the toxic $\alpha\beta$ dimer. 2. Otherwise unmodified Hb can be crosslinked to form polyhemoglobin. 3. Genetic modification allows for fusing of subunits as well as tuning of the oxygen binding properties of recombinant Hb. 4. Polymers such as poly(ethylene glycol) or poly saccharides can be chemically attached to the surface of the Hb molecule. 5. Encapsulation in a liposomal carrier or polymeric matrix protects the hemoglobin from degradation.

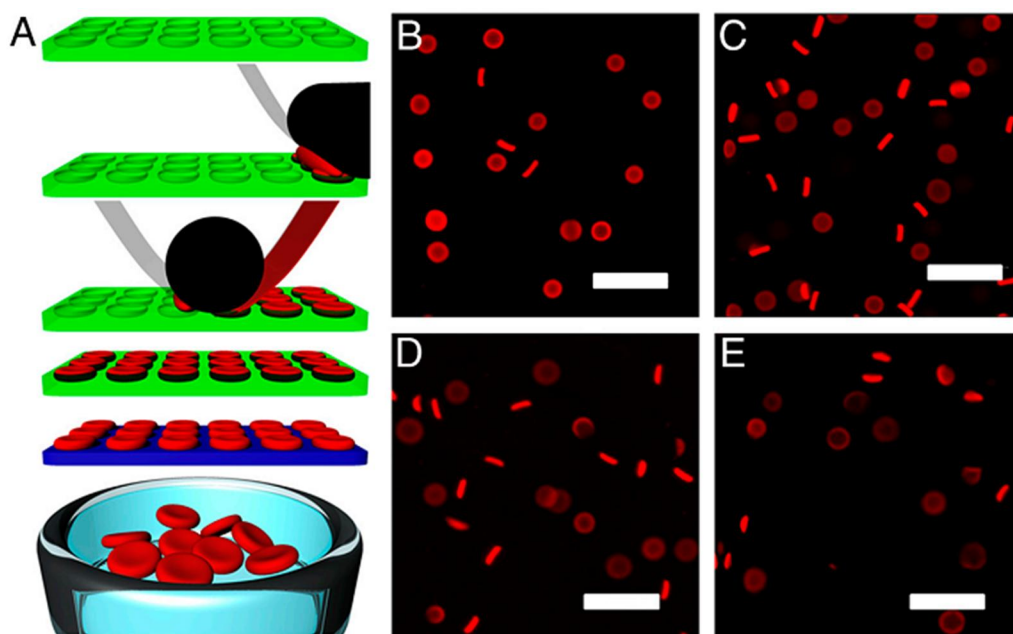


Figure 1.3 Blank RBC mimics. (A) A graphical depiction of the PRINT process to fabricate RBC mimics. Briefly, from top to bottom, an elastomeric fluoropolymer mold (green) with disc shaped wells was covered by an aliquot of the pre-polymer mixture (red). The mold was passed through a pressured nip (black) covered by a high energy sheet (grey), wicking away excess liquid from the mold surface while filling the wells of the mold. The filled mold was cured photochemically, yielding cross-linked hydrogel particles, which were harvested from the mold by freezing onto a thin film of 1% poly (vinyl alcohol) in water (blue) and peeling away the mold. Melting of this layer resulted in a suspension of red blood cell mimic (RBCM) hydrogel particles. (B-E) Fluorescent images of hydrated RBCMs with varying % crosslinker (B) 10% crosslinked (C) 5% crosslinked (D) 2% crosslinked and (E) 1% crosslinked. Scale bars are 20 μ m.

1.8 REFERENCES

- (1) *Blood: Principles and Practice of Hematology*; Lippincott Williams & Wilkins, 2003; p. 2304.
- (2) Jacobson, L. O.; Goldwasser, E.; Fried, W.; Plazk, L. *Nature* **1957**, *179*, 633-634.
- (3) Chien, S. *Annual review of physiology* **1987**, *49*, 177-92.
- (4) Mcwhirter, J. L.; Noguchi, H.; Gompper, G. *Proc. Natl. Acad. Sci.* **2009**, *106*.
- (5) Sutura, S.; Gardner, R.; Boylan, C.; Carroll, G.; Chang, K.; Marvel, J.; Kilo, C.; Gonen, B.; Williamson, J. *Blood* **1985**, *65*, 275-282.
- (6) Krücken, J.; Mehnert, L. I.; Dkhil, M. A.; El-Khadragy, M.; Benten, W. P. M.; Mossmann, H.; Wunderlich, F. *Infection and immunity* **2005**, *73*, 6390-8.
- (7) Deplaine, G.; Safeukui, I.; Jeddi, F.; Lacoste, F.; Brousse, V.; Perrot, S.; Biligui, S.; Guillotte, M.; Guitton, C.; Dokmak, S.; Aussilhou, B.; Sauvanet, A.; Cazals Hatem, D.; Paye, F.; Thellier, M.; Mazier, D.; Milon, G.; Mohandas, N.; Mercereau-Puijalon, O.; David, P. H.; Buffet, P. A. *Blood* **2011**, *117*, e88-95.
- (8) Card, R. T.; Mohandas, N.; Mollison, P. L. *British Journal of Haematology* **1983**, *53*, 237-240.
- (9) Mohandas, N.; Chasis, J. A. *Seminars in hematology* **1993**, *30*, 171-92.
- (10) Oldenborg, P.-A. *Science* **2000**, *288*, 2051-2054.
- (11) Bunn, H. F.; Forget, B. G. *Hemoglobin: Molecular, Genetic and Clinical Aspects*; W.B. Saunders Company, 1986; p. 690.
- (12) Geers, C.; Gros, G. *Physiol Rev* **2000**, *80*, 681-715.
- (13) Beutler, E.; Waalen, J. *Blood* **2006**, *107*, 1747-50.
- (14) Curry, S. *Annals of Emergency Medicine* **1982**, *11*, 214-221.
- (15) Goodnough, L. T.; Scott, M. G.; Monk, T. G. *Clin. Orthop. Relat. Res.* **1998**, 89-100.
- (16) Riess, J. *Chem. Rev.* **2001**, *101*, 2720-2797.
- (17) 2009 National Blood Collection and Utilization Survey Report - Section 508 Compliant - 09-nbcus-report-508.pdf.
- (18) Zubair, A. C. *American journal of hematology* **2010**, *85*, 117-22.

- (19) Alayash, A. I. *Nature reviews. Drug discovery* **2004**, 3, 152-9.
- (20) Shander, A. *Seminars in Hematology* **2004**, 41, 117-124.
- (21) Inayat, M. S.; Bernard, A. C.; Gallicchio, V. S.; Garvy, B. A.; Elford, H. L.; Oakley, O. R. *Transfusion and apheresis science : official journal of the World Apheresis Association : official journal of the European Society for Haemapheresis* **2006**, 34, 25-32.
- (22) Mozzarelli, A.; Ronda, L.; Faggiano, S.; Bettati, S.; Bruno, S. *Blood transfusion* **2010**, 8 Suppl 3, s59-68.
- (23) Blood collection and transfusion related fatality reports - UCM300764.pdf.
- (24) Cells, R. B. *Chemical Reviews* **2001**.
- (25) Biro, G. P.; Blais, P.; Rosen, A. L. *Crit. Rev. Oncol. Hemat.* **1987**, 6, 311-374.
- (26) Castro, C. I.; Briceno, J. C. *Artificial organs* **2010**, 34, 622-34.
- (27) Spahn, D. R. *Critical care* **1999**, 3, R93-7.
- (28) Jahr, J. S.; Varma, N. *IDrugs : the investigational drugs journal* **2004**, 7, 478-82.
- (29) Smani, Y. *Current opinion in investigational drugs (London, England : 2000)* **2008**, 9, 1009-19.
- (30) Bobofchak, K. M.; Mito, T.; Texel, S. J.; Bellelli, A.; Nemoto, M.; Traystman, R. J.; Koehler, R. C.; Brinigar, W. S.; Fronticelli, C. *American journal of physiology. Heart and circulatory physiology* **2003**, 285, H549-61.
- (31) Razack, S.; D'agnillo, F.; Chang, T. M. S. *Artificial Cells, Blood Substitutes and Biotechnology* **2009**, 25, 181-192.
- (32) Yu, B.; Chang, T. M. S. *Biotechnology and bioengineering* **2004**, 86, 835-41.
- (33) Tsuchida, E.; Sou, K.; Nakagawa, A.; Sakai, H.; Komatsu, T.; Kobayashi, K. *Bioconjugate chemistry* **2009**, 20, 1419-40.
- (34) Giarratana, M.-C.; Kobari, L.; Lapillonne, H.; Chalmers, D.; Kiger, L.; Cynober, T.; Marden, M. C.; Wajcman, H.; Douay, L. *Nature biotechnology* **2005**, 23, 69-74.
- (35) Giarratana, M.-C.; Rouard, H.; Dumont, A.; Kiger, L.; Safeukui, I.; Pennec, P.-Y. Le; Francois, S.; Trugnan, G.; Peyrard, T.; Marie, T.; Jolly, S.; Hebert, N.; Mazurier, C.; Mario, N.; Harmand, L.; Lapillonne, H.; Devaux, J.-Y.; Douay, L. *Blood* **2011**, 118, 5071-5079.

- (36) Olivier, E. N.; Qiu, C.; Velho, M.; Hirsch, R. E.; Bouhassira, E. E. *Experimental hematology* **2006**, *34*, 1635-42.
- (37) Piras, A. M.; Dessy, A.; Chiellini, F.; Chiellini, E.; Farina, C.; Ramelli, M.; Della Valle, E. *Biochim. Biophys. Acta* **2008**, *1784*, 1454-61.
- (38) Rolland, J. P.; Maynor, B. W.; Euliss, L. E.; Exner, A. E.; Denison, G. M.; DeSimone, J. M. *J. Am. Chem. Soc.* **2005**, *127*, 10096-100.
- (39) Gratton, S. E. A.; Williams, S. S.; Napier, M. E.; Pohlhaus, P. D.; Zhou, Z.; Wiles, K. B.; Maynor, B. W.; Shen, C.; Olafsen, T.; Samulski, E. T.; Desimone, J. M. *Acc. Chem. Res.* **2008**, *41*, 1685-95.
- (40) Xu, J.; Wong, D. H. C.; Byrne, J. D.; Chen, K.; Bowerman, C.; Desimone, J. M. *Angew. Chem. Int. Ed.* **2013**, *52*, 6580-9.

CHAPTER 2: PHARMACOKINETICS AND BIODISTRIBUTION OF LOW MODULUS HYDROGEL PARTICLES

2.1 Introduction

It has become a growing area of interest to study the effect of physical properties of nano- and microparticles on their *in vivo* behavior in the circulation, because of the increased attention to the design of functional particles for applications in the fields of medical imaging and drug delivery.¹⁻³ Many factors, including size, shape, charge, surface chemistry and modulus of particles, all influence their circulation behavior.⁴ Of these mentioned factors, size, is perhaps the most studied, though not necessarily the most dominant, factor. Many important *in vivo* functions of particles as drug carriers depend on particle size: circulation times, extravasation, targeting, immunogenicity, internalization, intracellular trafficking, degradation, flow properties, clearance and uptake mechanisms.⁵

To understand the effect of size of particles on circulation and uptake, it is critical to first recognize the biological barriers that may affect particle performance. Biological barriers exist to guard the human body from invasion by foreign particles from a systematic level, to the organ level, and the cellular level⁶. At the cellular level of biological barriers, different endocytotic modes determine the path of intracellular trafficking through various possible subcellular compartments.⁷ Ligands conjugated to the surface of engineered particles of particular sizes can influence the mode of cellular internalization.⁸ Cellular barriers are the last barrier nanoparticles have to overcome, i.e systematic and organ level barriers have already been bypassed. While

overcoming cellular barrier is important for most drug delivery systems, it is unnecessary for RBC mimics because the particles are desired to stay longer in blood.

Systemic and organ level barriers are what particles encounter in blood circulation. The blood-tissue interface is circumscribed by a layer of endothelial cells, which serve to demarcate the vascular and extravascular compartments, and to regulate the flow of solute molecules between these compartments⁹. A continuous endothelium is found in most tissues such as the capillaries of all muscles, the central nervous system and the lung, which presents a barrier for particles to pass. Exiting of particles from the circulation is normally restricted to fenestrated endothelium found in liver and spleen,^{10,11} or perturbed endothelium caused by inflammatory processes or by a tumor; the latter is how enhanced permeability and retention effect comes into play in cancer nanomedicine.¹²

In the sinusoids of the liver, the vascular endothelium is marked by openings or fenestrations at the size of about 100-150 nm¹³, which allow the ready passage of plasma proteins and lipoproteins, even permitting particles of less than about 100 nm to come into contact with the hepatocytes. Larger particles remain within the sinusoids where they come into contact with Kupffer cells, which are avidly phagocytic and the Kupffer cell population is extremely high comprising about 10% of total liver cells¹⁴. The abundant blood flow, tortuous circulation in sinusoids, and the abundance of Kupffer cells all together make liver the most efficient organ in the removal of circulating particles.

The spleen has two major functions: production of antibodies and clearance of senescent RBCs¹⁵. The two functions are approximately compartmentalized in the white pulp and the red pulp respectively. The red pulp is abundantly supplied with highly phagocytic macrophages for clearing old red blood cells. Blood flow slowly percolates into the splenic sinusoids, which are

comprised of a tight reticular mesh with interendothelial cell slits that are 200-500 nm in width. The large cross-sectional area for flow and slow blood velocity as well as the plentiful macrophages all facilitate the trapping of particles. The physical filtration of particles along with macrophage uptake in spleen makes it preferentially clear particles larger than 200 nm.

Macrophages that reside in the liver and spleen are in a good position to capture particles passing by, and there are also macrophages circulating that are capable of grasping particles too. Opsonization, that is the adsorption of plasma protein ligands capable of interacting with one or more receptors on the macrophage cell surface, is generally believed to be the major reason for macrophage recognition of foreign particles¹⁶. The opsonin proteins are present throughout the blood and are thought to come in contact as soon as particles are administered into blood; the binding to a particle surface can happen on a temporal scale ranging from a matter of seconds to many days for completion¹⁷. The exact mechanism has not been fully elucidated; yet, it is known that binding is followed by attachment of phagocyte to particle surface.

Based on the biological barriers discussed above, an optimal size is necessary for particles to avoid filtration by biological systems. The size cut-off for filtration no doubt varies considerably depending on animal species and the deformability of the particles administered. For particles lacking deformability, the upper limit would be in the range of a few microns in diameter (5-15 μm)¹⁸. Particles above this size are easily cleared by simple physical entrapment or filtration, usually in the lung capillary bed, which has a total surface area estimated at 40 m^2 . Small drugs, hydrophilic polymers, and very small nanoparticles will be renal filtered after injection due to their small size, which falls below the cut-off size of the kidney (~5.5 nm) as demonstrated using quantum dots studies¹⁹. Particles larger than 200 nm

would be filtered by the liver and spleen as mentioned above. Generally particle size has to be below 200 nm and above 5.5nm to be long circulating, and this has been the ‘gold-standard’ for particle design in most drug delivery systems.

The above results were gained from studies using rigid materials, ranging from metals, to resin or thermoplastics such as polystyrene or poly(lactic-co-glycolic acid) (PLGA) particles. While self-assembled particles, for example liposomes or micelles, may be made to be soft,²⁰ the difficulty in systematically controlling the size impedes a thorough study of similarly soft particles with varying sizes. Using the PRINT technology, however, it becomes readily feasible to maintain an identical low modulus for different-sized particles that are replicated from molds with varying sizes.

In this study, the behavior of monodisperse populations of extremely soft hydrogel particles was probed as particle size was varied in the micron range while composition and modulus were maintained as constants.

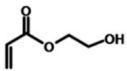
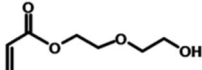
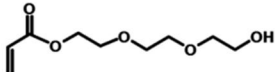
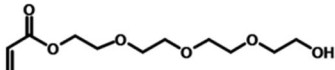
2.2 Results and Discussion

2.2.1 Hydroxyl PEG acrylate Monomers

Previous work in our group already demonstrated the importance of low modulus of particles on circulation time. However the monomer 2-hydroxyethyl acrylate (HEA), used for making RBC mimics from a mold with 2 μm disk cavities²¹, is volatile and cannot be used in PRINT process to replicate particles from smaller cavities due to increased surface-to-volume ratio²². Attempts to replicate particles from 1 μm cavities failed as the mold was mostly unfilled due to evaporation of HEA. The attempt to fabricate differently sized soft hydrogel particles including nanosized ones necessitated exploration of another photocurable monomer with a higher boiling point.

The intuitive way to fabricate smaller hydrogel particles is to synthesize analogues of HEA with a longer PEG side chain. However we know that longer side chains create a higher rotation barrier along the backbone, which may impair the softness of the resulting gel. Thus, we limited the side chain to be oligomeric chain ($n = 2, 3, \text{ or } 4$; **Figure 2.1**) of PEG groups. Rigorous purification of the HPA monomers was necessary to remove all of the diacrylate crosslinker, and cold storage ensured that the transesterified diacrylate did not form *in situ*. The properties of crosslinked hydrogels derive not just from the crosslink density of the gels, but also from the properties of the main-chain polymer and the amount of water uptake or swelling.

Table 2.1 Properties of lightly crosslinked hydrogels composed of different acrylic monomers containing 1% of a 4,000 g/mol PEG diacrylate crosslinker and 1% of HCPK photoinitiator, hydrated for 12 hours in deionized water at room temperature. Monomers are shown with increasing PEG chain length.

Monomer	E (kPa)	% strain at break	Swelling ratio, weight	Swelling ratio, length
HEA 	10 ± 1.6	270	13.6	2.9
HP ₂ A 	103 ± 8.6	60	5.8	1.9
HP ₃ A 	20 ± 1.7	83	10.9	2.4
HP ₄ A 	36 ± 4.8	52	8.8	2.2

The HPA monomers were successfully synthesized and confirmed by NMR and MS. Bulk samples based on HPA with 1% PEG4k diacrylate as crosslinker, 1% 1-hydroxycyclohexyl phenyl ketone (HCPK) as UV initiator were made and the resulting hydrogels after soaking in water after 24h were tested for mechanical properties, which are summarized in **Table 2.1**. Though HP4A hydrogels should have a greater hydrophilic character than HP3A hydrogels, the

longer PEG chain resulted in decreased water uptake, possibly because of the rotation barrier and entanglement impeding higher swelling.

2.2.2 Low Modulus HP3A Hydrogels

Based on previous work with low modulus hydrogels²³, an elastic modulus of < 20 kPa was targeted for HPA based hydrogels. With deformability similar to that of RBCs (15-26 kPa)^{24,25}, a modulus in the target range should be sufficient to show a large effect on particle circulation with 6 μm diameter particles. An acid containing monomer (2-carboxyethyl acrylate, CEA) was included in the hydrogel monomer mixture at 10 % (by weight) to give the particles a negative charge, thereby decreasing non-specific particle uptake.²⁶ Bulk samples of HPA hydrogels containing 10% CEA monomer, 1% HCPK and crosslinked with PEGDA (MW=4k and 6k Da) were hydrated in pH 7.4 PBS to simulate physiological conditions and tested with the Instron tensometer (**Table 2.2**).

No significant difference was observed between the two different crosslinkers. Since PEG4kDA dissolves more easily in HP3A than PEG6kDA, it is the preferred crosslinker to make particles. From the modulus data, we can see all the samples demonstrated modulus similar to RBCs.

Table 2.2 Mechanical properties of HP3A hydrogels with varying amounts of PEG4kDA crosslinker and 10% of 2-carboxyethyl acrylate. Swelling ratios were determined from one bulk sample hydrated for 24 hours in PBS. Modulus and strain at break represent an average value determined from three samples cut from the bulk gel, with error representing one standard deviation.

	A	B	C	D	E	F
HP3A	88	88.5	88.95	88	88.5	88.9
PEG6kDA	-	-	-	1	0.5	0.1
PEG4kDA	1	0.5	0.05	-	-	-
CEA	10	10	10	10	10	10
HCPK	1	1	1	1	1	1
E (kPa)	17± 2.2	13 ± 1.6	6.5± 1.3	17 ± 2.7	16 ± 1.5	12 ± 0.9
% strain at break	53 ± 19	46 ± 7	43± 7.5	50 ± 8	40 ± 7	38 ± 8
Swelling ratio (wt)	11.9	12.8	30	12.9	12.8	19.2
Swelling ratio (length)	2.4	2.6	3.5	2.5	2.5	2.8

2.2.3 RBC-sized HP3A Particles

According to the swelling ratio of bulk samples, PFPE mold with 2 μm cavities may generate RBC mimics with a similar size to those of mouse RBCs (5~6 μm). In a typical PRINT process, polymerizable liquid based on composition of **Table 2.2** were used to fill the PFPE mold and UV cured. The particles were then transferred onto poly(vinyl alcohol) (PVOH) film and then harvested into PBS. Depending on the amount of crosslinker in the composition, particles with slightly different sizes were obtained in the range of 5~6 μm in diameter and 1.6~1.8 μm in thickness. In **Figure 2.2(A-C)**, particles with 0.25 wt% PEG4kDA in different stages of the fabrication process: in the mold, transferred onto PVOH and suspended in PBS, were imaged with a fluorescent microscope. The soft nature of the particles could be visualized by SEM: **Figure 2.2D** illustrates that the particles with 1 wt% crosslinker collapsed and spread on the substrate. When the crosslinker density dropped to 0.5 wt%, however the dried sample could not be visualized using SEM because at such a low crosslinking density, the particles were unable to withstand the surface tension during drying process which tore them apart into broken pieces.

To obtain long circulation times, the deformability of the hydrogel particles must provide them with the ability to pass through smaller capillaries than their size as well as the fenestrations in the spleen *in vivo*. Before *in vivo* study, we utilized a microfluidic device with constricted passages to study the *in vitro* flow behavior mimicking what they might experience in traversing the microvasculature. Microfluidic devices modeling the vascular constrictions have been explored to evaluate the behavior of cells²⁷, including natural and diseased RBCs²⁸, and synthetic RBC mimics²⁹. A 3- μm tall channel packed passages that were 3 μm wide and 50 μm long and repeated many times was designed. There was also an unrestricted 15- μm wide path on each side of the restrictions running the length of the channel, providing an unhindered path for fluid flow to maintain reasonably low pressure through the constricted pathways (**Figure 2.3A**). A dispersion of 0.5 wt% PEG4kDA-crosslinked hydrogels (avg. diameter 5.4 μm) in PBS (containing 0.1 wt% PVOH) was tested in the channel at a flow rate of 0.1 mL/min controlled by a syringe pump. Using an inverted microscope, movies depicting the particles passing through the passages were taken. The image sequence in **Figure 2.3B** shows two particles traversing the passages: the particles stretched in the passages with an elongated shape followed by relaxation to the original discoid shape after exiting the passages. Particles with other crosslinker densities (from 1%-0.05%) were all tested in microfluidic devices and all demonstrated squishy characteristics that allow them to pass through channels narrower than their size.

2.2.4 Low Modulus HP3A Particles with Varying Sizes

The hydrogel formulation with the lowest modulus, as column C in **Table 2.2**, was used to fabricate super soft hydrogel particles, including 1% Dylight 680 maleimide for *in vivo* imaging, and 0.1% methacryloxyethyl thiocarbonyl rhodamine B for ease of particle analysis. To understand the effect of size on biodistribution of similarly soft particles, PRINT molds with

discoid wells of varying diameters of 0.2, 1, 2 and 3 μm were used to generate particles with hydrated diameters of 0.78, 3.79 ± 0.17 , 6.39 ± 0.56 , and 8.88 ± 0.47 μm in PBS, respectively (**Table 2.3**).

Fluorescent microscopy was used to measure the diameter of hydrated particles (n=50) for all except those molded at 0.2 μm . These particles were too small to accurately measure by fluorescence microscopy, but were evaluated using dynamic light scattering to determine their hydrodynamic diameter. The zeta potential of the particles was approximately -20 mV in all cases. The particles were suspended in 0.1 wt% 2,000 g/mol poly (vinyl alcohol) in PBS for *in vivo* applications. Fluorescent images of the low modulus particles can be seen in **Figure 2.4**.

Table 2.3 Characterization of particles fabricated for *in vivo* studies. Particles molded from 1, 2 and 3 μm features were measured by microscopy, with error representing one standard deviation from the mean with n=50 for particle diameters. Particles molded at 0.2 μm were measured by dynamic light scattering to determine their hydrodynamic diameter.

Mold diameter	Particle Diameter	Zeta Potential
0.2 μm	0.78 μm (PDI=0.219)	-17.9 \pm 7.8 mV
1 μm	3.79 ± 0.17 μm	-22.1 \pm 5.7 mV
2 μm	6.39 ± 0.56 μm	-17.6 \pm 10.8 mV
3 μm	8.88 ± 0.47 μm	-22.9 \pm 7.47 mV

2.2.5 Biodistribution of Soft Hydrogel Particles with Different Sizes

To examine the distribution and clearance profile of the particles, female Balb/c mice were injected intravenously at a dose of 20 mg particles/kg of body weight. The mice were sacrificed at time points of 0.2, 0.5, 1, 3, 7, 25, 56, and 104 hours post-dose and the tissues analyzed for fluorescent signal from the particles (**Figure 2.5** and **Figure 2.6**). The tissues were not perfused prior to analysis.

The smallest particles (hydrodynamic diameter = 0.78 μm) distributed primarily into the spleen and liver after injection. Particle accumulation in these tissues increased after injection, peaking 1 hour after dosing (**Figure 2.5**). After this initial 1 hour period, the signal in these tissues decreased steadily over the remaining 103 hours of the study. Clearance to the spleen and liver seems to have been the main mechanism of distribution for these particles, as the initial concentration in the blood dropped rapidly over the first hour post-dose. Accumulation in the lungs, heart and kidneys was minor over the course of the study. The particles were mostly concentrated in the spleen, though more total particles were sequestered in the liver. This difference can be seen in comparing Figure 2.5 and Figure 2.6, which present the biodistribution data on a per tissue and per gram of tissue basis, respectively. After 104 hours, the particles were largely cleared from the blood, with only 3.4% of the dose still circulating.

Particles with a hydrated diameters of 3.8 μm distributed primarily into the spleen and lungs immediately after injection. While signal in the lungs decreased after injection, signal in the spleen increased, peaking at 3 hours and staying fairly constant or slightly decreasing over the next 101 hours. These particles accumulated to some extent in the liver over the course of the study, with signal peaking 24 hours after injection and decreasing slightly thereafter. Liver accumulation was minor when viewed on a per gram basis (**Figure 2.6**). Accumulation in the kidneys and heart remained low at all times, decreasing over the course of the scan, possibly due to the small amount of blood remaining in these tissues. Particles were cleared to low, but still measurable, levels in the blood by the final time-point examined, with 4.1% of the injected dose in the blood at 104 hours.

Particles with 6.4 μm diameters distributed primarily into the spleen and lungs immediately after injection with a profile similar to what we observed in previous studies with

low modulus particles of this size. Signal in the lungs decreased after injection to low levels. Signal in the spleen and liver increased after injection, with signal in the spleen peaking at 3 hours and the signal in the liver peaking later, 7 hours after injection. Signal in the spleen dipped at the 24 hour time-point, correlating to an increase in signal in the blood. This effect may have been due to the release of physically entrapped particles from the spleen back into the circulation. Accumulation in the kidneys, heart, and muscle tissue remained low at all times, decreasing over the course of the scan, possibly due to the small amount of blood remaining in these tissues. At the final time-point examined, 104 hours post-dose, 13.2% of the injected dose remained in the blood.

The largest particles, with hydrated diameter of 8.8 μm , were sequestered primarily in the lungs after injection, likely due to their large size compared to the diameter of the capillary beds in this tissue, and only low amounts of particles remained in the circulation. Particles cleared from the lungs over the course of the study, with accumulation in the spleen and liver increasing over time. Liver accumulation was the most significant for these larger particles compared to the other sizes examined, especially when viewed on a per gram basis (**Figure 2.6**). As with the 6.4 μm diameter particles, a dip in the amount of particles in the spleen and a corresponding increase in the blood occurred. For these larger particles, this effect was more dramatic, and happened earlier in the study (7 hours post-dose). These particles were largely cleared from the circulation to below quantifiable levels by 24 hours post injection, correlating to less than 3% of the injected dose. It is noteworthy that even after 104 hours, the micron-sized particles seemed to be still retaining their shape in the MPS organs (**Figure 2.8**), indicating robust particle structure to withstand shear forces *in vivo*.

2.2.6 Pharmacokinetics of Soft Hydrogel Particles with Different Sizes

Particle concentration in the blood was determined from blood drawn via cardiac puncture at each time-point. Serial dilutions of particles in freshly drawn mouse blood allowed for the generation of standard curves which correlated fluorescent signal in whole blood to particle concentration. The signal from blood harvested from dosed mice fell within the linear region of these plots in most cases, with late time-points falling below quantification limits (where the plot deviated from linearity due primarily to interference from autofluorescence in blood) for the case of the 8.9 μm particles. A plot of particle concentration in whole blood over time for the four sets of particles is shown in **Figure 2.7**.

To evaluate the kinetics of clearance for the 0.78, 3.8 and 6.4 μm diameter particles, we used a two compartment pharmacokinetic model (**Table 2.4**), characterized by a bi-exponential decrease in particle concentration over time,³⁰ with parameters fit by non-linear regression analysis.³¹ This model, which has often been appropriate to describe the behavior of particles in the circulation,^{23,32} describes an initial (distribution) phase where the particles distribute from the plasma into various tissues, followed by a late (elimination) phase that describes the ultimate clearance of particles from the plasma. For small molecules and nanoparticles the distribution is attributed to extravasation into tissue; because of their size, the distribution of our hydrogel microparticles may be due to physical entrapment in constricted capillaries (as in the lung) or tissues with low blood flow (such as the spleen and liver) rather than by an extravasation process.

The clearance profiles were somewhat similar for each of the particles examined, with much of the dose distributing to tissues rapidly after injection and slow elimination half-lives. Elimination half-lives ($\beta t_{1/2}$) for the smaller particles, 31 and 60 hours for the 0.78 and 3.8 μm

particles, respectively, were shorter than for the red blood cell-(RBC) sized 6.4 μm particles (85 h), suggesting that this size may be crucial to the long circulation times of RBCs. Additionally, the area under the curve (AUC), was more than 3 times greater for the RBC sized particles than the smaller hydrogels (8.5 compared to 2.5 and 1.7 $\text{mg}\cdot\text{hr}/\text{mL}$, respectively), indicating that a much greater amount of particles stayed in the circulation over time. Parameters calculated with this model can be seen in **Table 2.4**.

Table 2.4 Pharmacokinetic parameters for low modulus hydrogel PRINT particles with increasing diameters. Parameters were determined from particle concentration in whole blood at times 0.2 - 104 hours post-dose using a standard two-compartment model.

Particle Diameter (μm)	0.78	3.79	6.39
A (mg/mL)	0.309	0.152	0.109
B (mg/mL)	0.0353	0.0268	0.0682
α (hr^{-1})	2.88	0.76	1.08
β (hr^{-1})	0.0224	0.0116	0.00810
$\alpha_{1/2}$ (hr)	0.2	0.9	0.6
$\beta_{1/2}$ (hr)	31.0	59.6	85.5
V_C (mL)	1.16	2.25	2.26
AUC ($\text{mg}\cdot\text{hr}/\text{mL}$)	1.69	2.50	8.51
CL_T (mL/hr)	0.24	0.16	0.047
Vd_β (mL)	10.60	12.68	5.73

The circulation profile of the largest particles examined in this study (8.8 μm) could not be described by a pharmacokinetic model because these were rapidly cleared below the limits of quantification, leaving too few data points for such analysis. These particles did not appear as if their clearance profile would be well described by a standard pharmacokinetic model due to the increase in particle concentration in blood at 3 and 7 hours, the explanation of which may require the application of more complicated models.³³ This effect of increases in particle concentration in the blood at later time points, correlated to decreases in particle signal in either the lungs or spleen in all cases. This strongly suggests that these deformable particles are physically trapped in these tissues, and are able to dislodge and re-enter the main circulation.

2.3 Conclusions and Future Directions

The above studies have shown the promise of HPA based hydrogels for PRINT applications where extremely low modulus particles are desired. Hydrogels made from HP3A were fabricated over a physiologically relevant range of moduli by varying the amount of PEG4kDA crosslinker. Particles with extremely high levels of deformability, characterized by a Young's modulus of 6.5 kPa, are able to avoid or escape filtration when injected intravascularly in mice. Evidence of avoidance is clear from the long (>30 hours) elimination half-lives of all but the largest of these particles.

The decrease in clearance rate is also clearly seen, as these particles tended to accumulate into the spleen over time, reaching a maximum value then decreasing. The decrease in accumulation in the spleen correlated with an increase in the concentration of particles in the blood, presumably due to the release of some of the physically entrapped particles. This was seen most dramatically in the largest of the microgels studied (8.9 μm), where the particle concentration decreased for the first hour of the study before increasing at the 3 and 7 hour time points, presumably due to the escape of particles from the lungs and spleen, which resulted in a corresponding decrease in particle accumulation. Finally, higher circulation persistence and slower clearance were seen for deformable particles that resembled red blood cells in size than for both larger and smaller particles, indicating that this combination of size, shape and deformability results in particles that are better adapted to the avoidance of natural clearance mechanisms in the body.

The results presented here demonstrate the importance of size and deformability for determining the biodistribution and circulation persistence of hydrogel particles. This information is expected to have a large impact on the design of hydrogel particles for therapeutic

or diagnostic applications and to provide a foundation for the use of such highly deformable particles for drug delivery.

The differences in PK and biodistribution among the particles of different sizes indicate the importance of size effects, which are affected synergistically by the flow dynamics and macrophage interactions. From the aspect of flow dynamics, 6.4 μm particles might have performed similarly to real RBCs in vasculatures in a sense that they were mostly in the center of blood vessels as defined by the Fåhræus–Lindqvist effect³⁴. Hence, they had less opportunity to marginate to blood vessel walls in liver sinusoids where Kupffer cells reside, while in spleen they had to pass through the pores that were guarded by macrophages. To study the distribution of the different particles in the cross-section of blood vessel, we may use intravital microscope to observe mouse's earlobe blood vessel, and see fluorescence pattern from RBC-sized particles and another-sized particle differently labeled. The smaller particles (3.79 μm , 0.78 μm) may tend to marginate more to the blood vessel wall than the RBC-sized particles.

The interaction between HP3A particles and macrophages in the spleen and other organs is not discussed here. It has been known that macrophages would have difficulty engulfing soft particles than rigid ones. Size also plays pivotal role regarding phagocytosis of particles by macrophages. Larger particles would be more difficult to engulf because macrophages need to deform the membrane more. By doing the same PK and BioD studies in mice with temporarily depleted macrophages by injecting clodronate liposomes, altered circulation profile and biodistribution of these hydrogel particles may be observed,³⁵ and can indicate the different roles played by physical sequestration of particles versus macrophage internalization.

All the particles were highly porous because of their high swelling. This characteristic may allow large cargoes like proteins, to diffuse into the interior. Different strategies can be

employed to secure the cargo inside. Proteins and nucleic acids can be secured within hydrogels that are oppositely charged due to electrostatic interactions. Pro-drug strategy can also be used to covalently link the cargo to the particle matrices. Degradation of the linker, either by low pH or reductive environment, could trigger release of the cargo. For hemoglobin, it is desirable to secure the protein inside without leaking out. Thus covalent conjugation can be utilized to ensure bond formation.

2.4 Materials and Methods

2.4.1 Materials

Acryloyl chloride (97%), triethylene glycol (99%), and 2-carboxyethyl acrylate (CEA, 97%) were purchased from Sigma-Aldrich and used as received. Photoinitiators 2,2-diethoxyacetophenone (DEAP), and 1-hydroxyl-cyclohexyl phenyl ketone (HCPK) were purchased from Aldrich and used as received. Poly(ethylene glycol) diacrylate (PEG4000DA) and methacryloxyethyl thiocarbamoyl rhodamine B (PolyFluor 570) were purchased from Polysciences, inc. and used as received. Dylight 680 maleimide was purchased from Thermo Scientific. All other reagents were purchased from Fisher and were used without further purification unless otherwise noted.

2.4.2 Synthesis of Hydroxy PEG Acrylate Monomers

Mixtures of hydroxy PEG acrylate and hydroxy PEG diacrylate were obtained by reaction of di-, tri-, or tetraethylene glycol and acryloyl chloride in anhydrous dichloromethane under a nitrogen purge with triethylamine present as a scavenger for HCl evolved during the reaction. In order to obtain a higher ratio of monoacrylate to the diacrylated product and a good yield, a 7:3 ratio of di-, tri-, or tetraethylene glycol to acryloyl chloride was used.³⁶ Addition of acryloyl chloride proceeded over 3 hours at room temperature, with stirring allowed to proceed for

another 12-15 hours. The ammonium chloride salts were removed via filtration. The filtrate was washed several times with deionized water to extract the glycols and monoacrylates. The aqueous phase was washed several times with diethylether to extract the monoacrylate. The ether washes were reduced by rotary evaporator in vacuo, and the product isolated via column chromatography. The product was eluted using a mixture of hexane, ethyl acetate and methanol in a 6:3:1 ratio. Free radical inhibitor 4-Methoxy Phenol (MEHQ) was added to the product fraction at 500 ppm of total acrylates prior to exhaustive vacuo rotoray evaporation to remove all of the residual solvent yielding a clear, colorless to pale yellow liquid. The acrylic monomers are referred to as hydroxyl PEG acrylates, with the length of the PEG chain attached to the acrylic moiety denoted by number. For example, HP4A refers to the tetraethylene glycol adduct, while HP2A refers to the diethylene glycol adduct.

2.4.3 Modulus Testing

To measure the mechanical properties of crosslinked HPA hydrogels, macroscopic coupons of the prepolymer mixtures were polymerized via UV light in a Teflon mold. Approximately 650 μL of freshly prepared prepolymer mixture was pipette into a 2.5 x 2.5 cm square mold. The mold was placed in a low-intensity UV oven, and nitrogen purged for 3 minutes prior to curing with UV light. The cross-linked hydrogels were removed from the mold, weighed, and placed in pH 7.4 PBS buffer for 24 hours to fully hydrate. The coupons were patted dry with paper towels and weighed again prior to sectioning into approximately 10 mm wide strips with a razor blade for testing with an Instron 5556 Universal Testing Machine (Instron) with a strain rate of 5 mm/min. Young's modulus was determined from the initial slope of the resultant stress-strain curves.

2.4.4 Particle Fabrication

Particles were fabricated using the PRINT (particle replication in non-wetting templates) process^{14,15}. PRINT molds for these studies were obtained from Liquidia technologies and consisted of a thin layer of a patterned, photocured perfluoropolyether (PFPE) on top of a flexible poly(ethyleneterephthalate) (PET) backing.

To fabricate particles, the pre-polymer mixture was spread onto a mold which was adhered to a silicon wafer and chilled to 2-5 °C on a custom built laminator platform. The reduced temperature prevented evaporation of the pre-polymer solution prior to photo-curing. A PET sheet was laminated to the top of the mold and pre-polymer solution, wetting the total mold area. The sheet was peeled away at the nip point of the laminator, leaving the wells of the mold filled while wicking away excess solution. The filled mold was immediately transferred into a chilled (~5 °C), nitrogen purged UV oven and cured with UV light ($\lambda = 365$ nm, 3 minutes, power ~ 20 mW/cm²).

Particles were transferred from the mold by laminating the filled, cured molds to a PET sheet which was coated with a thin film of Luvitec (BASF). The particle-filled mold and Luvitec coating were placed in contact and passed through the nip point of a laminator. To increase the yield of harvested particles, a heated laminator was used for this step, with roll temperatures hot enough to allow the Luvitec to flow and come into contact with the particles (typically >180 °F). Alternatively, it was possible in some cases to transfer the particles without added heat due to “sticky” adhesion of the particles to the Luvitec film. After cooling briefly, the mold was peeled away from the Luvitec sheet at a steep angle, leaving the particles on the Luvitec film in an ordered array.

Harvesting of the particles from the ordered array on Luvitec into solution was accomplished by “bead harvesting”. In this process, the particles on the harvesting film were passed through the vertical nip point formed by two rollers. At the nip point, a bead of water dissolved the Luvitec layer, suspending the particles in solution, as the rollers drew the film down through the nip. The particle solution was then collected using a pipette.

2.4.5 Particle Harvesting and Purification

The bead harvesting process leads to well stabilized particles, but leaves an abundance of dissolved Luvitec in solution. The particles were pelleted via centrifugation at 4 °C (12,000 rpm, 5-10 minutes depending on particle size) and the supernatant removed carefully so as not to disturb the pellet. The pellet was resuspended in a solution of 0.1% poly(vinyl alcohol) in Dulbecco’s pH 7.4 PBS buffer (Fisher Scientific) and this procedure was repeated 2-3 times to remove excess Luvitec and any soluble fraction of poly(HPA) or unreacted monomers.

2.4.6 Particle Characterization

To accurately determine particle concentration, thermogravimetric analysis (TGA) was used. To determine the weight of salts and polymer in the solution, 50 μ L of the particle solution was centrifuged exhaustively (14,000 RPM/20 minutes) to pellet the particles. The supernatant (20 μ L) was pipetted to a tared TGA pan and the weight was monitored on a Perkin Elmer Pyris 1 TGA under the following heating steps: 25-115 °C by 10 °C/minute followed by a 10 minute hold to drive off the water in the solution. The dried sample provided the weight of salts and dissolved polymer in solution. In parallel, a 20 μ L sample of the particle solution was analyzed under identical conditions, with the particle weight determined by subtracting the weight of salts and polymer in solution from this final weight.

Particles dimensions were determined by analysis of images from a microscope mounted camera (Zeiss AxioCam MRm) using a 100x objective (Zeiss Axio Imager D.1M), or by dynamic light scattering (DLS) for the 0.78 μm particles using a nano ZS zetasizer (Malvern Instruments). Over 50 fully hydrated particles in pH 7.4 PBS buffer were measured. Zeta potentials for particles were measured on a nano ZS zetasizer (Malvern Instruments) in water.

2.4.7 Microfluidics

Microfluidic masters were fabricated in the Chapel Hill analytical and nanofabrication laboratory (CHANL) cleanroom. Chrome on quartz masks were ordered from Benchmark Technologies. SU-8 was coated onto 6 inch wafers with film thickness equal to the desired feature height. The wafers were soft baked at 95 °C for 90 seconds. A Karl Suss MA6/BA6 mask aligner was used to bring the mask into contact with the wafer, followed by 10 second exposure time. Post-exposure bake at 95 °C for 2 minutes was followed by soaking in SU-8 developer for 3 minutes to remove unexposed resist. The masters were hard baked at 165 °C for 30 minutes prior to fabrication of devices. Feature heights were analyzed using a P-6 profilimeter (KLA Tencor). Microfluidic devices were fabricated from silicone (Sylgard 184, Dow Corning) sealed to glass after treatment with oxygen plasma. Flow in the devices was driven by a syringe pump at a fixed rate (0.06 $\mu\text{L}/\text{min}$). Dilute solutions of RBCMs (1-5 $\mu\text{g}/\text{mL}$ in PBS with 0.1% poly (vinyl alcohol)) were pumped through the channel and observed with a fluorescence microscope (Nikon TE2000). Videos were taken with a with a Photometrics Cascade II:512 camera. Particle stretching was analyzed with ImageJ software (NIH).

2.4.8 *In vivo* Studies

To track the plasma concentration and biodistribution of particles in mice, 20 mg articles/kg mouse weight was administered via a 2.0 mg/mL solution of particles in PBS with

0.1% poly(vinyl alcohol) via tail-vein injection to female BALB/c mice of 20-22 g body weight. Four mice were examined at each time-point, including points 0.2, 0.5, 1, 3, 7, 24, 56, and 104 hours post injection. At each time point examined, mice were sacrificed and tissues harvested. Harvested tissues included the lungs, liver, kidneys, spleens, heart and a posterior leg (thigh) muscle. Blood was collected via terminal cardiac puncture. Control mice were undosed.

2.4.9 Biodistribution

The fluorescent signal from the particles in the tissues and blood was measured using an IVIS Lumina fluorescent imager (Caliper Life Sciences) with excitation at 675 nm and emission measured at 720 nm. Harvested tissues including liver, lung, spleen, kidneys, heart, and intestines were weighed, then imaged. Blood was harvested via cardiac puncture, and pipetted in 100 μ L aliquots to black 96 well plates for analysis on the imager. Control mice without injection were sacrificed too and the tissues and blood used as background. The fluorescent signal for each tissue sample was background corrected by subtracting the signal from control tissues. Biodistribution profiles for the RBCMs at two hours post-dose were determined by percent of recovered fluorescence in the above tissues. Fluorescent signal in the blood was calculated by measuring the fluorescent signal from several aliquots of blood and extrapolating to account for the total blood volume in the mice (approximately 1.7 mL/20 g of body weight).

2.4.10 Pharmacokinetics of Particle Clearance from Blood

For determination of pharmacokinetic parameters including alpha and beta half-lives, we fit the data to a two-compartment model using non-linear regression analysis (Excel). The two-compartment model assumes that particles are transported between the central and eripheral compartments with first-order kinetics and that particles re eliminated from the central compartment with first-order kinetics. The data was fit to Equation 1, where C_p is the

concentration of the particle in the plasma, and α and β are rate constants for the distribution and elimination processes, respectively.

$$C_p = Ae^{-\alpha t} + Be^{-\beta t} \quad \text{Equation 2.1}$$

The fit was calculated by nonlinear regression, maximizing the R^2 value for the fit and producing best fit values for the coefficients and rate constants. Half-lives for the distribution and elimination process were calculated by equations 2.2 and 2.3, respectively.

$$\alpha t_{1/2} = \frac{\ln 0.5}{\alpha} \quad \text{Equation 2.2}$$

$$\beta t_{1/2} = \frac{\ln 0.5}{\beta} \quad \text{Equation 2.3}$$

AUC (area under the curve) was determined by integrating equation 2.1, which describes the plasma concentration/time profile (Equation 2.4).

$$AUC = \frac{A}{\alpha} + \frac{B}{\beta} \quad \text{Equation 2.4}$$

The volume of the central compartment, V_c , relates the dose administered and the initial particle concentration (equation 2.5).

$$V_c = \frac{\text{Dose}}{A+B} \quad \text{Equation 2.5}$$

Total body clearance, CL_T , describes the volume of blood cleared of particles over time, and is calculated from the dose administered and the AUC (equation 2.6).

$$CL_T = \frac{\text{Dose}}{AUC} \quad \text{Equation 2.6}$$

The volume of distribution in the elimination phase, Vd_β , describes the volume in which the particles would need to be disbursed to provide the observed concentration in blood for the elimination phase (equation 2.7).

$$Vd_\beta = \frac{CL_T}{\beta} \quad \text{Equation 2.7}$$

2.4.11 Histology

All tissues were frozen on dry ice shortly after imaging and 5 μ m frozen sections prepared for staining. Microscope slides with frozen tissue sections were allowed to thaw at room temperature for 20-30 min, at which point they were washed briefly with TBS. The sections were fixed with 2.5 % paraformaldehyde in TBS for 5 min, followed by two 5 minute washes with TBS. The excess paraformaldehyde was quenched with 10 mM ethanolamine in PBS for 5 min, followed by washing twice with TBS for 2 minutes. The sections were permeablized with 0.1% Triton X-100 (Alpha Aesar) in TBS for 5 min, and then washed with TBS twice for 5 min. The sections were incubated overnight at 4°C with DAPI (Invitrogen) prepared using 0.025 % Tween 20 (Fisher Scientific) in TBS. Following incubation, the sections were washed 4 times for 5 minutes prior to mounting with ProLong Gold antifade reagent (Invitrogen).

All samples were imaged with an Zeiss710 confocal laser scanning microscope with filters optimized for the different fluorescent probes, including the DyLight 680 dye in the RBCMs. Images were taken with a 40x objective lens.

2.5 Figures

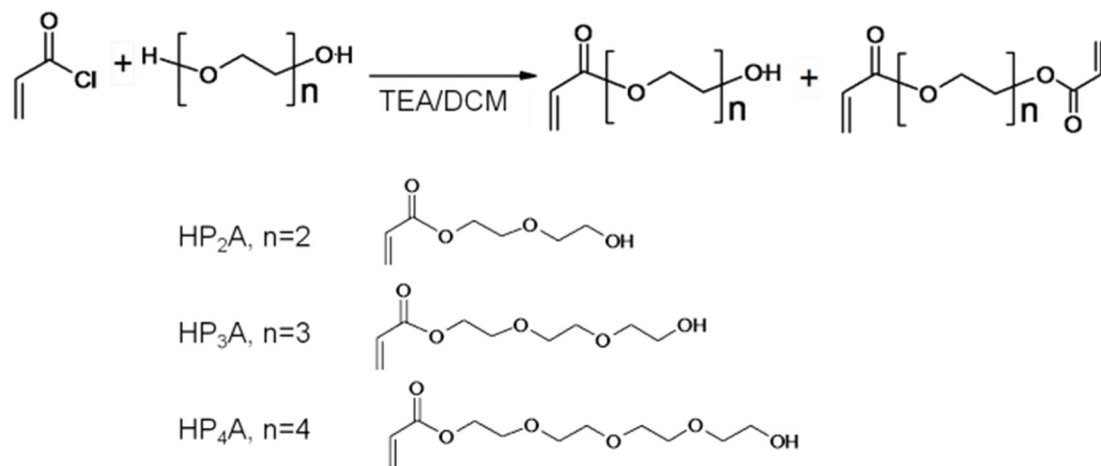


Figure 2.1 Synthetic scheme for hydroxyl PEG acrylates (HPAs). The structures of the monoacrylated products are shown below the reaction scheme, along with the naming convention.

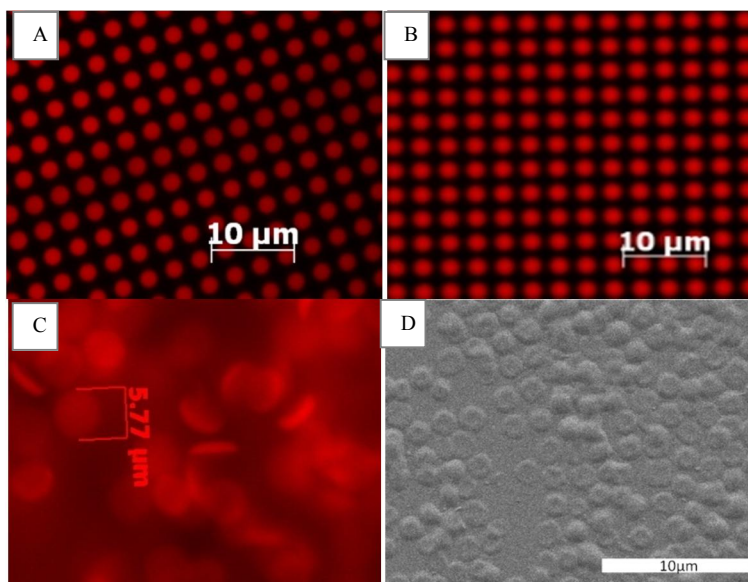


Figure 2.2 Microscopic images of HP3A particles with 0.25 wt% crosslinker in the mold (A), transferred on to PVOH (B) and suspended in PBS (C); SEM image of dried particles with 1 wt% crosslinker(D). Particles crosslinked with less than 1 wt% PEG4kDA were unable to retain integrity in the dry state that they could not be imaged by SEM.

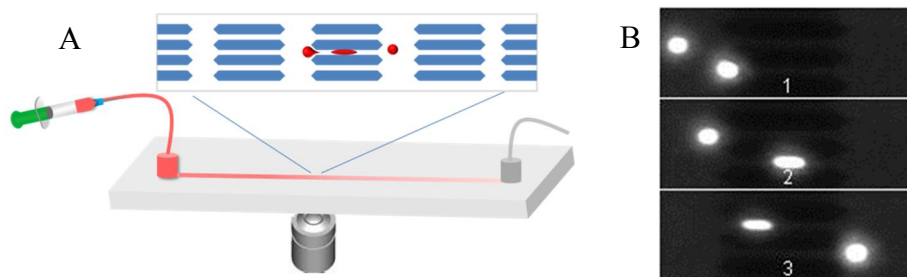


Figure 2.3 Microfluidic evaluation of HP3A-based RBC mimicking particles. (A) Schematic illustration of the microfluidic device used; (B) An image sequence showing 0.25 wt% crosslinked RBCM particles (5.4 μm in diameter) squeezing through the $3 \times 3 \mu\text{m}$ channels (190 ms between frames).

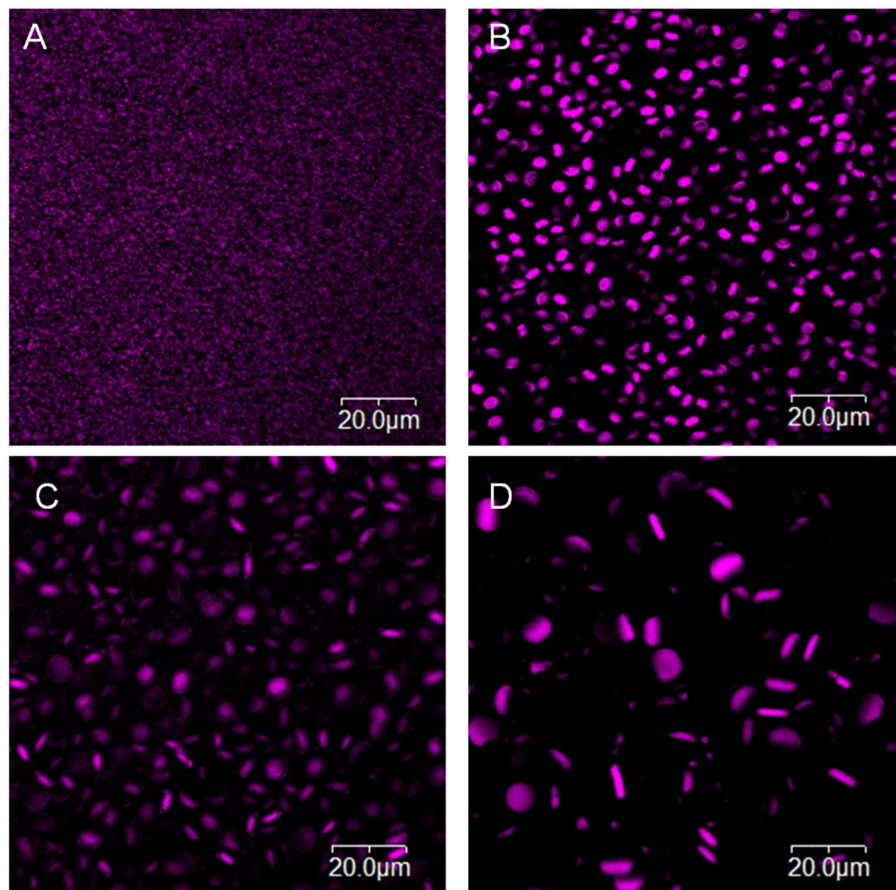


Figure 2.4 Fluorescent images of the particles used for the in vivo studies. The particles have hydrated diameters of (A) $0.78 \mu\text{m}$ (B) $3.79 \pm 0.17 \mu\text{m}$, (C) $6.39 \pm 0.56 \mu\text{m}$, and (D) $8.88 \pm 0.47 \mu\text{m}$. Scale bars are $20 \mu\text{m}$. The particles were imaged at the DyLight 680 channel.

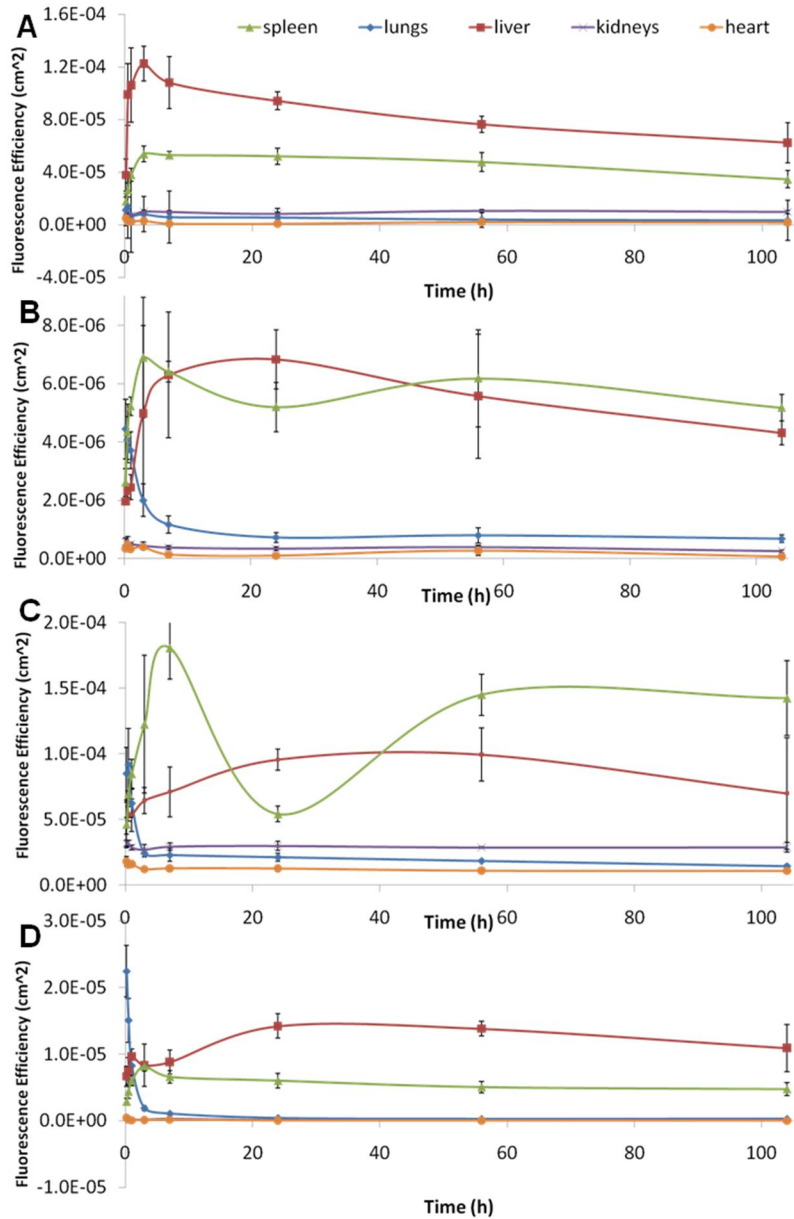


Figure 2.5 Biodistribution of extremely deformable particles of different sizes in mice over the course of 5 days. The total fluorescent signal from the particles in each tissue sampled is shown for particles with diameters of (A) 0.78 μm , (B) 3.8 μm , (C) 6.4 μm and (D) 8.9 μm . Four mice were examined per time-point, with error bars representing one standard deviation.

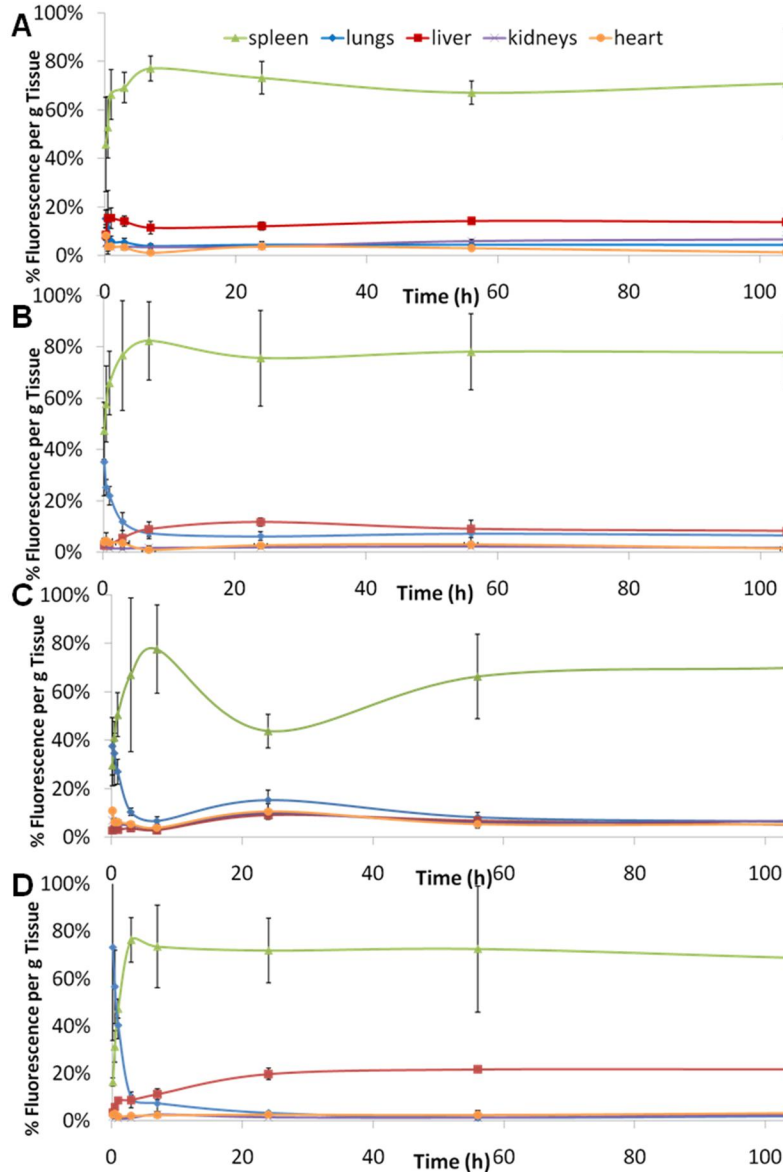


Figure 2.6 Biodistribution of extremely deformable particles of different sizes in mice over the course of 5 days. The percentage of the fluorescent signal recovered from the sampled tissues was adjusted by the weight of the tissue. Data is shown for particles with diameters of (A) 0.78 μm , (B) 3.8 μm , (C) 6.4 μm and (D) 8.9 μm . Four mice were examined per time-point, with error bars representing one standard deviation.

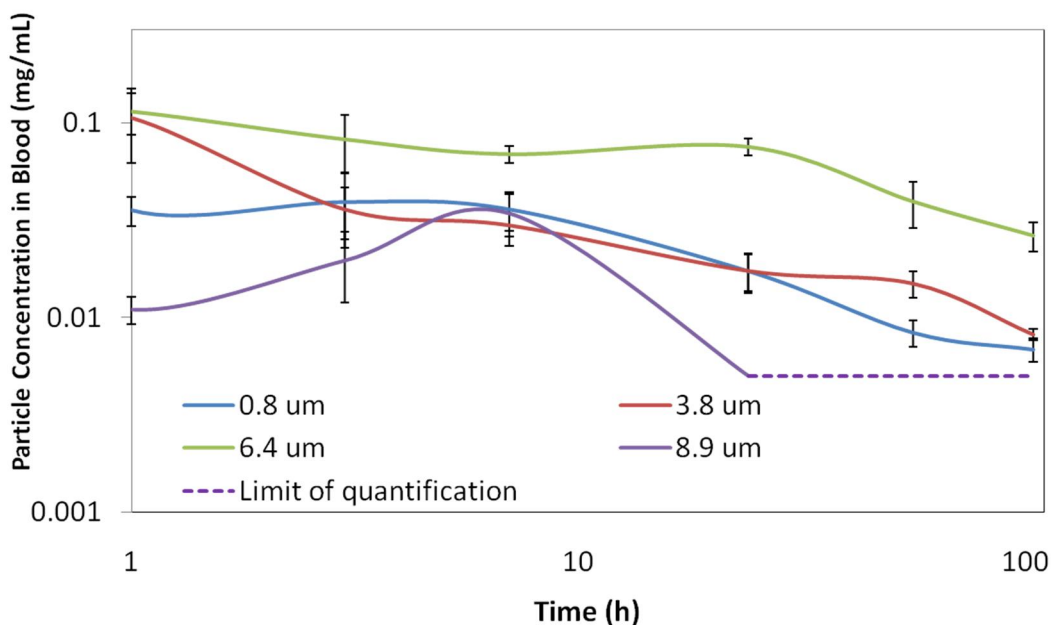


Figure 2.7 A plot showing the change in particle concentration in blood over time for deformable hydrogel particles of different sizes. Particles with a diameter of 6.4 μm , similar to that of mouse red blood cells, were cleared more slowly and remained in the circulation to a greater extent than both larger and smaller particles with identical mechanical properties and composition. The largest of these particles, with hydrated diameters of 8.9 μm , were cleared to concentrations in blood below our limits of quantification (indicated by the dashed line). Each data point represents 4 mice, with error bars representing one standard deviation.

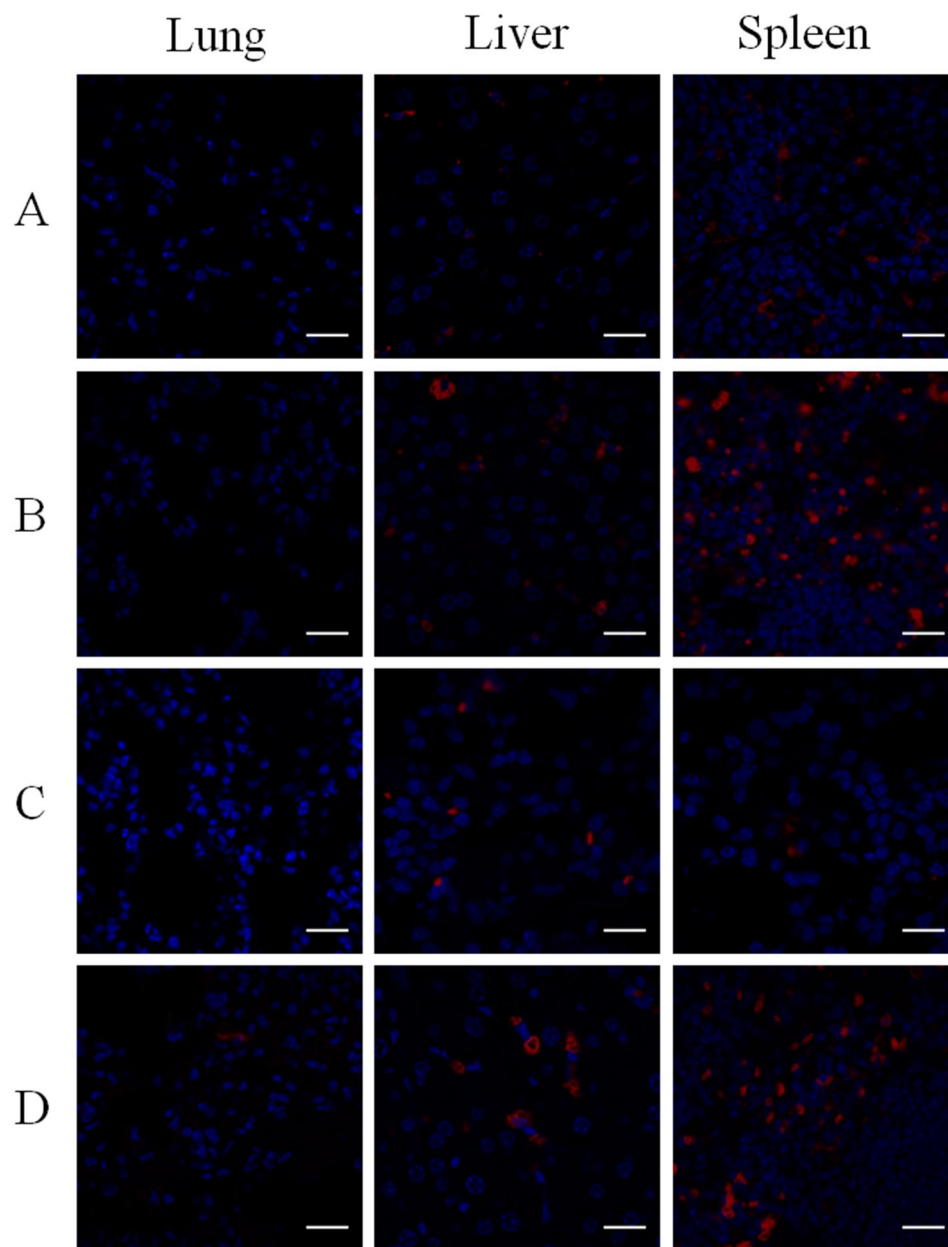


Figure 2.8 Histological sections of lung, liver and spleen tissue from mice sacrificed 104 hours after dosing with (A) 0.78 μm , (B) 3.79 μm , (C) 6.39 μm , and (D) 8.9 μm particles. Images are an overlay of fluorescence from DAPI staining (blue) and the Dylight 680 dye that is covalently bound to the hydrogel particles (red). Scale bars are 20 μm .

2.6 REFERENCES

- (1) Alexis, F.; Pridgen, E.; Molnar, L. K.; Farokhzad, O. C. *Molecular pharmaceutics* **2008**, *5*, 505-15.
- (2) Peer, D.; Karp, J. M.; Hong, S.; Farokhzad, O. C.; Margalit, R.; Langer, R. *Nature nanotechnology* **2007**, *2*, 751-60.
- (3) Sun, C.; Lee, J. S. H.; Zhang, M. *Advanced drug delivery reviews* **2008**, *60*, 1252-65.
- (4) Moghimi, S. M.; Hunter, A. C.; Murray, J. C. *Pharmacological Reviews* **2001**, *53*, 283-318.
- (5) Visscher, G. E.; Pearson, J. E.; Fong, J. W.; Argentieri, G. J.; Robison, R. L.; Maulding, H. V. *Journal of biomedical materials research* **1988**, *22*, 733-46.
- (6) Petros, R. A.; Desimone, J. M. *Nature reviews. Drug discovery* **2010**, *9*, 615-627.
- (7) Zhang, S.; Li, J.; Lykotrafitis, G.; Bao, G.; Suresh, S. *Adv. Mater.* **2009**, *21*, 419-424.
- (8) Verma, A.; Stellacci, F. *Small* **2010**, *6*, 12-21.
- (9) Sumpio, B. E.; Riley, J. T.; Dardik, A. *The international journal of biochemistry & cell biology* **2002**, *34*, 1508-12.
- (10) Warren, A.; Cogger, V. C.; Arias, I. M.; McCuskey, R. S.; Couteur, D. G. *Le Microcirculation* **2010**, *17*, 32-8.
- (11) Satchell, S. C.; Braet, F. *Am. J. Physiol. Renal. Physiol.* **2009**, *296*, F947-56.
- (12) Maeda, H. *Journal of Controlled Release* **2000**, *65*, 271-284.
- (13) Wisse, E.; Jacobs, F.; Topal, B.; Frederik, P.; Geest, B. *De Gene therapy* **2008**, *15*, 1193-9.
- (14) Bouwens, L.; Baekeland, M.; Zanger, R. de; Wisse, E. *Hepatology* **1986**, *6*, 718-722.
- (15) Mebius, R. E.; Kraal, G. *Nature reviews. Immunology* **2005**, *5*, 606-16.
- (16) FRANK, M. *Immunology Today* **1991**, *12*, 322-326.
- (17) Owens, D. E.; Peppas, N. a *International journal of pharmaceutics* **2006**, *307*, 93-102.
- (18) Azarmi, S.; Roa, W. H.; Löbenberg, R. *Advanced drug delivery reviews* **2008**, *60*, 863-75.
- (19) Choi, H. S.; Liu, W.; Misra, P.; Tanaka, E.; Zimmer, J. P.; Itty Ipe, B.; Bawendi, M. G.; Frangioni, J. V. *Nature biotechnology* **2007**, *25*, 1165-70.
- (20) Ogunsola, O. A.; Kraeling, M. E.; Zhong, S.; Pochan, D. J.; Bronaugh, R. L.; Raghavan, S. R. *Soft Matter* **2012**, *8*, 10226.

- (21) Merkel, T. J.; Jones, S. W.; Herlihy, K. P.; Kersey, F. R.; Shields, A. R.; Napier, M.; Luft, J. C.; Wu, H.; Zamboni, W. C.; Wang, A. Z.; Bear, J. E.; Desimone, J. M. *Proc. Natl. Acad. Sci.* **2011**, *586-591*.
- (22) Jackman, R. J.; Duffy, D. C.; Ostuni, E.; Willmore, N. D.; Whitesides, G. M. *Analytical Chemistry* **1998**, *70*, 2280-2287.
- (23) Merkel, T. J.; Jones, S. W.; Herlihy, K. P.; Kersey, F. R.; Shields, A. R.; Napier, M.; Luft, J. C.; Wu, H.; Zamboni, W. C.; Wang, A. Z.; Bear, J. E.; DeSimone, J. M. *Proc. Natl. Acad. Sci.* **2011**, *108*, 586-91.
- (24) Doshi, N.; Zahr, A. S.; Bhaskar, S.; Lahann, J.; Mitragotri, S. *Proc. Natl. Acad. Sci.* **2009**, *106*, 21495-21499.
- (25) Dulińska, I.; Targosz, M.; Strojny, W.; Lekka, M.; Czuba, P.; Balwierz, W.; Szymoński, M. *Journal of biochemical and biophysical methods* **2006**, *66*, 1-11.
- (26) Gratton, S. E. A.; Ropp, P. A.; Pohlhaus, P. D.; Luft, J. C.; Madden, V. J.; Napier, M. E.; DeSimone, J. M. *Proceedings of the National Academy of Sciences of the United States of America* **2008**, *105*, 11613-8.
- (27) Rosenbluth, M. J.; Lam, W. A.; Fletcher, D. A. *Lab Chip* **2008**, *8*, 1062-70.
- (28) Shevkoplyas, S. S.; Yoshida, T.; Gifford, S. C.; Bitensky, M. W. *Lab Chip* **2006**, *6*, 914-20.
- (29) Haghgoie, R.; Toner, M.; Doyle, P. S. *Macrom. Rapid Commun.* **2010**, *31*, 128-34.
- (30) Neubauer, A. M.; Sim, H.; Winter, P. M.; Caruthers, S. D.; Williams, T. A.; Robertson, J. D.; Sept, D.; Lanza, G. M.; Wickline, S. A. *Magnetic resonance in medicine* **2008**, *60*, 1353-61.
- (31) Brown, A. M. *Computer Methods and Programs in Biomedicine* **2001**, *65*, 191-200.
- (32) Gratton, S. E. A.; Pohlhaus, P. D.; Lee, J.; Guo, J.; Cho, M. J.; Desimone, J. M. *Journal of controlled release* **2007**, *121*, 10-8.
- (33) Li, M.; Al-Jamal, K. T.; Kostarelos, K.; Reineke, J. *ACS nano* **2010**, *4*, 6303-17.
- (34) Diez-Silva, M.; Dao, M.; Han, J.; Lim, C.-T.; Suresh, S. *MRS bulletin* **2010**, *35*, 382-388.
- (35) Jones, S. W.; Roberts, R. A.; Robbins, G. R.; Perry, J. L.; Kai, M. P.; Chen, K.; Bo, T.; Napier, M. E.; Ting, J. P. Y.; Desimone, J. M.; Bear, J. E. *J. Clin. Invest.* **2013**, *123*, 3061-3073.
- (36) J. Guzmán; M.T. Iglesias; E. Riande *Polymer* **1997**, *38*, 5227-5232.

CHAPTER 3: RBC MIMICS WITH HIGH LOADING OF HEMOGLOBIN

3.1 Introduction

The three major hurdles that impede application of HBOCs are: (1) renal toxicity¹ from hemoglobin dissociation; (2) vasoactivity² and (3) limited circulation time. While some of the first and second generations of RBC substitutes based on derivatized Hb could avoid renal toxicity, the circulation times were usually not long, and vasoactivity still remained because of interaction between nitric oxide and hemoglobin molecules.

Nitric oxide (NO) is a tiny molecule closely involved in many physiological functions, including but not limited to, blood vessel dilation,³ modulation of leukocyte adhesion⁴, and neurotransmission⁵. NO is produced in endothelial cells lining blood vessels, and normally targets the guanylate cyclase in the smooth muscle of blood vessels, leading to relaxation. In the vascular lumen, NO molecules have to traverse a significant distance across several diffusion barriers before reaching RBC: the 'RBC-free zone' adjacent to the vessel wall during blood flow, the unstirred plasma layer around an RBC, and the membrane of RBC. Therefore, reaction of Hb within RBCs is minimized and vasoconstriction prevented.^{6,7} Cell-free Hb, however, is not affected by intravascular flow due to its small size, and can therefore reach the site of NO production to consume NO, leading to vasoconstriction. This is why most of the early generations of RBC substitutes caused hypertension because the size of the carriers, either single or polymerized Hb, was too small. Therefore, increasing the hydrodynamic size of the carrier may help minimize vasoconstriction.

Encapsulating Hb within a carrier to mimic the cellular structure, can not only increase the hydrodynamic size, but also increase the diffusion barrier for NO, and is therefore being explored as a potent alternative to RBC substitutes based on Hb.

The idea to mimic the cellular structure using synthetic particles dates back to the 1950s, when Thomas Chang first described artificial RBCs with synthetic membranes encapsulating Hb and enzymes.⁸ This RBC mimic had an oxygen-dissociation curve comparable to that of true RBC; however, the size of the particles was in the range of 1 to 100 μm and could not be well regulated. The extreme difficulty in controlling particle size in these early days hampered further studies of these carriers because of possible blood flow issues in the capillaries. Biocompatibility was also a concern for these synthetic polymer membranes.

Recent years have witness increasing research on employing nanocarriers as RBC mimics by incorporating hemoglobin inside, probably as a result of the progress in nanotechnology. These new systems are considered as third-generation RBC substitutes. Liposomes (or vesicles) with sizes around 200 nm or smaller have been extensively used as RBC mimics ever since the 1980s because of technical advances in liposome formulation.^{9,10} Hb and other enzymes could be encapsulated within the lipid membranes, which better mimicked RBC surface than synthetic polymer membranes. These liposome-based HBOCs, termed as Hb-vesicles (HbVs), were found to remain longer in circulation than the earlier reported large artificial RBCs. Many groups have carried out research to further improve the circulation time of HbVs, and modification of surface was found to be effective when PEG-lipid was used to formulate the liposomes. Eishun Tsuchida's group had carried out many thorough studies on the tests of these HbVs, including biochemical characterization of hemoglobin inside the vesicles, and investigation of circulation, metabolism of the vesicles.¹¹⁻¹³

Alternative to HbVs, polymersomes^{14,15} and micelles¹⁶ have also been fabricated as RBC mimics. Similar to HbVs where lipids self-assembled to form liposomes, polymersomes and micelles were formed by the self-assembly of amphiphilic polymers. Palmer's group used diblock copolymer of PEG and poly(butadiene) (PBD) to formulate polymersomes. Polydisperse Hb-containing liposomes were extruded through polycarbonate membrane with pore size of either 100 or 200 nm, and monodisperse liposomes were formed. They also used diblock copolymer of PEG with either Poly(L-lactic acid) (PLA) or poly(ϵ -caprolactone) (PCL) to generate polymersomes because PLA and PCL are biodegradable. Jing's group used a triblock copolymer to produce micelles and encapsulated Hb inside. Rather than mixing Hb with the polymer to physically encapsulate Hb, they used click chemistry to covalently link Hb into one block of the polymer.¹⁵

Biodegradable polymers have also been used to form porous particles encapsulating Hb. Double-emulsion techniques were generally used in these studies to form nanoparticles with hollow interiors where Hb was loaded. The size of these particles is similar to that of HbVs and they could circulate in blood, though not long enough. To increase the biocompatibility, stability, and to extend circulation time of the nanoparticles, block copolymers of these thermoplastics with PEG were also used to fabricate nanoparticles with PEG on the surface.^{17,18} Although oxygen binding properties of the encapsulated Hb were not affected, it took longer times to saturate Hb within the particles and to deliver oxygen because of the shell thickness in the particles.

Hydrogels are promising biomaterials extensively explored in both tissue engineering and drug delivery because of their hydrophilicity and biocompatibility.¹⁹ Hydrogels with submicron sizes, named nanogels, have also been used as RBC mimics.^{20,21} In Palmer's work, acrylamide

monomers were polymerized within liposomes to form monodispersed nanogels after removal of the lipids. Once Hb was loaded into the liposomes with monomers, polymerization of the monomers could retain Hb inside probably due to chain transfer of monomer radicals to the protein. An obvious advantage of using nanogels as RBC mimics is the rapid gas exchanged rate through the particles because of the high water content, and this is also why our RBC mimics based on PRINT hydrogels are attractive as oxygen carriers.

To extend our mimicry of RBCs, the RBC-sized deformable particles discussed earlier were loaded with bovine hemoglobin. The low mesh density allowed Hb molecules to diffuse into the interior of the particles. Carboxyl group from CEA was used as a reacting handles to be conjugated with lysines of hemoglobin. Similar conjugation of Hb to poly(acrylic acid) had been carried out before and was found to cause no adverse effect on the structure and function of the protein.²²

3.2 Results and Discussion

3.2.1 Fabrication and characterization of blank particles

To maximize the potential of soft particles for long circulation times, we used only 0.05 wt% PEG4kDA in particle formulation as in **Table 2.2C**, resulting in hydrogels with a modulus of 6.5 kPa. Elastomeric fluoropolymer molds with patterned wells of 2 μm in diameter, 0.6 μm in height, were used to fabricate particles crosslinked with 0.05 wt% PEG4kDA. **Figure 3.1A** shows particles with polymerized Rhodamine dye confined in the mold. Once transferred out of the mold and suspended in PBS, the particles hydrated and swelled to 6.3 μm in diameter and 1.8 μm in height (**Figure 3.1B**), with ζ -potential of of -23 mV in 0.1X PBS.

3.2.2 Conjugation of Hb into the RBCM particles

To avoid the complications of allosteric effectors such as 2,3-diphosphoglycerate, which are required for the native operation of human Hb²³, we used bovine Hb. Bovine Hb only requires chloride ion for native operation,²⁴ which can be provided by buffers like PBS and is present in the blood. The conjugation of bovine Hb to the particles was carried out using EDC/sulfo-NHS chemistry to couple carboxylic acids in the particles to amines of the lysines of Hb²⁵ (**Figure 3.2**). In the first step, carboxyl groups in the particles were activated by EDC/sulfo-NHS in 0.1 M MES buffer with pH = 4.5. Then the activated particles were transferred to PBS (pH = 7.4) after removing excess EDC and sulfo-NHS. Bovine Hb was added to react with the amine-reactive NHS esters in the particles. A low concentration of particles (1 mg/mL) was employed during reaction to avoid inter-particle crosslinking by Hb to form larger aggregates. Sulfo-NHS was also used to maintain the negative charge of the particles, helping to avoid aggregation.

We confirmed that Hb had indeed reacted with the particles by directly observing the particles conjugated with dye-labeled Hb under a fluorescent microscope. Both Fluorescein and Rhodamine labeled bovine Hb were synthesized using the corresponding dye-NHS to react with Hb at a molar ratio of 15:1. Excess dye-NHS was used to ensure Hb molecules were labeled with several dye molecules per protein. There are 42 lysine amino groups on the surface of a single Hb molecule²⁶; therefore, the dye-labeled Hb possessed multiple unfunctionalized amine groups for use in coupling to the particles. After reacting with dye-free particles through the EDC/sulfo-NHS coupling method, the resulting particles obtained fluorescence arising from the dye-labeled Hb (**Figure 3.3A, B**).

To determine whether the dye-Hb was covalently conjugated to the RBCMs or more loosely associated via non-covalent interactions, we fabricated Fluorescein-labeled particles by copolymerizing Fluorescein-o-acrylate into the polymer network (**Figure 3.3C**). We incubated the particles with Rhodamine-tagged Hb (Rh-Hb) in PBS overnight, then pelleted and washed 3 times to remove unassociated protein. The washed particles had no fluorescence in the Rhodamine channel under a fluorescent microscope, indicating a lack of non-specific binding of Hb to the RBCMs. Considering that Hb acquires slightly negative charge at pH = 7.4 (pI = 6.8)²⁷, a lack of electrostatically driven association with negatively charged particles is reasonable. In contrast, when the particles were first activated by EDC/sulfo-NHS and then incubated with Rh-Hb followed by washing, they displayed red fluorescence from the covalently conjugated Rh-Hb (**Figure 3.3D**). The red fluorescence from Rhodamine overlapped perfectly with the green fluorescence from Fluorescein (**Figure 3.3E**). The covalent conjugation of Hb into the RBCM particles was also confirmed by FTIR spectroscopy (**Figure 3.3F**). The peaks at 1650 and 1550 cm^{-1} corresponding to the amide I and amide II region of hemoglobin²⁸ were also present in the spectrum of the Hb-RBCM particles, which were thoroughly washed to remove unassociated Hb. The peak at 1579 cm^{-1} , characteristic of the carboxylate moiety that was consumed by the conjugation chemistry²⁹, was attenuated in the Hb-RBCM particle sample, indicating a decrease in the prevalence of this functionality as a result of conjugation to Hb. Combining the spectroscopic result from FTIR and the microscopic observations, we concluded that Hb was covalently conjugated to the hydrogel matrix of RBCM particles.

Besides Hb, other proteins bearing lysine groups on the surface could possibly also be conjugated into the particles. We used Alexa Fluor® 488 (AF488) labeled bovine serum albumin (BSA) as a representative protein to demonstrate this. By incubating AF488-BSA with activated

dyeless particles, the resulting particles gained fluorescence from AF488 (**Figure 3.4**), indicating covalent conjugation of BSA to the particles.

3.2.3 Confocal studies of the Hb-RBCM particles

While the free volume fraction was very high in the particles due to the low mesh density and high water content, we wanted to determine if the protein was distributed throughout the bulk of the particles or limited to the surface. For these experiments, we made larger (18 μm tall, 18 μm diameter cylinders) hydrogel particles with identical composition to facilitate confocal imaging analysis. These large model particles, which were fabricated without the inclusion of a fluorescent dye, were allowed to react with Fluorescein-Hb under the same conditions as discussed above. Confocal laser scanning microscopy (CLSM) was used to scan the particles at various cross sections due to the narrow depth of focus of this technique. We randomly selected a representative particle and collected a stack of scans in the xy plane while varying the focal depth in the z direction to cover the entire particle. All of the xy scans obtained showed fluorescence associated with the covalent attachment of fluorescein-Hb to the particle matrix, indicating that Hb had been distributed throughout the particle interior. A reconstructed 3D view of the model particles is shown in **Figure 3.5**, with orthogonal cross-section views of the representative particle. Although the particles used for the confocal experiments were larger than the $\sim 6 \mu\text{m}$ RBCMs, they were polymerized under the same condition with identical compositions and it is reasonable assumption that the mesh size, which depends on crosslinker density, in both sets of particles were similar.

3.2.4 Hb loading efficiency of RBCM particles

By varying the initial Hb concentration for the conjugation, the loading ratio of Hb into the RBCM particles could be adjusted. We define the weight ratio of conjugated Hb to the

polymer network of particle as the loading ratio, R . The maximum theoretical value of R would be greater than 60 for the case of every carboxyl group in the particles being conjugated to one Hb molecule. While steric effects make saturation unlikely, we observed that very high loading resulted in the undesirable effects of particle aggregation and sedimentation. Loading ratios as high as 5.1 were obtained without any observable aggregation or sedimentation effects. The loading ratio was changed by varying the amount of Hb added to a fixed amount of carboxyl-activated particles (1mg/ml; **Figure 3.6A**). The amount of Hb loaded into the particles was determined by measuring depletion of free protein in the supernatant solution by UV-vis spectroscopy through adaption of the standard cyanometHb method²¹. The encapsulation efficiency for these particles was defined as the amount of the Hb loaded into particles divided by the overall starting amount of Hb. Generally, incubation of particles with higher concentrations of Hb led to increased R and decreased encapsulation efficiency. The highest stable loading achieved, with $R = 5.1$, resulted in an encapsulation efficiency reduced to 50%. Although the encapsulation efficiency was not very high for higher Hb loadings, unbound Hb could be collected from the particles and reused for conjugation. The size of the particles decreased slightly with increased Hb loading (**Figure 3.6B**).

High loading of Hb into oxygen carriers is desirable for blood substitutes, which would require large doses administered with high concentration of Hb to have oxygen carrying capacity similar to that of blood. The high Hb concentration in normal blood (14 g/dL) has been approached by some HOBCs (5~10 g/dL¹). The weight ratio of Hb to the lipids (as in liposomes) or polymers (in polymersomes) used to constitute those carriers, similar to R defined above, has varied widely in different cases, from 0.3 to 9.36.³⁰ The values of R here arose from RBCM particles that were composed of only 10% of a monomer capable of conjugation to Hb (CEA). It

is possible that even higher loading ratios could be obtained when the amount of CEA in the particles is increased.

3.2.5 CD and UV-vis spectroscopic study

Retention of the structure and activity of the encapsulated Hb is a crucial consideration for the application of this protein towards carrying oxygen. The secondary structure of proteins is essential to their function; retention of this structure can be used to infer protein activity³¹. Protein secondary structure can be monitored by far UV-CD spectroscopy³². We measured the UV-CD spectra, in the range of 185 to 260 nm, for Hb conjugated to RBCM particles, a mixture of particles and free Hb, and unmodified free Hb in identical buffer conditions to look for structural changes in the protein (**Figure 3.7A**).

The strong maximum at 194 nm and double minima at 208 and 222 nm in the CD spectrum of free Hb (**Figure 3.7A**), are characteristics of α -helix²². The CD spectrum of the suspension of particles mixed with free Hb (Hb+particles) was very similar to the spectrum of free Hb, with the peak at 194 nm slightly decreased in intensity. For Hb conjugated to the particles (Hb-c-particles), the peak positions were the same, with slightly decreased intensity at 208 nm, and dropped larger dip in intensity at 194 nm. When the sample of Hb-c-particles was half diluted and subjected to CD study, the obtained spectrum also crossed over the same point (**Figure 3.7A**). So the percentage helicity of Hb in the particles could be assessed by comparing the ellipticity at 222 nm³³. As the minimum at 222 nm for Hb-c-particles only shows minor different from that of free Hb, we can conclude that the percentage helicity of Hb conjugated to particles was close to native Hb, indicating negligible change in the secondary structure of Hb-c-particles.

Although it has been reported that secondary structure of Hb could be changed when interacting with nanoparticles due to hydrophobic interactions or changes in ionic strength near the particles^{28,34}, we do not anticipate this effect in our case as the microgels are very soft and hydrophilic, and the large pores in the particles allowed the ions of PBS to diffuse into the interiors fairly easily to maintain uniform ionic strength. In a recent study where bovine Hb was conjugated to high molecular weight poly(acrylic acid) using similar coupling chemistry, the authors observed the secondary structure of Hb to be unchanged²².

The Soret CD of Hb, arising from the interaction between π - π^* transition of the heme groups and the surrounding aromatic amino acids, is greatly influenced by the orientation and position of the aromatic amino acid residues^{35,36}. Changes in the Soret CD of Hb can be an indication of differences in the heme environment as well as the electronic state of the heme. The Soret CD of Hb, Hb+particles, and Hb-c-particles were recorded in the wavelength range of 350 to 450 nm in **Figure 3.7B**. Comparing the three spectra in **Figure 3.7B**, the peak positions at 416 nm remained unchanged, implying that the heme environment was well preserved in the conjugated Hb compared to the starting Hb. The reduction in the peak intensity was most likely caused by light scattering³⁷. The electronic state of heme was in the oxidized form for all three samples as the starting Hb had mostly been automatically oxidized into metHb, which is unable to bind oxygen.

To obtain Hb-RBCM particles capable of binding oxygen with low metHb, the suspension of Hb-RBCM particles was added with reducing agents. Sodium dithionite (10 molar equivalents to total Hb concentration) was first added to reduce metHb back to deoxyHb, and excess dithionite was removed by spinning down the particles and decanting for 3 times. Then ascorbic acid (10 mM) was added to the suspension for long term reduction. Sodium dithionite is

very efficient in reducing metHb back to deoxyHb; however, excess dithionite may be oxidized by residual oxygen in solution to generate reactive oxygen species (ROS) that in return would accelerate the oxidation of Hb³⁸. **Figure 3.7C** shows the UV-vis spectra of Hb-particle ($R = 2.8$) suspension. The as prepared particle suspension showed a Soret peak at 405 nm, characteristic of metHb. After reducing iron(III) back to iron(II) by dithionite, the Soret peak moved to 430 nm, characteristic of deoxyHb³⁹. Carbon monoxide could bind to deoxyHb in the particles to shift the Soret peak to 419 nm¹⁶. To the carbonized Hb-particle suspension, air was bubbled for 20 min under light and the spectrum of the resulting suspension showed a Soret peak at 412 nm, characteristic of oxyhemoglobin, along with two feature peaks at 542, 576 nm⁴⁰.

An indirect method was used to estimate the metHb level in the particles. Generally, the difference in absorbance at 540 nm of a hemoglobin-containing solution before and after addition of KCN can be used to calculate the metHb concentration using UV-vis spectroscopy²¹. Since the absorbance at 540 nm is much lower than that at the Soret peak, accurate measurement would require higher concentration of Hb (therefore higher particle concentration) than that used for the UV-vis spectra in **Figure 3.7C**. However, higher concentration of particles would cause more light scattering that interfered with the absorbance measurement. To circumvent this problem, we polymerized HP3A with 10 wt% CEA and 1 wt% initiator, but without crosslinker to make un-crosslinked polymer that could represent the formulation of the particles. The resulting polymer ($M_n = 41$ kDa, $M_w = 233$ kDa) was conjugated with Hb to generate poly(HP3A-co-CEA)-Hb conjugate, in which the loading ratio was 0.8 (high loading ratio would result in polymer precipitation). The poly(HP3A-co-CEA)-Hb conjugate was reduced by sodium dithionite, and excess dithionite was removed. Ascorbic acid (10 mM) was added to the resulting solution with $[Hb] = 5$ mg/mL. For as prepared, un-reduced Hb-polymer solution, the metHb

level is 75 %, similar to the metHb level (69 %) in the stock solution of Hb. The metHb level immediately after the reduction dropped to 1.4 %. The solution was kept under aerobic condition, and the metHb formation over time was measured over 1 month as summarized in **Figure 3.7D**. After 1 month, the metHb level rose to 25 %, and within 10 days the metHb did not exceed 10 %.

3.2.6 Oxygen dissociation and NO oxidation kinetics

We used a stopped-flow spectroscopy to study the kinetics of oxygen dissociation and NO induced oxidation of oxyHb following established methods.⁴¹⁻⁴³ Both free Hb and Hb-RBCM were saturated with oxygen before measurement. By quickly mixing 0.5 μM free Hb (thus 2 μM heme) or Hb-RBCM ($R = 0.9$, with the same Hb concentration), with 0.9 mM sodium dithionite, the absorbance change at 436 nm was recorded to monitor the decrease of oxyHb. Since light scattering from particles also contributed to absorbance, the absorbance change was normalized to plot the change versus time, as shown in **Figure 3.8A**. The oxygen dissociation rate for Hb in Hb-RBCM was almost 2 fold slower than that of free Hb.

NO induced oxidation of oxyHb was studied by measuring the absorbance change at 419 nm after quickly mixing 0.5 μM free Hb or Hb-RBCM with 14 μM NO solution. The absorbance change was normalized to plot the change versus time, as shown in **Figure 3.8B**. At the concentrations used, NO was in excess so that the kinetics could be regarded as pseudo-first-order. By fitting the curves, the calculated rate constants were 18 and 7.4 $\mu\text{M}^{-1} \cdot \text{s}^{-1}$ for free Hb and Hb-RBCM, respectively. The former agrees very well with literature value around 20 $\mu\text{M}^{-1} \cdot \text{s}^{-1}$ [65], indicating high measurement fidelity. The rate constant of Hb-RBCM is 2.5-fold less than that of free Hb, probably from slowed diffusion secondary to the gel structure of the RBCM.

3.2.7 Mechanical and fluidic properties of Hb-RBCM particles

The RBCM particles were fabricated from a low modulus material to take advantage of the increased circulation times seen with such highly deformable RBC-like microgels⁴⁴. However, it stands to reason that the cargo loaded into these gels (Hb) could increase the modulus of the resultant gels. To test the effect of loading these gels with Hb on the elastic modulus, we incubated bulk polymer samples with Hb and carried out the conjugation under identical conditions used for Hb conjugation to particles. At low loading of Hb, this strategy seemed to be effective; the modulus of bulk samples with loading ratio of 0.38 increased somewhat compared to Hb-free polymer gel, with $E = 9.1$ kPa and 6.5 kPa, respectively. However, higher loadings of Hb could not be obtained, likely as a result of the vastly reduced surface area to volume ratio in the bulk samples compared to the microparticles. The diffusion-limited conjugation reaction was likely much slower in the bulk samples, leading to hydrolysis of the reactive NHS ester before reaction could proceed fully.

To directly evaluate the deformability of the Hb loaded particles, the same microfluidic device as in **Figure 2.3** was used. Dilute suspensions of particles were flowed through the devices via a syringe pump at a constant rate of 60 $\mu\text{L}/\text{min}$. The Rhodamine dye labeled particles could be tracked as they traveled through the channel of the microfluidic device using an inverted fluorescent microscope focused on restrictions close to the outlet of the channel. We found that moderate ($R \leq 2.8$) loading of Hb had no noticeable effect on the ability of the particles to deform to elongated shape and navigate the pores (see image sequence in **Figure 3.9A**). The shape change of the particles was reversible as after coming out of the pores they could return to the original disc shape. However, when the R increased to 5.1, the majority of the stiffer particles became lodged in the entrances to the pores (**Figure 3.9B**), although a minor

fraction of the particles could still pass through. Therefore, with a loading ratio of Hb as high as 2.8, the RBCM particles were still very deformable.

A high concentration of Hb in a HBOC fluid is necessary to fulfill oxygen transport targets. We could concentrate the Hb-RBCM particles by centrifugation in order to increase the overall Hb concentration. However, a fluid packed with very high density of Hb-RBCM particles may become very viscous, and hence is inappropriate for transfusion. To mimic the hematocrit (i.e., packed cell volume fraction) of blood (40-45%), we spun down particles and decanted to obtain a pellet with a volume fraction around 40%. While the fluid with particles whose $R = 2.8$ became quite viscous at this packed particle volume fraction (PPVF), particles with $R = 1.3$ could flow easily at the same PPVF with the overall Hb concentration in the suspension to be 5.2 g/dL. The viscosity of this fluid was evaluated using a rheometer that could control the shear rate and measure the corresponding shear stress and viscosity. As a control, collected mouse blood (in heparinized tube to avoid clotting) was also subjected to the rheometer. By ramping the shear rate from 0.1 to 1,000 1/s, covering the shear rates found in blood flow⁴⁵, the rheological properties of the Hb-particle suspension and mouse blood were compared as in **Figure 3.9C, D**. As can be seen, over different shear rate ranges, the shear stress and viscosity of the Hb-RBCM fluid was mostly lower than the blood from two mice. The Hb-RBCM fluid displayed rapid decrease in viscosity leading to a local maximum in the stress, which may indicate phase separation and formation of shear band^{46,47}. This behavior will be investigated in future work.

To test if the particles can survive at high shear rate, the same suspension ($R=1.3$, [Hb] = 5.2 g/dL) was sheared on the rheometer at a constant rate of 1,000 1/s for 10 min, and the resulting suspension was observed under optical microscopy to check the integrity of the particles. The particles were indeed intact after shear as shown in **Figure 3.9E**. When the

suspension was spun down, the supernatant was completely colorless, indicating no release of dye or Hb because of particle breakdown.

3.2.8 Cytotoxicity of the RBCM particles

Human vascular endothelial cells (HUVEC) and HeLa cells were chosen as in vitro models to assess the cytotoxicity of the RBCM particles. To investigate the possible effect of CEA on cytotoxicity, RBCM particles with even higher content of CEA (20 and 50 wt%) were also fabricated following similar procedure for the 10 wt% CEA particles, and were dosed to the cells. Hb-RBCM particles ($R=2.8$) with and without reduction of metHb were also dosed to both cell lines. To ensure similar numbers of Hb-particles dosed to the cells, the concentration of the Hb-particle suspensions were calculated based on the weight of polymers only, excluding Hb. After incubation the cells with different particles for 72 h, the cell viability was quantified by MTS assay. The results in **Figure 3.10** show that, for both cell lines, unloaded particles had minimal cytotoxicity, although with more CEA the cell viability was slightly lower. Unreduced Hb-RBCM particles showed cytotoxicity to both cell lines, probably because of the oxidative stress from metHb in the particles⁴⁸. For reduced Hb-RBCM particles, in the lower dose range, there is little cytotoxicity, while at higher dose, the viability of the cells decreased with increasing particle concentration, possibly due to higher metHb formed in the cell culture. Therefore, for our goal to increase the loading of Hb into RBCM particles by charging particles with more CEA, the biocompatibility issue of the resulting particles would rely less on CEA, but more on the metHb level in the particles. We already started to investigate incorporating ROS scavenging enzymes to solve this issue for future application.

3.2.9 Conclusions and Future Work

Here we have demonstrated the synthesis of RBC-like hydrogel microparticles that retain their deformability with covalently bound Hb, which retained native secondary structure, homogeneously distributed throughout the particle matrix. The particles could be loaded with over 70 wt% Hb (loading ratio $R = 2.8$) and the metHb level under aerobic condition could be controlled to be less than 10 % within 10 days. We demonstrated that Hb in the particles could bind oxygen when carbonized Hb in the particles was purged with air.

Given that hemoglobin, a 64 kDa protein (~8 nm in hydrodynamic diameter), uniformly distributes throughout the lightly crosslinked RBCM particles, we can infer a large pore size for these particles. Therefore, reducing agents like ascorbic acid may only work when the particle fluid is stored, while not work effectively after injection of the fluid. Instead, larger enzymes which act on Hb found in RBCs to regulate metHb level, such as superoxide dismutase (SOD) and catalase (CAT) may be conjugated to the particles through the same conjugation chemistry, but at much lower concentration. Chang, et al. polymerized SOD, CAT with Hb to obtain polyHb-SOD-CAT using glutaraldehyde, which prevented problems related to oxidation of Hb⁴⁹. Inclusion of low amount of these enzymes into the particles may be efficacious in scavenging ROS, resulting in low level of metHb over a long time even under aerobic conditions.

While added Hb could act as crosslinker to shrink the particles and increase the modulus, this effect was not observed to be dramatic except for cases with very high loading of Hb. This may be due to inclusion of Hb without the formation of crosslinks because of a low density of reactive sites on the RBCM particle. Hb-RBCM particles ($R = 1.3$) could also survive high shear rate (up to 1,000 1/s) as the particle remained intact after the suspension with 5.2 g/dL Hb was sheared for 10 min.

The method of protein loading reported here should be general with respect to other proteins of similar or smaller size to Hb due to the ubiquitous presence of the lysine residues essential to the conjugation reaction, as BSA was also successfully loaded into the particles. Advantageously, the loading of a protein to the RBCM particle matrix were both carried out in aqueous conditions, avoiding potential solvent based denaturation of protein⁵⁰. For example, butyrylcholinesterase, a native protein that can degrade nerve agents, may be conjugated to the particles to synthesize nerve agent scavenger that may take effect over extend times.

3.3 Experimental Section

3.3.1 Materials

Acryloyl chloride, triethylene glycol, CEA, 1-hydroxycyclohexyl phenyl ketone (HCPK), fluorescein-o-acrylate, bovine Hb, Dulbecco's phosphate buffer saline (PBS), potassium cyanide (KCN) and potassium ferricyanide ($K_3Fe(CN)_6$), sodium dithionite, ascorbic acid, carbon monoxide, were all received from Sigma-Aldrich. Polyethylene glycol (MW=4,000 g/mol) diacrylate (PEG4kDA), methacryloxyethylthiocarbamoyl rhodamine B (PolyFluor® 570) were from Polysciences, Inc. Sulfo-N-Hydroxysuccinimide (NHS), 1-ethyl-3-(3-dimethylaminopropyl) carbodiimide hydrochloride (EDC), Fluorescein-NHS, Rhodamine-NHS, AF488-BSA and 2-(N-morpholino) ethanesulfonic acid (MES) buffer were all received from Thermo Scientific. Perfluoropolyether molds were received from Liquidia Technologies. Sylgard® 184 for making microfluidic devices was from Dow Corning. DI water was used and all the other organic solvents were received from Fisher Scientific.

3.3.2 Synthesis of dye-labeled Hb

To 1 mL Hb solution (20 mg/mL) in borate buffer (pH=8.5), 220 μ L DMF solution of fluorescein-NHS or rhodamine-NHS (10 mg/mL) was added and allowed to react at RT for 1 h.

The resulting solution was transferred to Slide-A-Lyzer dialysis units (Thermo Scientific) with a cut-off size of 20 kDa. The dye-labeled Hb solution was dialyzed against 1L DI water for 12 h (water changed twice) to completely remove the excess dye-NHS. The purified dye-Hb solution was collected into an eppendorf tube covered by aluminum foil and stored at 4 °C before use.

3.3.3 Synthesis of poly(HP3A-co-CEA)

A mixture of HP3A (899 mg) and CEA (100 mg) with 1% HCPK (1 mg) was purged with nitrogen for 15 min. Deoxygenated methanol (6 mL) was added to the monomer mixture to obtain a homogenous solution. The solution was irradiated by UV light ($\lambda=365$ nm, power =20 mW/cm²) for 8 min under nitrogen purge. After curing, water was added to the polymer solution and dialyzed using a Slide-A-Lyzer dialysis unit with a cut-off size of 3 kDa. The dialyzed polymer solution was lyophilized to weigh the dry sample. About 5 mg of the dry polymer was dissolved in 1 mL filtered DMF and subjected to GPC (Waters) analysis on the molecular weight using PEO standard.

3.3.4 Modulus Testing

Refer to 2.4.3.

3.3.5 Particle fabrication and characterization

Refer to 2.4.4 and 2.4.5.

3.3.6 Protein Conjugation to particles and polymers

In a typical reaction of Hb to particles: to 0.4 mg particles suspended in 0.5 mL MES buffer (pH = 4.5) was added with 100 μ L EDC solution in MES (0.7 mg/mL) and 100 μ L sulfo-NHS solution in MES (2 mg/mL). The resulting suspension was allowed to shake at RT for 20 min. Then the particles were spun down at 10,000 g centrifugation and washed for 3 times with PBS to remove excess EDC, sulfo-NHS. The particles were resuspended into 200 μ L PBS; to

this suspension, different amounts of Hb (from 0.2 mg to 4 mg) were added and the final volume of reaction was remained at 0.4 mL. The conjugation continued for 12 h at 4 °C in a shaker (Eppendorf) at 1,000 rpm. After the reaction, the resulting Hb-particles were washed 3 times in PBS and resuspended into 0.4 mL PBS for future characterizations. Dye-labeled Hb and AF488-BSA were conjugated to the particles following a similar protocol. To calculate the loading ratio of BSA, a Coomassie assay was used to measure the depletion of BSA in the solution after conjugation with the particles.

To conjugate Hb to poly(HP3A-co-CEA), the polymer was dissolved in MES buffer and added with EDC, sulfo-NHS similarly to the above procedure for particles. After activation for 20 min at RT, the solution was added with PBS and filtered using a centrifugal filtering device (cut-off size = 3k Da; Millipore) to quickly remove excess EDC/NHS, and increase the pH to 7.4. To the resulting solution containing 1 mg/mL polymer, Hb (2 mg/mL) was added and the reaction continued for 6 h at 4 °C. After the reaction, the solution was purified using a centrifugal filtering device with cut-off size of 100 kDa to remove un-conjugated Hb.

3.3.7 CSLM study of model particles

CLSM images were collected with an Olympus FV 500 microscope with filters optimized for fluorescein dye in the RBCMs. Images were taken using a 60X oil objective lens. Confocal sections were collected in the image scan x-y-z mode. A single particle that was vertically standing on the slide was chosen. By focusing both the bottom and top of that particle, the starting and ending focus positions were selected with an increment of 0.414 μm . The scanning of the sections generated a series of images, which were reconstructed into a 3D view using the software MetaMorph®.

3.3.8 Reduction of metHb and Hb binding to CO and oxygen

To Hb-particle suspension in PBS, the particles were spun down and resuspended in deoxygenated PBS (deoxy-PBS: PBS purged with Argon for 30 min). Sodium dithionite (10 equivalent molar ratio to Hb) dissolved in deoxy-PBS was added to the particle suspension, and the reduction continued at RT for 5 min. Excess dithionite was removed by spinning down particles and washing with deoxy-PBS 3 times, followed by addition of ascorbic acid (10 mM). CO was purged to reduced Hb-particle suspension to convert deoxyHb to CO-Hb with the suspension in a tube covered by aluminum foil. When CO-Hb-particle suspension was purged with air for 20 min under light, oxygen could replace CO to bind Hb.

3.3.9 UV-vis spectroscopy of Hb and Hb-RBCM particles

The UV-vis spectra were measured on a Cary-50 UV-vis spectrometer in the wavelength range of 200 nm to 800 nm. The scan rate was 300 nm/min with 0.5 nm interval. PBS solution was used as the background and subtracted. For the determination of total Hb concentration in solution, a standard curve of cyanmethemoglobin was obtained by measuring the absorbance of the cyanmetHb solution at 540 nm with concentrations of 0.05, 0.1, 0.2, 0.4 and 0.8 mg/mL. The metHb level was measured by adding 15 μ L KCN (10 wt% solution) to the Hb containing solutions/suspensions (1 mL) and the difference in the absorbance at 540 nm before and after addition of KCN was used to calculate the metHb concentration²¹. To test the metHb formation over time, the reduced Hb-polymer solution was dispensed as 1 mL aliquots into multiple Falcon tubes (50 mL) with the top of solution filled with air in the tubes. The concentration of the particles used for the UV-vis spectroscopy was only 0.05 mg/mL, with Hb concentration of 0.14 mg/mL to ensure absorbance lower than 1. With the low concentration used, light scattering became minimal.

3.3.10 Circular Dichroism (CD) spectroscopy studies

The CD spectra of unmodified Hb, Hb physically mixed with RBCM particles and Hb-RBCM particles were recorded using a Chirascan Plus CD spectrometer (Applied Photophysics, Inc.) at 23 °C. Each sample was diluted in 10 mM K₂HPO₄ buffer (pH=7.2; K₂HPO₄ buffer was used to avoid the absorbance below 200 nm associated with the chloride in PBS), and the buffer spectrum was subtracted. The step resolution was kept at 0.5 nm/data point, and the bandwidth and sensitivity were 1 nm and 20 millidegrees respectively. Particles lightly loaded with Hb (R=0.4) were used for the CD study because higher Hb loading resulted in increased light scattering that interfered with the measurement⁵¹. For the determination of secondary structure change, the samples were diluted to contain 0.16 mg/mL Hb, and particle concentration maintained at 0.4 mg/mL where applicable. The samples were scanned from 190 to 260 nm, the scan speed was maintained at 50 nm/min. To record the Soret CD bands, each sample contained 1mg/mL Hb and scanned from 350 to 450 nm at a scan speed of 50 nm/min, a path length of 1 mm, and eight accumulations. The higher concentration of Hb (1 mg/mL) was used for the Soret CD spectra because the absorbance of Hb in this wavelength range is much weaker than that in far UV.

3.3.11 Stopped-Flow Spectroscopy

A stopped-flow, rapid mixing instrument (Applied Photophysics) was used to study the kinetics of oxygen dissociation and NO caused oxidation of oxyHb. Both free Hb and Hb-RBCMs were saturated with oxygen before measurement by purging air into the solution or suspension for 0.5 h. NO stock solution with 2 mM concentration was received from Shoenfisch's group and stored in tightly sealed tube in 4 °C, and was used within 2 days.

Dilutions of NO solution were prepared using deoxygenated PBS by purging PBS with Argon for 0.5 h.

For oxygen dissociation study, by quickly mixing 0.5 μM free Hb (thus 2 μM heme) or Hb-RBCMs ($R=0.9$) with the same Hb concentration, with 0.9 mM sodium dithionite, the absorbance change at 436 nm was recorded to monitor the decrease of oxyHb. Since light scattering from particles also contributed to absorbance, the absorbance change was normalized to plot the change versus time. NO caused oxidation of oxyHb was studied by measuring the absorbance change at 419 nm after quickly mixing 0.5 μM free Hb or Hb-RBCMs with 14 μM NO solution. Excess NO was used to ensure the kinetics followed pseudo-first-order. The absorbance change was normalized to plot the change versus time.

3.3.12 Microfluidics

Refer to 2.4.7 for device fabrication. Dilute solutions of Hb-particles (1–5 $\mu\text{g}/\text{mL}$ in PBS with 0.1% PVOH) were pumped through the channel and observed with a fluorescence microscope (Olympus IX81). Videos were taken with a CCD camera (Hamamatsu). Particle stretching was analyzed with ImageJ (NIH) software.

3.3.13 Rheological measurement

A rotational rheometer (ARES-G2, TA instrument) was used for the measurement of viscosity at different shear rates. To obtain fluid packed with more particles, the particle suspension was spun down and decanted to adjust the volume fraction of the pellet to the overall fluid volume. Briefly, for a 10 mL suspension containing 10 mg of particles (only considering the weight of the polymer), the volume of the pellet after centrifugation at 8,000 g for 8 min was around 100 μL . The volume of PBS buffer on top of the pellet could be decanted to be 150 μL , resulting in a packed particle volume fraction of 40%. The final hemoglobin concentration

$$[\text{Hb}] = \frac{10 \text{ mg} \times R}{250 \mu\text{L}} = 40 \cdot R \frac{\text{mg}}{\text{mL}} = 4R \text{ g/dL} \quad (R: \text{loading Ratio})$$

Two hundred microliters of blood or particle suspension ([Hb]=5.2 g/dL; R=1.3) were loaded onto the rheometer stage. The stainless steel plate had a diameter of 40 mm with a cone angle of 0.0399 rad. The samples were sheared from 0.1 to 1,000 1/s within 3 min while the temperature was maintained at 25 °C. The mouse blood samples were collected from Balb/c mice into heparinized eppendorf tubes kept at 4 °C and tested within 24 h.

3.3.14 Cytotoxicity study

Human umbilical vein endothelial cell (HUVEC) or HeLa cells were seeded in 200 μL of media (HuMEC containing HuMEC supplement and bovine pituitary extract or MEM containing Earle's salts and both supplemented with 10% fetal bovine serum) at a density of 5,000 cells per cm^2 into a 96-well microtiter plate. Cells were allowed to adhere for 24 h and subsequently incubated with RBCM particles at concentrations ranging from 200 $\mu\text{g/mL}$ to 1.56 $\mu\text{g/mL}$ for 72 h at 37 °C in a humidified 5% CO_2 atmosphere. After the incubation period, all medium/particles were aspirated off cells. The ATP-luciferase assay requires 100 μL fresh medium, which was added back to cells, followed by the addition of 100 μL CellTiter-Glo® Luminescent Cell Viability Assay reagent (Promega). Plates were placed on a microplate shaker for 2 min, then incubated at room temperature for 10 min to stabilize luminescent signal. The luminescent signal was recorded on a SpectraMax M5 plate reader (Molecular Dynamics). The MTS [(3-(4,5-dimethylthiazol-2-yl)-5-(3-carboxy-methoxyphenyl)-2-(4-sulfophenyl)-2H-tetrazolium)] viability assay utilizes 20 μL of CellTiter 96® AQueous One Solution Reagent (Promega) into each well of the 96-well assay plate containing the samples in 100 μL of culture medium. Plates were incubated at 37 °C for 1–4 h in a humidified, 5% CO_2 atmosphere. The absorbance at 490 nm was recorded using a SpectraMax M5 plate reader (Molecular Dynamics).

The viability of the cells exposed to the RBCM particles was expressed as a percentage of the viability of cells grown in the absence of particles.

3.4 Figures

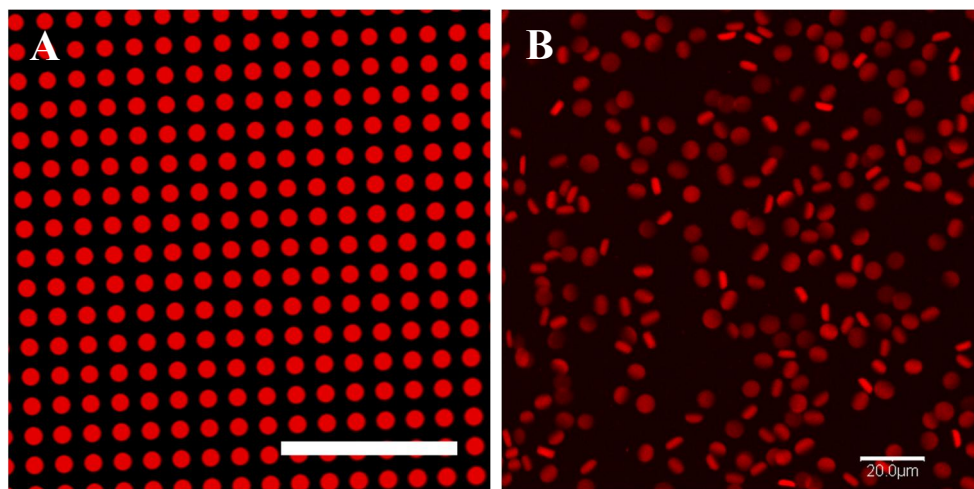


Figure 3.1 Fluorescent micrograph of polymerized particles (fabricated from 88.85 wt% HP3A, 10 wt% CEA, 0.05 wt% PEG4kDA, 1 wt% photo-initiator, 0.1 wt% PolyFluor 570) in the mold (A), and fully hydrated particles free of the mold, suspended in PBS (B). Scale bars=20 μm .



Figure 3.2 Scheme for the conjugation chemistry between carboxyls of particles and lysines of Hb.

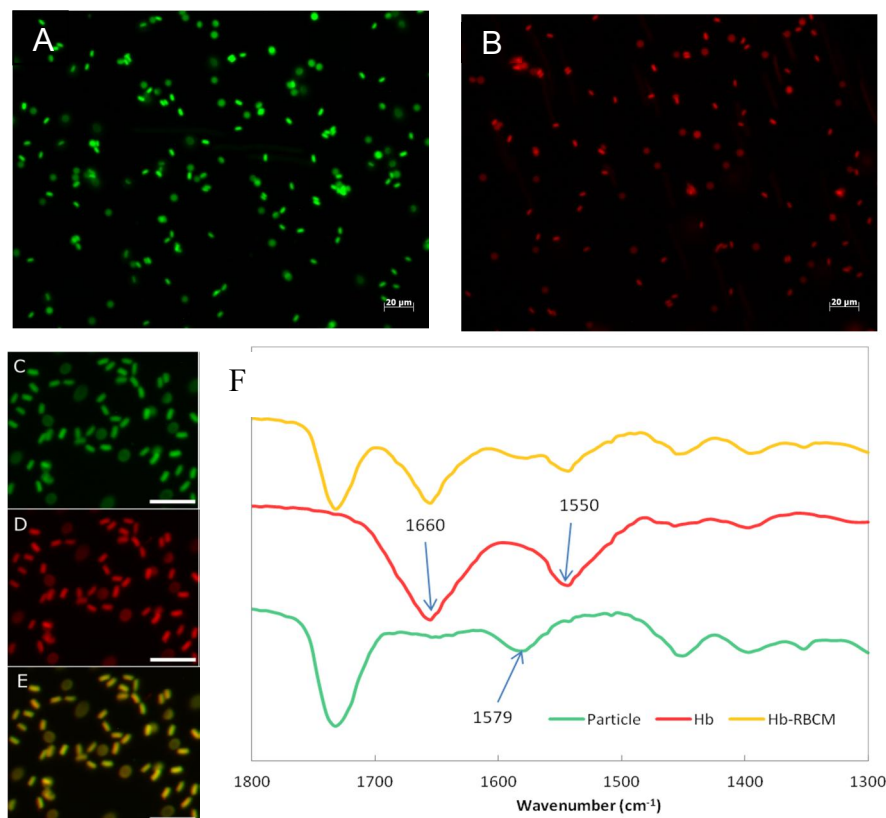


Figure 3.3 Conjugation of Hb to RBCM particles. Dyeless particles reacted with Fluorescein-tagged Hb (A) and Rhodamine tagged Hb (B). Fluorescein-labeled RBCM particles reacted with Rhodamine-tagged Hb were observed in the (D) Fluorescein, (E) Rhodamine channels of fluorescence; (F) overlay of D and E. Scale bars=20 μm. (G) FTIR spectra of blank particles, Hb, and Hb-RBCM conjugate. The arrow pointing to 1579 cm^{-1} denotes the peak of carboxylate in the particles; the two arrows pointing to 1550 and 1660 cm^{-1} denote the amide groups in Hb.

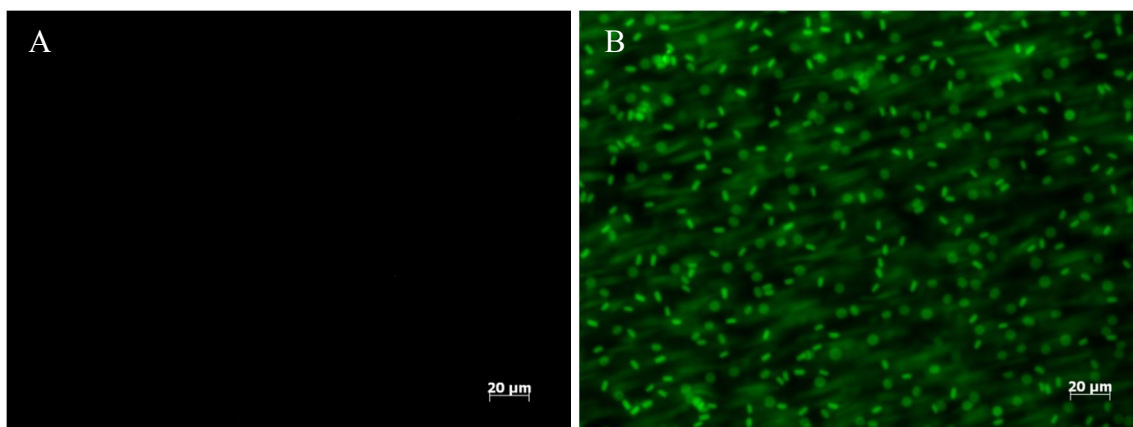


Figure 3.4 Dyeless particles (A) conjugated with AF488-BSA (B). The green background in B is actually stream of particles flowing during the capturing of the image. For determination of loading ratio, dyeless BSA was conjugated to particles with a feeding ratio of 1 mg particle : 2 mg BSA, and we found that 0.4 mg BSA (using Coomassie's assay and plate reader to determine the difference before and after reaction) became conjugated after reaction for 12h.

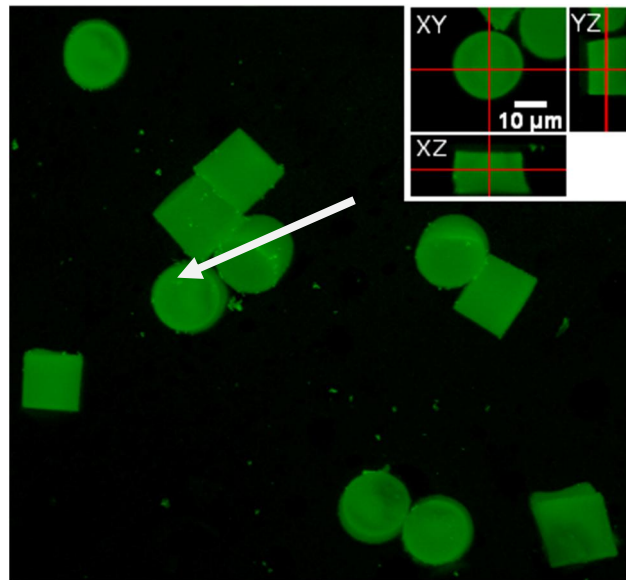


Figure 3.5 A 3D reconstruction view of fluorescein-Hb-conjugated particles observed using xyz scan mode of the confocal laser scanning microscope, with the inset showing orthogonal cross-section views of a representative particle (indicated by the white arrow). The fluorescent protein seems to be homogenously distributed throughout the hydrogel particle.

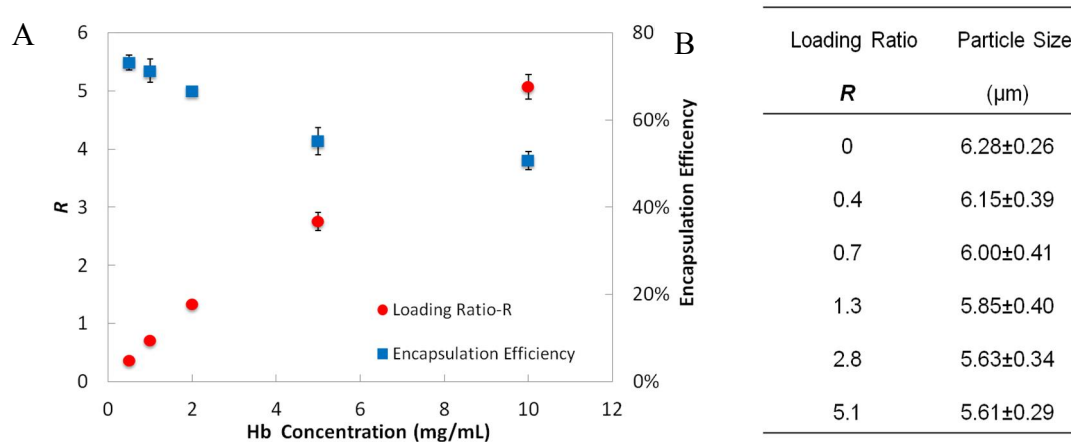


Figure 3.6 (A) Loading ratio R and the encapsulation efficiency of Hb into the RBCM particles with respect to different starting concentration of Hb for the conjugation while the particle concentration was maintained at 1mg/mL ($n = 3$). (B) RBCM particle size with respect to different loadings of Hb; the size of the particles were measured by analyzing fluorescent micrographs of the particles ($n = 50$) which had polymerized Rhodamine dye inside.

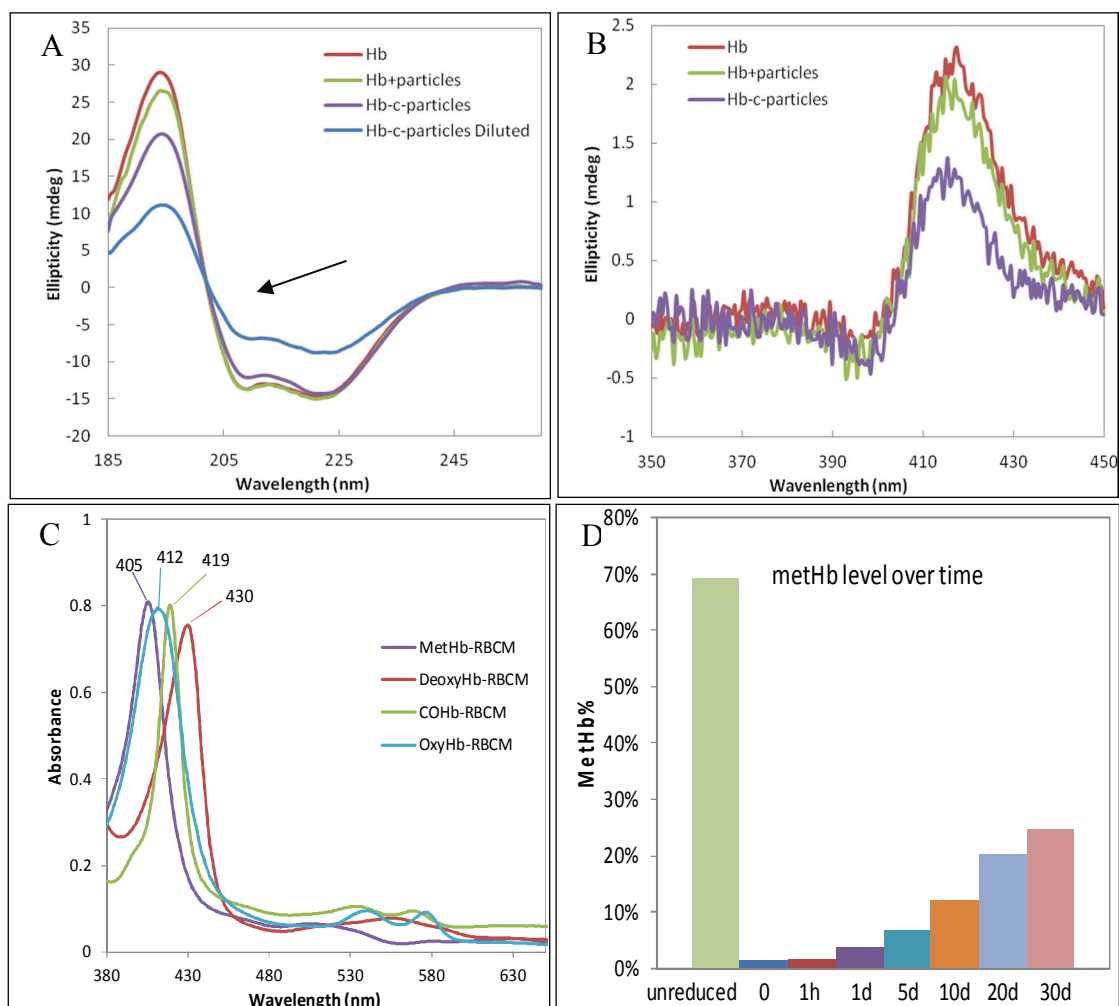


Figure 3.7 (A) Far-UV circular dichroism spectra of pure Hb, Hb physically mixed with particles (Hb+particles), and Hb conjugated to particles (Hb-c-particles). For Hb-c-particles, the sample was half diluted as Hb-c-particles Diluted to confirm the isodichroic point as denoted by the arrow. The spectra were all measured in 10 mM K₂HPO₄ buffer with a path length of 1 mm. (B) Soret CD of the first three samples with Hb concentration of 1 mg/mL in 10 mM K₂HPO₄ buffer. (C) UV-vis spectra of Hb-particles with the hemes of Hb at different binding states. Particle concentration in the sample was 0.05 mg/mL with Hb concentration of 0.14 mg/mL. The as prepared Hb-particles showed a Soret peak at 405 nm, indicating mostly metHb in the particles. When sodium dithionite was added to the particle suspension, metHb was reduced back to deoxyHb, characterized by the Soret peak at 430 nm. Carbon monoxide purged into the

suspension converted deoxyHb into CO-Hb as the Soret peak moved to 419 nm. When exposed to light and air, the Soret peak of the suspension moved to 412 nm, indicating formation of oxyHb. (D) MetHb level in polymer-Hb conjugate over time. The polymer was based on a similar formulation as for the particles but without crosslinker. Overall Hb concentration in the conjugate solution was 5 mg/mL.

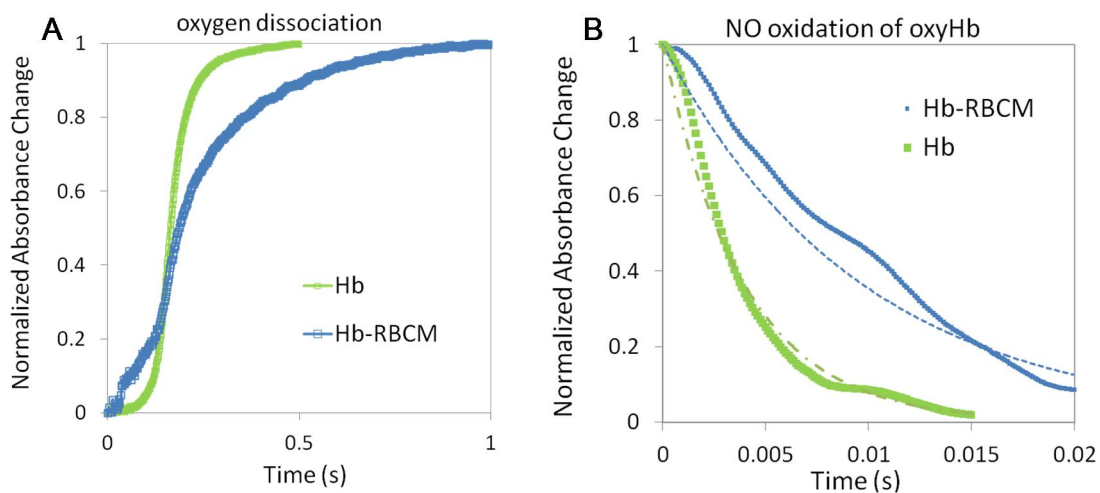


Figure 3.8 Time courses of (A) oxygen dissociation and (B) NO oxidation of oxyHb. Hb concentration was $0.5 \mu\text{M}$ after mixing in all the studies with $14 \mu\text{M}$ NO solution to ensure pseudo-first-order reaction by large excess of NO. All the measurement carried out at $23 \text{ }^\circ\text{C}$.

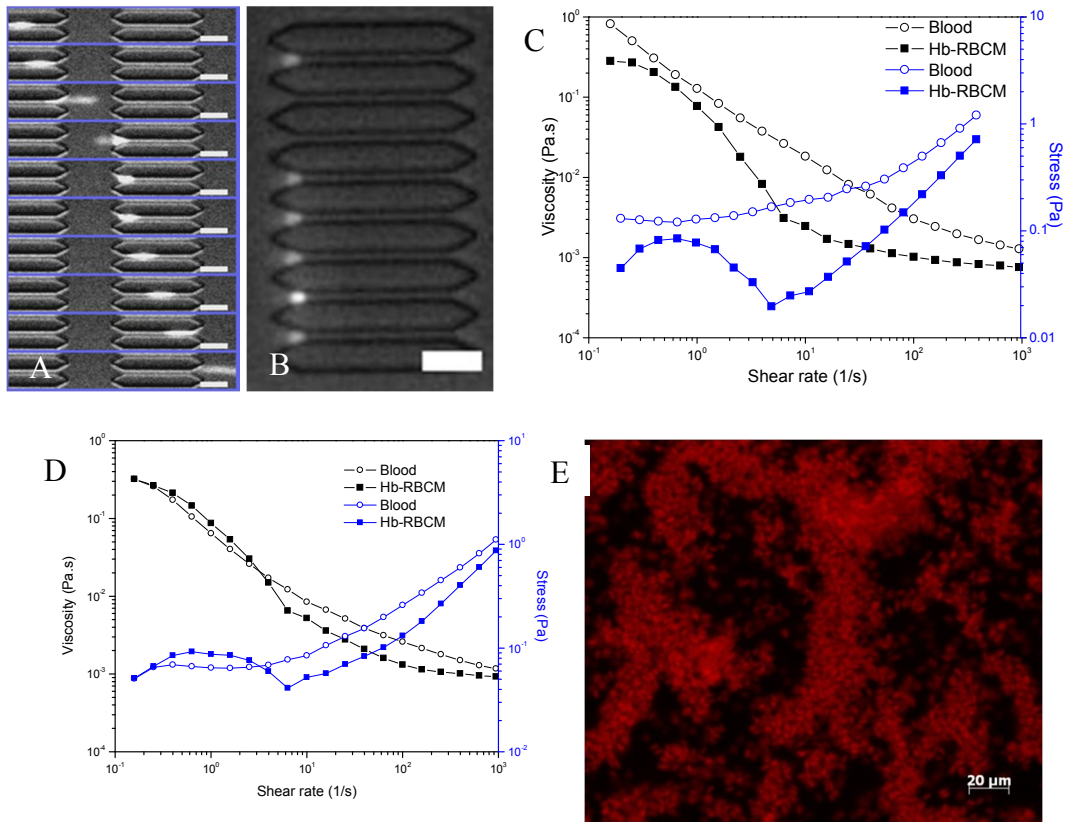


Figure 3.9 (A) Image sequence (top to bottom) showing how a single particle ($R = 2.8$) passed through a constricted pore (from left to right). The time lapse between the frames was 31 ms. (B) Clogged pore entrance by Hb-RBCM particles with $R = 5.1$. (C) and (D) Rheological results showing viscosity and shear stress versus shear rate for blood of two mice and Hb-RBCM suspension ($[Hb] = 5.2$ g/dL) that had been subjected to a rheometer. The shear rate ranged from 0.1 to 1,000 1/s, covering the possible shear rates in blood flow. (E) Microscopic image showing intact Hb-RBCM particles after being sheared at a constant rate of 1,000 1/s for 10 min. Scale bars = 20 μ m.

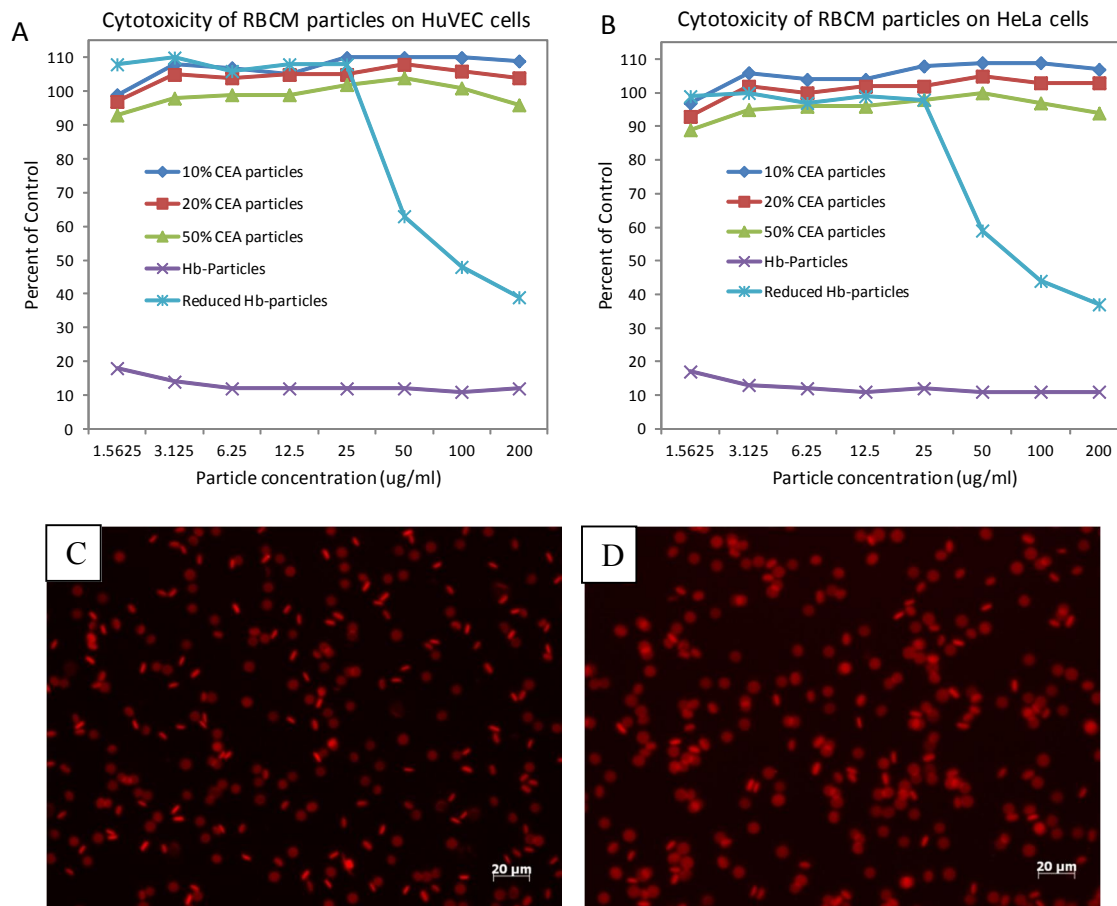


Figure 3.10 Cytotoxicity of the RBCM particles tested on (A) HUVEC and (B) HeLa cells after 72 h. RBCM particles with 10, 20, and 50 wt% CEA, but unloaded with Hb were studied to assess the biocompatibility of CEA. Hb conjugated particles (10 wt% CEA; $R=2.8$) with metHb reduced were tested with their un-reduced counterparts. Fluorescent micrographs of (C) 20 wt% and (D) 50wt% CEA particles. The size of the particles were 6.5 and 7.5 μm , and the zeta-potential were -23.5 and -29.9 mV respectively.

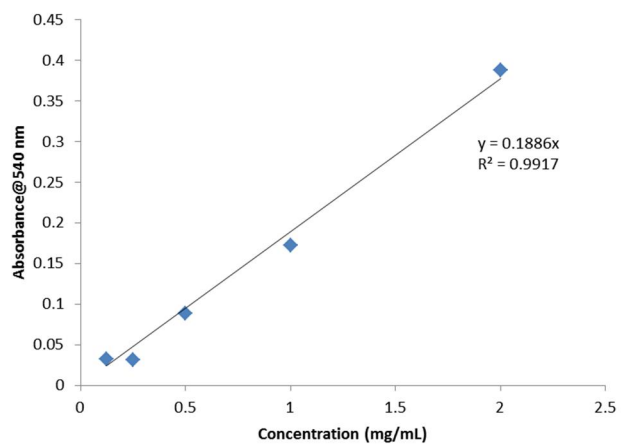


Figure 3.11 Standard curve of Hb measured by UV-vis spectroscopy, and fitted by linear regression. At 540 nm, the molar absorbance of oxyHb, deoxyHb, and metHb are the same.

3.5 REFERENCES

- (1) Tsuchida, E.; Sou, K.; Nakagawa, A.; Sakai, H.; Komatsu, T.; Kobayashi, K. *Bioconjugate Chem.* **2009**, *20*, 1419-40.
- (2) Goodnough, L. T.; Scott, M. G.; Monk, T. G. *Clin. Orthop. Relat. Res.* **1998**, 89-100.
- (3) Huang, P. L.; Huang, Z.; Mashimo, H.; Bloch, K. D.; Moskowitz, M. A.; Bevan, J. A.; Fishman, M. C. *Nature* **1995**, *377*, 239-42.
- (4) Kubes, P.; Suzuki, M.; Granger, D. N. *Proc. Natl. Acad. Sci.* **1991**, *88*, 4651-4655.
- (5) Garthwaite, J.; Boulton, C. L. *Annual review of physiology* **1995**, *57*, 683-706.
- (6) Joshi, M. S.; Ferguson, T. B.; Han, T. H.; Hyduke, D. R.; Liao, J. C.; Rassaf, T.; Bryan, N.; Feelisch, M.; Lancaster, J. R. *Proc. Natl. Acad. Sci.* **2002**, *99*, 10341-6.
- (7) Liao, J. C.; Hein, T. W.; Vaughn, M. W.; Huang, K. T.; Kuo, L. *Proceedings of the National Academy of Sciences of the United States of America* **1999**, *96*, 8757-61.
- (8) Chang, T. M. S. *Science* **1964**, *146*, 524-525.
- (9) Kaneda, S.; Ishizuka, T.; Goto, H.; Kimura, T.; Inaba, K.; Kasukawa, H. *Artificial organs* **2009**, *33*, 146-52.
- (10) Alayash, A. I. *Nat. Biotechnol.* **1999**, *17*, 545-9.
- (11) Tsuchida, E.; Sou, K.; Nakagawa, A.; Sakai, H.; Komatsu, T.; Kobayashi, K. *Bioconjugate chemistry* **2009**, *20*, 1419-40.
- (12) Sou, K.; Klipper, R.; Goins, B.; Tsuchida, E.; Phillips, W. T. *The Journal of pharmacology and experimental therapeutics* **2005**, *312*, 702-9.
- (13) Sakai, H.; Sou, K.; Horinouchi, H.; Kobayashi, K.; Tsuchida, E. *Advances in experimental medicine and biology* **2010**, *662*, 433-8.
- (14) Rameez, S.; Alost, H.; Palmer, A. F. *Bioconjugate Chem.* **2008**, *19*, 1025-32.
- (15) Sun, J.; Huang, Y.; Shi, Q.; Chen, X.; Jing, X. *Langmuir* **2009**, *25*, 13726-9.
- (16) Shi, Q.; Huang, Y.; Chen, X.; Wu, M.; Sun, J.; Jing, X. *Biomaterials* **2009**, *30*, 5077-5085.
- (17) Xu, F.; Yuan, Y.; Shan, X.; Liu, C.; Tao, X.; Sheng, Y.; Zhou, H. *International journal of pharmaceutics* **2009**, *377*, 199-206.
- (18) Sheng, Y.; Yuan, Y.; Liu, C.; Tao, X.; Shan, X.; Xu, F. *Journal of materials science. Materials in medicine* **2009**, *20*, 1881-91.
- (19) Langer, R.; Peppas, N. A. *AIChE Journal* **2003**, *49*, 2990-3006.

- (20) Patton, J. N.; Palmer, A. F. *Biomacromolecules* **2005**, *6*, 2204-12.
- (21) Patton, J. N.; Palmer, A. F. *Biomacromolecules* **2005**, *6*, 414-24.
- (22) Thilakarathne, V.; Briand, V. A.; Zhou, Y.; Kasi, R. M.; Kumar, C. V. *Langmuir* **2011**, *27*, 7663-71.
- (23) Lalezari, I.; Lalezari, P.; Poyart, C.; Marden, M.; Kister, J.; Bohn, B.; Fermi, G.; Perutz, M. F. *Biochemistry* **1990**, *29*, 1515-1523.
- (24) Sakai, H.; Masada, Y.; Takeoka, S.; Tsuchida, E. *J. Biochem.* **2002**, *131*, 611-7.
- (25) Sinz, A. *J. Mass Spectrom.* **2003**, *38*, 1225-37.
- (26) Zhang, N.; Palmer, A. F. *Biotechnol. Bioeng.* **2011**, *108*, 1413-20.
- (27) Shukla, R.; Balakrishnan, M.; Agarwal, G. P. *Bioseparation* **2000**, *9*, 7-19.
- (28) Henzler, K.; Wittemann, A.; Breininger, E.; Ballauff, M.; Rosenfeldt, S. *Biomacromolecules* **2007**, *8*, 3674-81.
- (29) Gershevitz, O.; Sukenik, C. N. *J. Am. Chem. Soc.* **2004**, *126*, 482-3.
- (30) Arifin, D. R.; Palmer, A. F. *Biomacromolecules* **2005**, *6*, 2172-81.
- (31) Pelton, J. T.; McLean, L. R. *Anal. Biochem.* **2000**, *277*, 167-76.
- (32) Kelly, S. M.; Jess, T. J.; Price, N. C. *Biochimica et biophysica acta* **2005**, *1751*, 119-39.
- (33) Lu, S.; Ciardelli, T.; Reyes, V.; Humphreys, R. *J. Biol. Chem.* **1991**, *266*, 10054-10057.
- (34) Zolghadri, S.; Saboury, A. A.; Golestani, A.; Divsalar, A.; Rezaei-Zarchi, S.; Moosavi-Movahedi, A. A. *J. Nanoparticle Res.* **2008**, *11*, 1751-1758.
- (35) Sugita, Y.; Nagai, M.; Yoneyama, Y. *J. Biol. Chem.* **1971**, *246*, 383-388.
- (36) Liu, C. *Biochim. Biophys. Acta* **1998**, *1385*, 53-60.
- (37) Urabe, Y.; Shiomi, T.; Itoh, T.; Kawai, A.; Tsunoda, T.; Mizukami, F.; Sakaguchi, K. *Chembiochem* **2007**, *8*, 668-74.
- (38) Takeoka, S.; Sakai, H.; Kose, T.; Mano, Y.; Seino, Y.; Nishide, H.; Tsuchida, E. *Bioconjugate Chem.* **1997**, *8*, 539-44.
- (39) Wallace, W.; Houtchens, R.; Maxwell, J.; Caughey, W. *J. Biol. Chem.* **1982**, *257*, 4966-4977.
- (40) Zijlstra, W. G.; Buursma, A. *Comp. Biochem. Physiol.* **1997**, *118*, 743-749.

- (41) Eich, R. F.; Li, T.; Lemon, D. D.; Doherty, D. H.; Curry, S. R.; Aitken, J. F.; Mathews, a J.; Johnson, K. a; Smith, R. D.; Phillips, G. N.; Olson, J. S. *Biochemistry* **1996**, *35*, 6976-83.
- (42) Vandegriff, K. D.; Bellelli, A.; Samaja, M.; Malavalli, A.; Brunori, M.; Winslow, R. M. *The Biochemical journal* **2004**, *382*, 183-9.
- (43) Rameez, S.; Palmer, A. F. *Langmuir* **2011**, *27*, 8829-40.
- (44) Merkel, T. J.; Jones, S. W.; Herlihy, K. P.; Kersey, F. R.; Shields, A. R.; Napier, M.; Luft, J. C.; Wu, H.; Zamboni, W. C.; Wang, A. Z.; Bear, J. E.; Desimone, J. M. *Proc. Natl. Acad. Sci.* **2011**, 586-591.
- (45) Replogle, R.; Meiselman, H.; Mirrill, E. *Circulation* **1967**, *36*, 148-160.
- (46) Vermant, J.; Solomon, M. J. *J. Phys.: Condens. Matter* **2005**, *17*, R187-R216.
- (47) Lerouge, S.; Decruppe, J.; Humbert, C. *Phys. Rev. Lett.* **1998**, *81*, 5457-5460.
- (48) Meguro, T.; Chen, B.; Lancon, J.; Zhang, J. H. *J. Neurochem.* **2001**, *77*, 1128-1135.
- (49) D'Agnillo, F.; Chang, T. M. *Nat. Biotechnol.* **1998**, *16*, 667-71.
- (50) Rusmini, F.; Zhong, Z.; Feijen, J. *Biomacromolecules* **2007**, *8*, 1775-89.
- (51) Bustamante, C.; Tinoco, I.; Maestre, M. F. *Proc. Natl. Acad. Sci.* **1983**, *80*, 3568-72.

CHAPTER 4: MODULATING BIODISTRIBUTION AND EXTENDING CIRCULATION OF HB-LOADED RBC MIMICS

4.1 Introduction

Most mammalian cells bear a negative surface charge as measured by electrophoresis. This means that, despite presence of both cationic and anionic groups from carbohydrates and proteins on the cell surface, overall there are more anionic groups than the cationic ones. RBCs, are generally more negatively charged on the surface than other cells resulting from carboxyl groups of sialic acid distributed on their membrane.¹ The negative surface charge makes RBCs stable in plasma, preventing aggregation.² The amount of sialic acid is a major factor in distinguishing young and senescent RBCs. It has been suggested that senescent RBCs are less negatively charged, due to reduction in sialic acid, than normal ones, hence being recognized and destructed by macrophages.³ Removal of sialic acid on healthy RBCs by neuraminidase could also lead to recognition of the RBCs by the MPS.^{4,5}

Increasing the negative charge on RBC surface, however, would also lead to removal of the RBCs. There are four major types of lipids making up the RBC membrane, and phosphatidyl serine (PS) is a negatively charged lipid that is exclusively distributed within the inner leaflet of RBC membrane. Exposure of PS, under certain circumstances like sickle cells,⁶ leads to more negative charge on RBC surface, and removal of the cells by macrophages. Therefore, it seems that there is a window for ζ -potential of RBCs to ensure sufficient circulation time of the cells; too high or too low of a negative charge would lead to recognition and clearance of RBCs by the MPS. Although it has not been fully elucidated how the surface charge of RBCs influence their

function and clearance in details, it is clear that the surface properties follow design rules, which may have implications for design of synthetic particles.

For micro- or nanoparticles, surface charge, along with other physical parameters including size, shape and modulus, affects the circulation in blood. Macrophages in the MPS are highly capable of recognizing and phagocytizing alien particles or cells depending on all these parameters. For surface charge alone, it is generally accepted that macrophages tend to recognize charged particles easier than neutral ones, and this tendency intensifies as the absolute value of ζ -potential of particles increases.⁷ Once administered to blood, cationic particles are known to form aggregates in the presence of the negatively charge serum proteins.⁸ The aggregates can be too large to flow through capillaries in the lung. Positively charge particles may also cause several complications such as hemolysis and platelet aggregation.^{9,10}

A general method to avoid scavenging by the macrophages of the MPS, and to extend circulation time of particles, is to camouflage the surface of particles with neutral, hydrophilic polymers like poly(ethylene glycol) (PEG). PEGylation, generally indicating attachment of PEG to particle surface, can make the resultant particles stealthy to macrophages by repelling plasma protein from coating the particle surface.^{11,12} The molecular weight and conformation of PEG are important parameters governing the clearance of PEGylated particles. In our lab, 200×200 nm PRINT nanoparticles had been PEGylated to obtain a “brush conformation”, i.e. densely packed PEG layer, resulting in much longer half-life than the unPEGylated particles, or particles less densely packed with PEG that exhibited “mushroom conformation”.¹³ Another polymer of interest for this purpose is zwitterionic polymer that contains both cationic and anionic charges in the same molecule. For liposomes, PEG may destabilize the lipid membrane because of the amphiphilic property of PEG, while zwitterionic polymers could make liposomes stable as

studied by Jiang's lab.¹⁴ They tested liposomes coated with zwitterionic polymers, and found extended circulation time for the resultant liposomes.¹⁵

For Hb-loaded RBC mimics, the particle surface became attached with Hb, a protein that is supposed to be encapsulated within cells. Exposure of Hb on particle surface may impair the *in vivo* circulation either due to particle aggregation or easier recognition by the MPS.

Methods are needed to avoid exposure of Hb on particle surface. While different PEGylation methods have been employed to functionalize a wide variety of particles, one thing in common is that the intent is for PEG molecules to provide dense protective conformation on the surface of particles. For Hb loaded PRINT RBC mimics, however, it would be impossible to obtain a dense layer of PEG on the particle surface because there is no solid, continuous surface that is generally found in other nanoparticle systems. PEGylating Hb on such a particle surface would probably result in a low density of PEG and loss of extended conformation. Moreover, there are both carboxyl and amine groups on Hb surface; PEGylation through linkage to lysines would make surface-bound Hb more negatively charged, driving the charge of particle surface further away from neutral. While it is possible to PEGylate both carboxyl and amine groups of Hb attached, it is very complicated and may also cause adverse effect to the structure and function of Hb.

Herein, a strategy to solve the above-mentioned problem is proposed and tested. The idea is to load Hb into the interior of PRINT particles but not on the surface. To realize this, a particle with conjugation handles only in the interior is needed. The surface, rather than attached with protein, should remain neutral and hydrophilic. Because of the chemical homogeneity of PRINT particles, post-modification of as-prepared particles is necessary to construct such a particle structure. After obtaining PRINT particles with a uniform distribution of functional groups,

PEGylation will be carried out to quench the functional groups on particle surface only while preserving them inside. However, for PRINT RBC mimics fabricated in previous chapters, the highly swollen nature in aqueous solution made them permeable even to large PEG molecules up to 30 k Da, making functional groups in the interior also available and reactive toward the PEGylation strategy. While these soft RBC mimics could deswell in a non-polar solvent to a dense state that may impede diffusion of PEG molecules, the particles were severely aggregated due to insufficient surface charge for stabilization. In an alternative approach here, an acid-labile crosslinker was used in the particle formulation to yield a high crosslink density, and PEGylation was conducted on the surface only, followed by swelling of the particles through degradation of the crosslinker. Through the new strategy, swollen particles with neutral surface and charged groups in the interior can be obtained. Conjugation of Hb into the particles could generate new RBC mimics with Hb loaded predominantly into the interior of the particles. The scheme in **Figure 4.12** illustrates the procedure for constructing the new RBC mimics. Primary-amine containing particles were fabricated as the starting point rather than CEA containing ones because primary amines can be simply converted to carboxyls when needed and are much easier to quench than carboxyls.

In addition, we tested the new particles both *in vitro* and *in vivo* to demonstrate the effect of surface properties of the RBC mimics on their interaction with biological barriers.

4.2 Results and Discussions

4.2.1 Synthesis of Acid-labile Crosslinker

An acetal-based diacrylate (ADA; **Figure 4.13A**) was synthesized and characterized by NMR (**Figure 4.13B**). ADA, as a hydrophobic crosslinker, is derivatized from HEA, which has been proven to be great material in fabricating highly deformable gels in our previous study.¹⁶

Acetals, with a general structure of $R_2C(OR')_2$, are stable under neutral and alkaline conditions but readily undergo hydrolysis in aqueous acidic solutions, hence being widely used in drug delivery for controlled release.¹⁷⁻²⁰ The R group can be selected to control the degradation rate, which can be estimated by the stability of the liberated oxonium ion as degradation intermediate.²¹ For example, methyl as R would make the oxonium ion more stable than hydrogen, leading to faster degradation rate. Here we used two methyl groups as R because of ease for synthesis and an optimal degradation rate ADA demonstrated. After degradation, a single ADA molecule would generate two HEA molecules with one acetone molecule, making purification of degraded particle easy by centrifugation.

The reaction between HEA and 2-methoxypropene in the presence of organic acid PPTS to synthesize ADA is not new. Similar reactions had been done by Frechet¹⁷ and Willson²² before where a high temperature was required. However, we found that at high temperature, there was a trans-esterification reaction between HEA molecules, generating ethylene diacrylate, a non-degradable crosslinker. Even very low amount of this short-chain non-degradable diacrylate as byproduct in ADA could make PRINT particles unable to swell to desired size even after complete degradation of ADA. And ethylene diacrylate was very difficult to remove from ADA since they had almost the same mobility on TLC plate for many elution combinations tested. Therefore, to avoid the complication of ethylene diacrylate generation at high reaction temperature, we carried out the ADA synthesis in an ice bath, and found that the reaction could still continue, with a 1:1 molar ratio of the two products generated. ADA could easily be separated from the mono-protected HEA by common column chromatography.

4.2.2 ADA-crosslinked PRINT Particles

Using the 2 μm PRINT mold, tightly crosslinked particles containing either AEM or CEA with the formulations in **Table 4.1** could be fabricated. For AEM containing particles, HP3A was used to increase the solubility of AEM because the major component ADA (50 wt%) was not polar enough. HP3A was also used in the formulation for CEA containing particles for better comparison with AEM particles. Non-degradable crosslinker PEG4kDA, a long chain PEG diacrylate used to crosslink previous blank RBC mimics, was also lightly used in both scenarios to ensure swelling but not complete dissolution of particles after acetal degradation.

The size of the as prepared particles with CEA or AEM was 2.5 μm (**Figure 4.14A**) and 2.3 μm (**Figure 4.15A**) respectively when suspended in PBS, with zeta-potential of -28 mV and 22 mV measured in 0.1X PBS. When suspended in pH=3 buffer, the CEA containing particles could swell to a maximal size of 5.5 μm after 3 h (**Figure 4.14B**), while AEM containing particles swelled to a maximal size of 5.0 μm after 2 h (**Figure 4.15B**). It took longer time for ADA to completely degrade in CEA containing particles because the carboxyl groups of CEA would be protonated at pH = 3 (pKa of CEA around 4), making the particles more hydrophobic for diffusion of proton and acetone.

Table 4.1 Compositions used to fabricate tightly crosslinked particles. Both AEM and CEA containing particles were fabricated.

Component	Weight percent (wt%)		Function
	Cationic	Anionic	
HP3A	28-28.9	27-27.9	Improving solubility of AEM
AEM	18	0	Amine containing monomer
CEA	0	20	Carboxyl containing monomer
PEG4kDA	2	1	Non-degradable crosslinker
DEAP	1	1	Photoinitiator
ADA	50	50	Degradable crosslinker
fluorescent dye	0.1-1	0.1-1	Imaging

4.2.3 PEGylation of ADA-crosslinked Anionic Particles

Our initial attempt was to start with CEA containing particles with a high crosslinking density, to obtain a neutral surface but with an anionic interior for loading with Hb. By adding EDC/NHS or EDC/sulfo-NHS to activate the carboxyl groups in particles, methoxyl-PEG-amine (mPEG-amine) was added with the intention to react with carboxyl groups on particle surface only. We found that mPEG-amine with molecular weight (MW) ranging from 5 k to 30 k Da could all screen the surface charge of the particles, as zeta-potential of the PEGylated particles could decrease to neutral, with high MW mPEG-amine being more efficient. However, after treatment of the PEGylated CEA particles in pH = 3 buffer even for extended hours, the expected swelling did not occur as the particles just slightly increased their size (**Figure 4.14C, D**).

The insufficient swelling of PEGylated CEA particles was found to be caused by side reactions of the activated carboxyls. It has been known that carboxyl activated by carbodiimide can undergo the [O→N]-Acyl migration reaction to generate O-acylisoureas.²³ This side reaction could happen within the particle interior, resulting in a decrease in the available amount of carboxyls because EDC or other carbodiimides are small molecules and could penetrate the

particle even highly crosslinked by ADA. The generated O-acylisoureas are positively charged, and could interact with negatively charged carboxyls remained to form physical crosslinks.

To avoid the side reactions of using carbodiimide, other carboxyl-activators including the uranium reagent TSTU and HATU, and triazine reagent DMT-MM,^{23,24} had also been tested, yet the same problem remained. What probably happened was that these small-molecule activators infiltrated into the interior of particles to activate the carboxyls, which had no amine to react with because of the size exclusion for mPEG-amine, leading to crosslinking with hydroxyls of HP3A. Even when HP3A was replaced by another hydroxyl-free monomer, methoxyl-PEG (MW = 480 Da) acrylate, insufficient swelling still occurred, possibly because of trace amount of hydroxyl impurities in the new monomer, or hydroxyls generated by partially degraded ADA.

Overall, even though highly crosslinking of the CEA containing particles by ADA could ensure confined PEGylation only on the particle surface, carboxyls within the particle interior could readily be activated toward undesirable side reactions that caused extra crosslinking. The final size and deformability of the particles even after ADA degradation would be greatly affected. To circumvent the problem, AEM particles crosslinked by ADA were used as alternative, since the primary amines could be easily converted to carboxyl.

4.2.4 PEGylation of ADA-crosslinked Cationic Particles

The AEM containing particles with the formulation in **Table 4.1**, denoted as particle **A** as following the nomenclature in **Figure 4.12**, could degrade quickly in pH = 3 buffer, while remained minimally swollen in PBS (pH = 7.4) for an extended time (**Figure 4.15C**). This pronounced difference in degradation rate in different pHs made ADA crosslinked particles attractive for our purpose, as rapid degradation in pH = 3 could shorten the work-up time, yet stability in PBS allowed storage before further reactions were carried out.

Amine reactive PEGs such as mPEG-NHS are extensively used to PEGylate both proteins²⁵ and particles¹³. However, in our study here, we found that all the commercially available mPEG-NHS reagents needed to be purified for the quenching of surface amines, otherwise a similar problem of insufficient swelling of particles after acid treatment always occurred without exception (**Figure 4.16A**). The reason was probably due to a β -alanine impurity in the commercial products. Generally, mPEG-NHS is synthesized by activation of the carboxyl of mPEG-COOH using combination of DCC and NHS, or similar activators in organic solvents. However, excess DCC and NHS can form a byproduct β -alanine, which is a small molecule having NHS groups at both ends.²⁶ Even though the impurity quantity may be low, it could act as a short-chain crosslinker within the interior of particle **A**.

Since the β -alanine impurity is a small molecule, it has distinct solubility from mPEG-NHS in IPA, based on which we purified mPEG-NHS with different MWs. AEM particles PEGylated with the purified reagents could swell to the desired size after acid treatment (**Figure 4.16B**).

Table 4.2 ζ -potential of particle **B** and **C** when mPEG-NHS with MW of 2k, 5k and 30 k Da were used for the PEGylation for 4h.

MW of mPEG-NHS (Da)	2k	5k	30k
Zeta potential (mV) — B	2.23	2.12	0.85
C	2.54	4.86	5.27

The efficiency of mPEG-NHS with MW of 2k, 5k and 30k Da on quenching the amines on particle surface was compared by measuring the ζ -potential of particles after PEGylation under similar conditions. At the same molar stoichiometry of mPEG-NHS used for the same weighted particles, higher MW PEG was more efficient in screening the surface charge as the corresponding ζ -potential of particle **B** (PEGylated version of particle **A**) became closer to 0 mV

(**Table 4.2**). This is reasonable because longer PEG chains could extend out to shield the charge better. However, after pH = 3 degradation to swell the particles, ζ -potential of particle **C** (degraded derivative of particle **B**) showed the opposite trend against MW. Therefore, longer PEG could shield the charge more efficiently in particle **B**, yet was less efficient in actually quenching the amines because the larger size limited efficient grafting of PEG molecules to surface of **B**, making more remaining amines exposed to surface of **C**. As a trade-off between an efficient quench of amines on the particle surface and limited diffusion into interior of particles, we chose an optimal MW of 2k Da for the quench reaction without trying lower MWs.

We confirmed that PEGylation was limited to the particle surface using a confocal microscopic method. A fluorescent probe, fluorescein-PEG_{2k}-NHS was used to react with a dyeless model particle that were fabricated with the same composition as particle **A** but in PRINT mold with larger cavities (7×7×3 μm) for better visualization. After PEGylation under the same condition as particle **A** was treated with mPEG_{2k}-NHS, the model particles were thoroughly washed and observed under a confocal microscope. As can be seen in **Figure 4.16C**, a ring-like fluorescence pattern was present, indicating distribution of fluorescein-PEG_{2k}-NHS only on the particle surface. In a control, when fluorescein-NHS (MW=473 Da) was used to quench the particles under the same condition, a disc-like fluorescence pattern was shown instead (**Figure 4.16D**). With identical compositions, particle **A** should have similar pore size as the model particle, therefore similar diffusion barrier for mPEG_{2k}-NHS. We could therefore infer that PEGylation on particle **A** was limited to the surface only.

4.2.5 Quantifying Amine Contents in Particles

The fluorescence-based microscopic method described above implies that mPEG_{2k}-NHS reacted with amines of particle **A** in a gradual way from surface toward the interior, and the

reaction was possibly limited to a certain depth. However, it would be inaccurate to assess the diffusion depth by measuring the width of the fluorescence band. Instead, we used a quantitative fluorescent assay to measure how much primary amine is left in the particles. In this method, fluorescein-PEG_{2k}-NHS was added to particles of interest to label the amines by fluorescein. PEG was used to ensure stability of some particles that otherwise aggregated when fluorescein-NHS was used. From the 1 : 1 stoichiometry, the amine content can be calculated from the quantity of dye, which can be fitted using the standard curve of fluorescein-PEG_{2k}-NHS regarding excited fluorescence.

Direct degradation of particle **A** generated particle **F**. Using the fluorescent assay describe above to, we found that from 1 mg **A**, there were 0.82 μmol NH_2 in generated particle **F**. When particle **F** was PEGylated even using the largest MW PEG-NHS available, mPEG_{30k}-NHS, the remaining amount of $-\text{NH}_2$ was quantified to be less than 10% of the original total. In contrast, in particle **C**, there were 72.1% NH_2 as of **F** from the same starting amount of particle **A**.

The results of amine quantification confirmed it was necessary to develop the confined PEGylation on tightly crosslinked particles so that most interior amines could be preserved, while direct PEGylation of swollen particles led to excessive consumption of amines. It is noteworthy that, swollen particles like **F** would further swell after PEGylation because the incorporated PEG molecules could absorb water and repel each other, even though the charged groups were diminished.

4.2.6 Succinylation of AEM-particles

Succinic anhydride (SA) was used to convert the amines of AEM into carboxyls. The reaction was carried out in 10X PBS to retain a stable pH. When 1X PBS was used, the pH

could, due to hydrolysis of largely excess SA, decrease to around 3, at which amines would be so protonated that succinylation could not continue.

Succinylation of particle **C** into particle **D**, reversed the ζ -potential to slightly negative as -6 mV (**Figure 4.18A**), which could be considered as near-neutral generally. In contrast, particle **G**, succinylated derivative of particle **F**, reversed the charge from 28 mV to -32 mV (**Figure 4.18B**).

The succinylation reaction was very efficient in converting amines to carboxyls, as no remaining NH_2 was detectable using the fluorescent assay described in **4.2.5**.

4.2.7 Conjugation of Hb

Conjugation of bovine Hb into particle **D** or particle **G** followed previous method explicitly described in **3.2.4**. For particle **D**, because of absence of carboxyl on the surface, conjugation could be carried out in concentrated suspension without inter-particle crosslinking or aggregation. However for particle **G**, as there were many carboxyl groups on particle surface implied by a ζ -potential of -32 mV, which was even more negative than blank particles made in **3.2.1** (ζ -potential = -18 mV), the conjugation had to be conducted with low concentration; otherwise, severe aggregates and sedimentation would form during the reaction (**Figure 4.19A**). We maintained low concentration during conjugation for both particle types for comparison. By normalizing the numbers of particles to fixed weight of particle **A**, we could calculate the loading of Hb into particles generated from 0.2 mg (ca. 10 million) particle **A** as: 0.21 mg Hb in **E**, and 0.19 mg Hb in **H**.

A turbidity assay was applied to both particles **E** and **H**, when the two suspensions with optical density (OD) of 1 were quickly mixed with fetal bovine serum (**Figure 4.19B**). The OD at 720 nm, at which absorbance of Hb was negligible, decreased gradually because of particle

sedimentation due to their large size. The rate of OD change for particle **E** was slower than that of particle **H**, indicating less inter-particle aggregation.

4.2.8 Particle Interaction with Macrophage

To assess the effect of surface properties of these RBC-sized particles on their *in vivo* circulation and biodistribution, we first studied their interaction with macrophages *in vitro*. We dosed all the different types of particles from **A** to **H** to the Raw264.7 (mouse leukaemic monocyte macrophage) cell line, with about 400 particles/cell to a total of 10^5 cells. After incubation for 4 and 24 h, percent of macrophages that were associated with particles were measured by flow cytometry and presented in **Figure 4.20A**. Particles with quenched surfaces (**B**, **C**, **D**, **E**) all showed much lower association than the starting particle **A** and unquenched particles (**F**, **G**, **H**), indicating reduced interaction between quenched particles and macrophages. Hb loaded particles **H**, counterpart of **E**, were highly associated with the macrophages probably due to presence of Hb on particle surface. Our results agreed with previous knowledge that neutral particles have less interaction with macrophages than charged particles.⁷ While particle **A** and **F**, amine containing particles, displayed cytotoxicity to the cells (**Figure 4.20B**), PEGylated particle **C** with interior amines showed minimal cytotoxicity similarly to other particles, confirming effective surface quenching.

4.2.9 *in vivo* Studies

To compare the *in vivo* performance of all the RBC-sized particles (**C** to **H**), an intravital microscopic imaging method, was used to observe the particles when intravenously injected into balb/c mice. Intravital microscopy (IVM) has been used to assay the accumulation of targeted particles in tumors²⁷ and tissues,²⁸ it has also been proven to be a reliable method in evaluating the circulation of both micro- and nanoparticles in our previous studies.^{13,16,29} DyLight 680 was

copolymerized into all the particle sets; we observed the peripheral vasculature through the skin of an anesthetized mouse's ear to track the near-IR fluorescence of injected particles every 5 s for 2 h (**Figure 4.21A**). Elimination curves could be generated by plotting the change in fluorescent signal from the particles over time normalizing each scan to the maximum intensity slice.

As anticipated, particles with quenched surface showed extended circulation than their unquenched controls. Particle **D** demonstrated the longest circulation (**Figure 4.21B**) of all the particles tested. With a small bump in the clearance curve, indicating release of some of the physically entrapped particles back to blood similar to what we had observed before for blank RBC mimic (**Figure 2.7**),³⁰ the clearance curve of particle **D** cannot be fitted for a conventional pharmacokinetic model, at least within the 2 h time frame. After 2h, particle **D** was highly concentrated in the spleen, a characteristic of highly deformable particles of this size.³⁰ Negatively charged particle **G** (ζ -potential = -32 mV) had a clearance curve that could be well fitted using the two-compartment pharmacokinetic model (**2.4.10**), which has often been appropriate to describe the behavior of particles in circulation.³¹ The calculated elimination half-life ($t_{1/2\beta}$) of 0.5 h is much shorter than that of blank RBC mimics (ζ -potential = -18 mV; $t_{1/2\beta}$ = 85 h³⁰), yet the biodistribution of **G** was very similar to both **D** and previous blank RBC mimics, indicating quicker clearance of **G** by the MPS system since it is known that more charged particles tend to attract macrophages more.^{32,33}

Loaded with hemoglobin, particle **E** also showed similar biodistribution pattern as **D** and **G**. The fitted elimination half-life of 1.2 h, was way more better than particle **H**, which was rapidly removed from circulation as only insignificant fluorescence observed all through the imaging process (**Figure 4.21A** shows the fluorescence after 100 secs post injection).

Biodistribution after 2 h showed drastically high accumulation of **H** in the lung (**Figure 4.23**). Since the lung is the first downstream tissue with microvasculature post injection, we could speculate that most of the dose sequestered immediately after injection of **H** because of aggregates formed as evidenced by tissue staining result (**Figure 4.22**).

Table 4.3 Two-compartmental analysis of RBC-sized particles from intravital microscopy experiments. The clearance curve of Particle **D** cannot be fitted using 2-compartment model.

Particle	Distribution half-life, min	Elimination half-life, min	AUC, fluorescence×min
C	1.3	20.5	10.7
E	6.2	73.9	25.3
G	5.4	29.1	29.8
D	NA	NA	62.3

Compared to neutral or negatively charged particles, positively charged ones tend to interact more with plasma proteins, most of which are negatively charged,⁷ leading to fast removal. Indeed, positively charged particle **F** was instantly removed from circulation (**Figure 4.21A**) similarly to **H**, and most of the particles ended up in the lung (**Figure 4.23**). Adsorption of proteins onto **F** probably led to aggregation and hence sequestration in the lung. Interestingly for particle **C**, we observed strong fluorescence from the particles in the early time points post injection (**Figure 4.21A**). However, compared to particle **D**, the clearance rate of **C** was much faster ($t_{1/2} = 20.5$ min), with both spleen and liver as the major disposition tissues. Because of the deformability and neutral surface of **C**, the bulk of the dose were able to traverse the lung post injection in contrast to **F**. However, the high porosity in these swollen microgels might have allowed plasma proteins to infiltrate into the particles gradually, leading to easier recognition of **C** by the MPS system most prevalent in the spleen and liver.

4.2.10 Conclusions and Future Work

To further mimic true RBCs in regard to confined distribution of Hb, we designed a new particle **D** with neutral surface and charged groups inside, and loaded Hb into the particle in a confined fashion without or with only minimal exposure of the protein to particle surface. Through the IVM and tissue imaging studies, we found that surface properties indeed dictated both circulation and biodistribution when other factors were similar. All the particles with quenched surface, i.e. PEGylated surface, showed longer circulation than the corresponding counterparts with charged surface.

For the proposed PEGylation method here, the selection of an optimal MW is critical. In the tight state before degradation, the particle surface could be easily neutralized due to charge screening by PEG. However, after degradation of ADA and swelling of particles, physically screened but not chemically quenched charges could come into effect. Moreover, some charges close to the surface but originally buried inside may become exposed after degradation. This is why from particle **B** to **C**, increase of ζ -potential was always observed for the different PEG-NHS used. Therefore, the PEG reagent used should be able to diffuse toward the interior to certain extent in order to quench charges on and close to the surface. To this end, the smaller MW of PEG-NHS, the better. However, PEG-NHS with too small MW may permeate into the particles so easily and fast that most of the interior charges would also be quenched. We opted to use PEG-NHS with MW of 2 k Da because of its smaller size compared to the more generally used PEG of 5 k Da or higher MW, and its limited diffusion rate compared to PEG-NHS with MW < 1 k Da (as tested with MW of 510 and 686 Da). If our goal is to merely increase circulation time of blank microgels without intention to further functionalize the particles like

loading protein, using PEG-NHS to quench charged groups of already-swollen particles may be sufficient enough to extend the circulation.

Compared to conventional PEGylation on nanoparticles, where a dense layer of PEG on particle surface was necessary to achieve the “mushroom conformation”, our PEGylation was primarily intended to quench the surface charge while maintain particle stability. While it may be possible that particle **B** had a dense layer of PEG covering its surface, the swollen, RBC-sized particles from **C** to **E** would only have separated PEG chains because of an almost 6 times $\left(\left(\frac{5.5\mu\text{m}}{2.3\mu\text{m}}\right)^2\right)$ increase of particle surface area after degradation of ADA.

While anionic particles could mimic RBCs regarding negative surface charge, there may be a strict window for ζ -potential, as decrease from -18 mV (blank RBC-sized particle in **Chapter 2**) to -32 mV (particle **G**) caused quicker clearance of anionic particles. PEGylation to quench the negative charge on particle surface, not only provided stability to the particles, but also reduced interaction between the particles and macrophages, leading to the longest circulation ever observed in IVM for RBC-sized particles. Therefore, even for highly swollen particles that are unable to obtain high density of PEG coverage, PEGylation to neutralize surface charge may still extend circulation as it does to solid nanoparticles.

Using the IVM method here, we could definitely compare circulation half-lives of the different particles and confirm the advantage of surface-quenched particles. The calculated clearance half-life from the 2 h intravital curve was 1.2 h for particle **E**, similar to the half-life of cell-free Hb. To accurately evaluate the half-life of particle **E**, blood draw method will be needed and a longer circulation time may possibly be calculated. Some long circulating particles may still be within the distribution phase during the 2 h scan by IVM. Blood draw method spans

longer time to ensure coverage over the distribution phase, and can provide more accurate estimation of the circulation life.

Particle **E** can be potent candidate as oxygen carrier, despite its decreased circulation time compared to the blank particles. With such a large size, vasoconstriction may possibly be avoided for particle **E**, because vasoconstriction is inversely proportional to the size of the HBOC.³⁴ While early HBOCs based on large sized particles (1-100 μm) were abandoned for further test because of blood flow issues, particle **E** could avoid accumulation in the capillary beds in the lung. This feature of particle **E** is critically important, otherwise particle **H** would be deteriorating cases where an oxygen carrier is needed since particle **H** would severely block capillaries in the lung.

It has been well known that cationic particles would be cleared from the circulation faster than neutral or anionic particles. Our study confirmed this as particle **F** was rapidly removed by the lung. However, by quenching the surface positive charge via PEGylation while retaining the cationic charge inside particles, an extended circulation for **G** was observed, making particle **G** possible to be used for *in vivo* applications. It is noteworthy that for particle **G**, spleen and liver were the two major organs with similar levels of particle disposition, while for all the other RBC-sized particles, either lung or spleen was the only leading organ for particle disposition. Since macrophages are most abundant in the spleen and liver, it is hypothesized that some plasma proteins could gradually infiltrate into particle **G**, leading to recognition of particle **G** by the MPS.

In the future, we can test particle **E** regarding vasoconstriction. First, we can compare cell-free Hb and particle **E** in an *ex vivo* model. Solution of cell-free Hb or suspension of particle **E** containing equal concentration of Hb can be perfused through isolated arterioles,^{34,35} and

possible diameter change of the arterioles can be monitored. With or without flow, cell-free Hb would always cause vasoconstriction in this model as Hb molecules could diffuse into the endothelial to scavenge NO. In this model, equal amount of Hb either in particles or as free form is distributed in the arteriole of interest, so the result can clearly imply how vasoactive the particle is compared to free Hb. Once no vasoconstriction observed for particle **E** using this model, we can continue to study vasoactivity *in vivo*.

We can use IVM to study arteriole diameter change in mice dosed with particle **E** and free Hb. Because of different pharmacokinetics of free Hb and particles **E**, the distribution of Hb in particle **E** into the arteriole of interest may be quite different from that of free Hb even when the same dose of Hb administered, so this *in vivo* study must be accompanied by the *ex vivo* model. Compared to a single time flow in the *ex vivo* model, there are numerous flows passing the arteriole of interest, so the vasoconstriction study *in vivo* can further reveal vasoactivity of particle **E** under continuous intravascular flow compared to free Hb.

Besides Hb, particle **D** can also be installed with other proteins of interest. The two enzymes, superoxide dismutase (SOD) and catalase (CAT) responsible for maintaining low metHb in RBCs, can be conjugated to the particle with lower loading prior to Hb conjugation, resulting in particles mimicking the enzyme system of RBCs.

The long circulation time of particle **D** can possibly be maintained when low amount of protein is loaded compared to particle **E** which was highly charged with Hb. Enzymes that can work in plasma without necessity to be delivered into specific cells can be installed into particle **D** at low loading for extended effect. For example, butyrylcholinesterase (BuChE), a natural enzyme that can degrade organophosphorus nerve agents, can be loaded into the particles as nerve agent scavenger for defense purpose. A pro-drug strategy can also be used to link BuChE

to particle **D** so that the protein can be release over a long time to scavenge nerve agent not only in blood but also in muscles and other tissues.

The scavenging idea can also be applied to cationic particles. Surface neutral, interior cationic particle **C** can bind to nucleic acids through electrostatic forces. After binding, the deformability of particle **C** may be decreased that the particle would be cleared in the spleen. In situations where free plasma nucleic acids may cause inflammation,³⁶ the particles can act as scavenger to remove the free nucleic acids. As discussed above, the current form of particle **C** might possibly be easily accessible by plasma proteins, leading to clearance in the spleen and liver. We can finely tune the pore size in such a surface-neutral, interior-cationic particle so that it can selectively bind nucleic acids while excluding proteins that are generally larger. Scaling down the pore size may mean higher crosslinking density and less deformability for the particles than blank particles studied here. To extend circulation of such particles even after modulating the pore size, a smaller particle size than that of RBC may be used so that there is still long enough circulation despite less deformability. Because particles for this purpose does not have to be in the RBC size range in order to mirror RBC hydrodynamics in intravascular flow to avoid vasoconstriction, microgels with smaller size than RBCs may still be a good selection to fulfill both specific binding of nucleic acids and extended circulation until becoming too stiff after scavenging enough nucleic acids.

By incorporation of other functionalities into the interior of surface-neutral particles, more scavenging functions can be explored, such as removal of lipid,³⁷ and removal of glutamate for brain neutraprotection.³⁸ Overall, we believe, by combining PRINT and the proposed strategy for selective surface modification, new particles can be created not only as potent oxygen carriers, but also as bioscavengers for therapeutic purposes.

4.3 Materials and Methods

4.3.1 Materials

HP3A was synthesized according to 2.4.2. Pyridinium p-toluenesulfonate (PPTS), 2-hydroxyethyl acrylate (HEA), 2-methoxypropene, diethoxyacetophenone (DEAP), 2-aminoethyl acrylate (AEM), succinic anhydride, bovine hemoglobin, Dulbecco's phosphate buffer saline (PBS) were all received from Sigma-Aldrich. Polyethylene glycol (MW=4,000 g/mol) diacrylate (PEG4kDA), methacryloxyethylthiocarbamoyl rhodamine B (PolyFluor[®] 570) were from Polysciences, Inc. Sulfo-N-Hydroxysuccinimide (NHS), 1-ethyl-3-(3-dimethylaminopropyl) carbodiimide hydrochloride (EDC), Fluorescein-NHS, and 2-(N-morpholino) ethanesulfonic acid (MES) buffer, were all received from Thermo Scientific. DyLight 680 was from Piercenet. Methoxy-PEG-NHS with MW of 2k, 5k, 30k were all received from Creative PEGworks; fluorescein-PEG_{2k}-NHS was received from Nanocs Inc, and all the PEG reagents were purified before use with procedures described later. All organic solvents and acidic buffers were received from Fisher Scientific unless otherwise noted. Perfluoropolyether molds were received from Liquidia Technologies.

4.3.2 Synthesis of ADA

In a typical procedure, 15 g (129 mmol) HEA with 1.5 g (6 mmol) PPTS was dissolved in 50 mL dichloromethane (DCM) in a 3-neck flask charged with nitrogen purge and a stir bar. The flask was kept submerged in an ice bath. Then 5 g (69.4 mmol) 2-methoxypropene dissolved in another 50 mL DCM was gradually added to the flask from an addition funnel during a 0.5 h course. The reaction was allowed for 4h. After the reaction, the DCM solution was washed with 6 wt% NaHCO₃ solution 3 times (100 mL each time). To the washed DCM phase, anhydrous Na₂SO₄ was added to dehydrate. The solids were filtered, and then DCM was removed on a

rotovap in vacuo to obtain colorless oil (10.5 g). ADA was separated from the other product in the oil using a silica column with elution comprising of 5:1:0.03 of hexane/ethyl acetate/triethylamine. Triethylamine was used to avoid degradation of ADA in the column because silica gel is slightly acidic. About 3 g of ADA could be obtained. Even though the final yield was not high because of the byproduct, we confirmed high purity as no ethylene diacrylate was present characterized by HPLC.

4.3.3 Purification of mPEG-NHS

For PEG of 5k Da and larger MW, dissolve ~100 mg mPEG-NHS in 50 μ L anhydrous methanol (Acros), then add 1 mL anhydrous isopropanol (IPA; Acros) to the solution and after ~5 min, mPEG-NHS would precipitate out. For mPEG-NHS with MW of 2k Da, dissolve ~100 mg PEG2k-NHS in ~500 μ L IPA, and sonicate to dissolve completely. Store the solution at -20 $^{\circ}$ C for 3 min and mPEG-NHS would precipitate out. Spin down the PEG solid and repeat the corresponding process another 4 times. Collect the final solid and dry in vacuo. Store purified solids in a vial top-filled with nitrogen for future use if not used immediately. Purified PEGs were used within 2 weeks.

4.3.4 Fabrication of Particle A

About 50 μ L of the pre-particle solution with formulation in **Table 4.1** was applied to a PRINT mold using a pipette tip. A polyethylene terephthalate (PET) sheet was applied on top of the mold, and this assembly was passed through a small, non-heated laminator with pressure of 50 psi to wet the mold completely. After passing through, the assembly was subjected to another hot laminator set at 60 $^{\circ}$ C, 40 psi, and the PET sheet was peeled away at the nip point of the laminator, leaving the cavities filled while wicking away excess solution. The filled mold was immediately transferred into a nitrogen purged UV oven and cured with UV light ($\lambda = 365$ nm,

power = 20 mW/cm²) for 3 min. After curing, the filled mold was placed face down on a thin film of 0.1% Plasdone (GAF) in water on top of another PET sheet. This assembly was placed in a cooler half-filled with dry ice, allowing the water to freeze and adhere to the particles. After freezing, the mold was peeled away from the particles trapped in the ice layer, and the ice was allowed to thaw. Particles and water were collected, then washed and concentrated via repeated centrifugation at 10,000 rpm (4×3 min each time) in PBS. The concentration of particle suspensions was determined by thermogravimetric analysis (TGA) on a Perkin Elmer Pyris TGA. Both the suspension and the supernatant after spinning down the particles were subjected to TGA at the same volume (20 μL) to obtain the dry weight. The difference in the weight divided by the volume was the concentration of that particle suspension.

4.3.5 Particle characterization

Particle dimensions were determined by analysis of images taken from a microscope mounted camera (Zeiss AxioCam MRm) using a 100× objective (Zeiss Axio Imager D.1M). Over 50 fully hydrated particles in PBS were measured for each case. The ζ-potentials for particles were measured on a Malvern nano-ZS zetasizer. The particle suspension was spun down and resuspended into 0.1X PBS for the measurement at a concentration of around 0.3 mg/mL. All the experiments were performed at 25 °C.

4.3.6 Particle A Degradation

Particle A was dispersed in buffers with different pHs at a concentration of about 0.8 mg/mL. After certain time points, 100 μL of the suspension was taken out and washed by PBS by 3 runs of centrifugation circles. The washed particles in PBS were dropped onto a glass slide, covered by a thin glass slip, and then observed under microscope for the size.

4.3.7 PEGylation of Particle A

Typically, 1 mg particle **A** was suspended in 500 μ L PBS. Then 6 mg of mPEG_{2k}-NHS (or 15 mg mPEG_{5k}-NHS, or 90 mg mPEG_{30k}-NHS to ensure the same moles of PEG per mg particles) in 100 μ L PBS was added to the particle suspension and reacted for 4 h on a shaker set at 1000 rpm at room temperature. After reaction, the particles were purified by repeated circle of centrifugation/washing 3 times.

4.3.8 Succinylation

Particle **C** or **F** in 1X PBS was spun down and re-suspended in 10X PBS to a concentration around 1 mg/mL. To the suspension, 4 mg SA dissolved in 50 μ L acetonitrile (Acros) was added and reacted for 2h by shaking at RT. After that, the particles were spun down and resuspended in 10X PBS, followed by another 4 mg of SA in 50 μ L acetonitrile and reacted another 1 h. Finally particles were purified by repeated centrifugation/washing circles for 4 times.

4.3.9 Hb Conjugation

Refer to **3.3.8** for the method of conjugation and Hb quantification. For **D** to **E**, 2.5 mg Hb was added to 1 mg particle **D** (2 mL PBS), while for **G** to **H**, 2 mg Hb was added to 1 mg **G** (in 2 mL PBS) to ensure that no less Hb loaded in **E** than **H** because quenching the surface led to less carboxyls in **E**.

4.3.10 Model Particle PEGylation using Fluorescein-PEG-NHS

Commercial Fluorescein-PEG-NHS was made by reacting FITC to amine-PEG-COOH followed by conversion of COOH to NHS ester. Therefore, there may be remaining FITC in the final product. When unpurified product was used to react with dyeless model particles, fluorescence was seen all over the particles because FITC could diffuse in to react with interior

amines. To purify, dissolve 1 mg fluorescein-PEG_{2k}-NHS in 50 μ L PBS and load the solution to a small column (Diameter: 0.5 cm, length: 5 cm) packed with Sephadex G-25. Elution with PBS could separate fluorescein-PEG-NHS from FITC as PEG would come out first. The collected solution of fluorescein-PEG-NHS was added with another 5 mg purified mPEG_{2k}-NHS to 1 mg model particles for PEGylation which lasted 4 h by shaking at RT. After reaction, the particles were thoroughly washed by PBS 4 times with centrifugation. In a control experiment, the same moles of fluorescein-NHS were used to replace fluorescein-PEG-NHS for the reaction.

4.3.11 Amine Quantification in Particles

For swollen particles **C** and **F**, we used a fluorescent assay to quantify the amine content. Both **C** and **F** were prepared starting from 1 mg of particle A. To suspensions of **C** or **F** in 500 μ L PBS, 10 mg fluorescein-PEG_{2k}-NHS was added and allowed to react for 12 h followed by purification. The purified particles were resuspended and diluted to measure fluorescence (excited at 492 nm, emission at 518 nm). A standard curve of fluorescein-PEG_{2k}-NHS at different dilutions was prepared. Based on the standard curve of fluorescein-PEG_{2k}-NHS, the amount conjugated to the particles could be fitted. Based on a 1:1 stoichiometry, the amine content was calculated. Herein, fluorescein-PEG_{2k}-NHS was used rather than the small molecule fluorescein-NHS because otherwise particle **F** would stick to reaction vials and could not be spun down because of quenching of amines on the surface.

4.3.12 Normalizing Particle Numbers

To better compare the performance of all the particles regarding their interaction with macrophages, and *in vivo* circulation, we decided to dose the same numbers of particles rather than the same weight because the particles (**B** to **H**) had similar shape, size, yet their individual weight vary more especially after Hb conjugation.

First of all, we could estimate the weight of a single particle **A**, knowing the dimensions of PRINT mold and the pre-mix density,

$$m_A = \rho h \pi r^2 = \frac{1.1\text{g}}{\text{cm}^3} \times 0.6 \mu\text{m} \times 3.14 \times 1 \mu\text{m}^2 = 2.1 \text{ pg}$$

Then, for a single well with 1×10^5 macrophages, the dose would be 400 particles per cell, as in weight of $2.1 \text{ pg} \times 400 \times 10^5 = 80 \mu\text{g}$ for total **A** dosed.

For the other particles, to ensure same numbers as $80 \mu\text{g}$ **A**, we could start with 8 mg **A** to fabricate different particles and divide the final volume of each particle 100 times to obtain the same numbers of particles.

For animal studies, 10^7 particles/g mouse weight was dosed for the RBC-sized particles from **C** to **H**. The dose, in numbers of particles, equaled to the number of 0.4 mg of starting particle **A** for mouse of 20 g body weight.

4.3.13 Macrophage Interaction Study

The Raw264.7 cells were cultured with Dulbecco Eagle media which was supplemented with 1% penicillin/streptavidin and 10% fetal bovine serum. Cells were grown in standard culture conditions (37°C and 5% CO_2). The cells were seeded in 24 well plates at a concentration of 1×10^5 per well and left overnight in the incubator. On the next day, the media was replaced with fresh media warmed to 37°C just prior to the experiment. The particle samples ($80 \mu\text{g}$ in 1 mL water) were incubated with the cells for 4 and 24 h. Cells grown without any particles were used as control. At the set time points, cells were washed three times with $500 \mu\text{L}$ 1X PBS and detached by the addition of 1X trypsin/EDTA ($300 \mu\text{L}$) to each well. Following a 5 minute incubation (37°C), 1X DBPS/10% FBS ($500 \mu\text{L}$) was added to each well and was mixed vigorously. This final solution was then transferred to a polypropylene tube and analyzed using flow cytometer.

4.3.14 Intravital Microscopy

Animal studies were carried out in accordance with an animal use protocol approved by the University of North Carolina Animal Care and Use Committee. IVM experiments were performed using an IV 100 laser scanning microscope (Olympus) on female balb/c mice of 18 to 26-g body weight (Jackson Lab). Hair was removed from the ear and a tail vein catheter was applied. The mice were anesthetized with isoflurane and placed onto a heated stage (37 °C) in a prone position, with an ear immobilized by taping to an aluminum block. Vasculature was located by injection with a solution of 5 mg / mL rhodamine B labeled 70-kDa dextran (Invitrogen) in PBS and visualized by excitation with a 568-nm laser. A suspension of particles in PBS with 0.05% Tween 80 was then injected and visualized using a 633-nm laser. Imaging scans proceeded for 2 h, with an image taken every 5 s. We analyzed the region of interest containing vasculature for fluorescent signal in each scan and corrected for variation in laser intensity or autofluorescence by background correcting each image with the signal from a region of the scan that was free of vasculature. For comparison, we normalized each scan to the maximum intensity slice for that scan, providing curves that measured the clearance of particles from the peripheral vasculature over time as a percentage of the maximum signal. Harvested tissues including liver, lung, spleen, kidneys, heart were weighed, then imaged using an IVIS Kinetic fluorescence imaging system (Caliper Life Sciences) with excitation at 675 nm and emission measured at 720 nm (NIR dye). Blood was harvested via cardiac puncture and pipetted in 100- μ L aliquots to black 96-well plates for analysis on the imager. The fluorescent signal for each tissue sample was background corrected by subtracting the signal from control tissues. Biodistribution profiles for the particles at 2 h postdose were determined by percent of recovered fluorescence in the above tissues.

4.3.15 Histology

Refer to **2.4.11** for detailed procedure applied here.

4.4 Figures

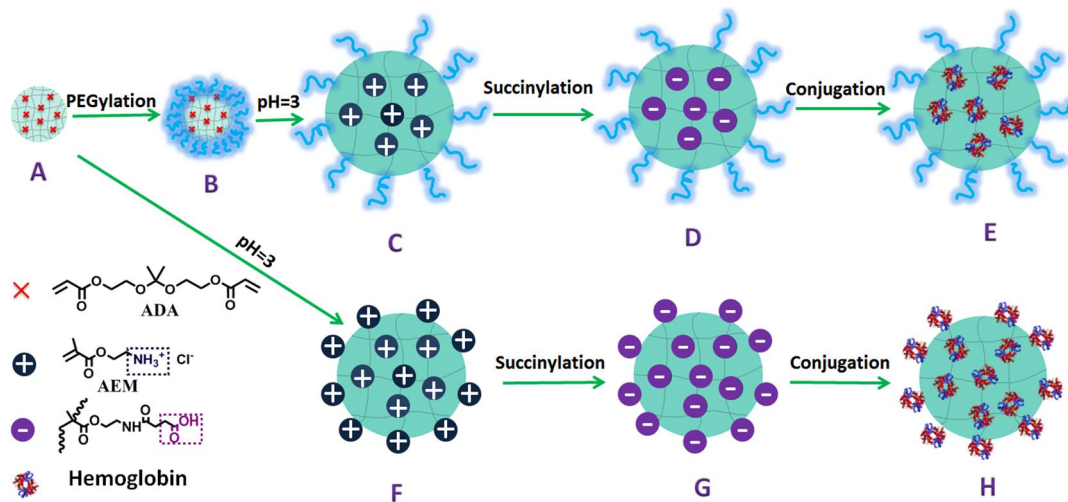


Figure 4.12 Scheme showing synthetic route from PRINT particles to surface-neutral microgels with charged interiors and functionalization of the microgels (A to E). Control particles with charged surface were produced following route A to H.

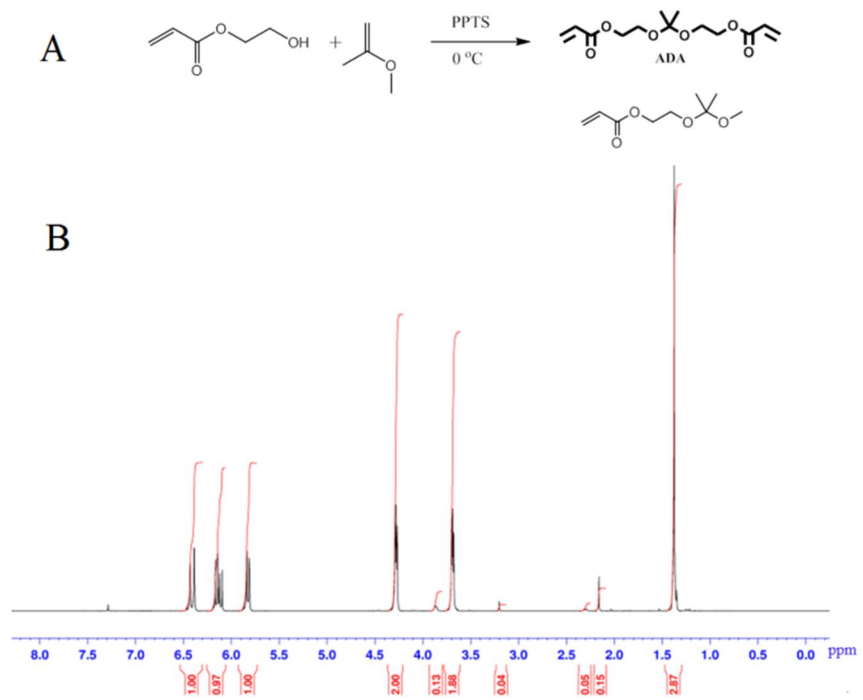


Figure 4.13 (A) Synthetic scheme for ADA by reacting HEA with 2-methoxypropene in the presence of an organic acid PPTS. (B) NMR spectrum of ADA in CDCl_3 measured at 25 °C.

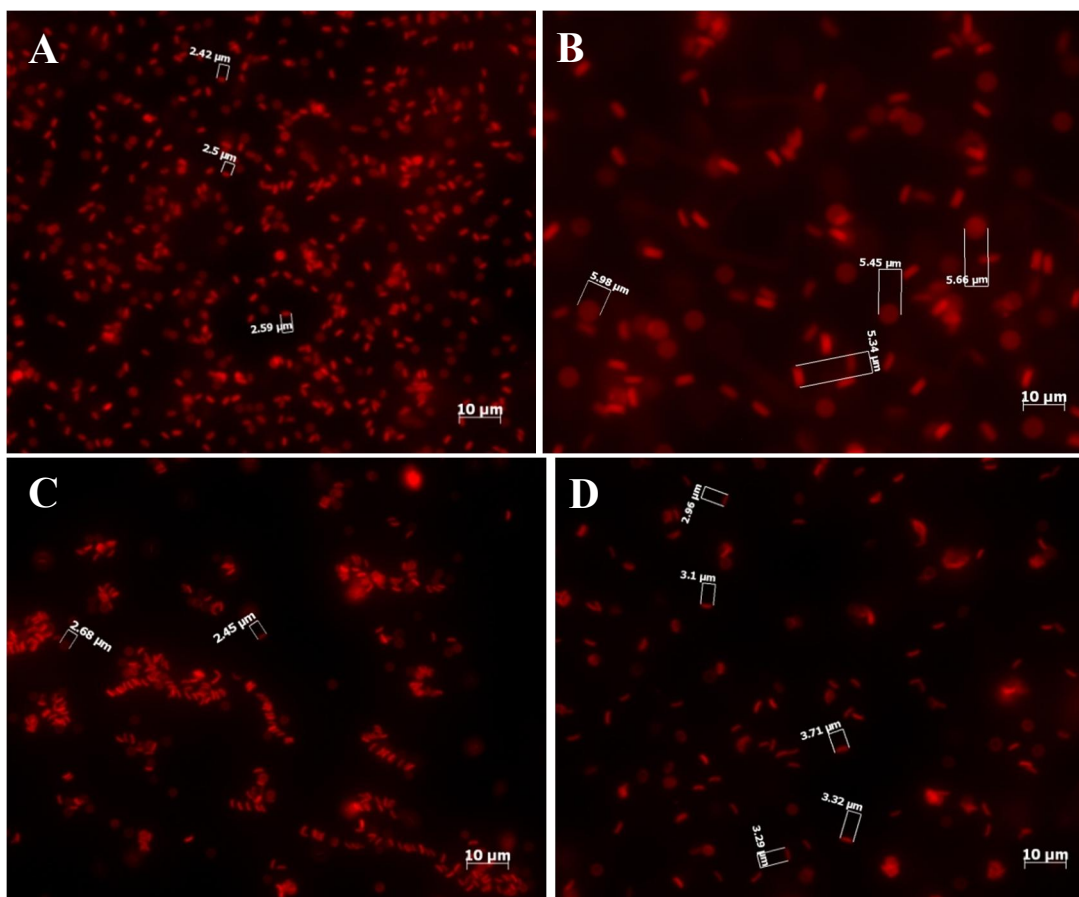


Figure 4.14 ADA crosslinked CEA containing particles at different stages. (A) as prepared; (B) after pH=3 treatment for 3 h; (C) PEGylated by mPEG_{5k}-amine using EDC/NHS; (D) pH=3 treatment for 18 h after PEGylation.

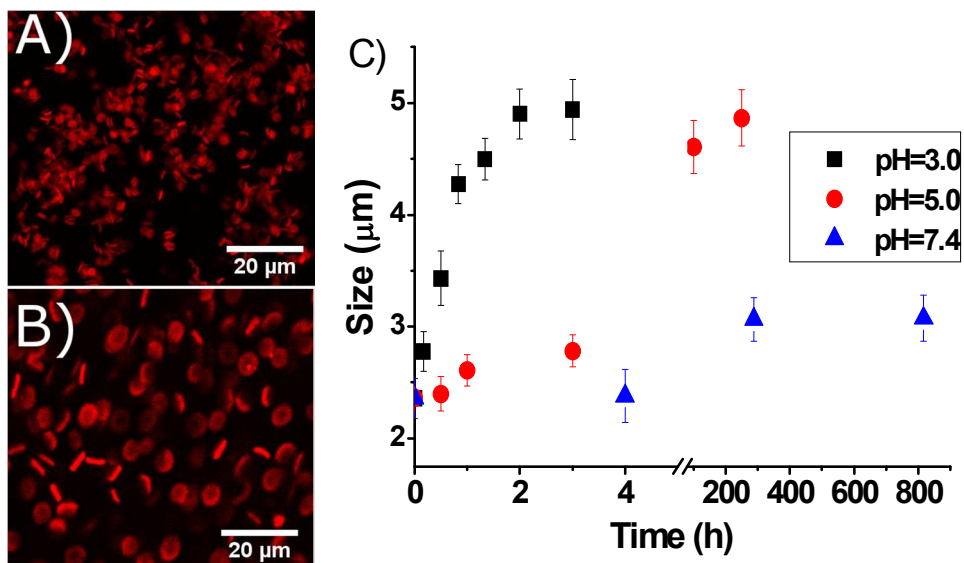


Figure 4.15 Fluorescent microscopic image of (A) freshly prepared particle A and (B) swollen particle F after acetal degradation in pH=3 buffer for 2 h. (C) Size increase of particle A overtime in different pHs. Aliquots of particle suspensions were taken out and re-suspended in PBS for sizing by averaging diameter of particles under microscope (n=50).

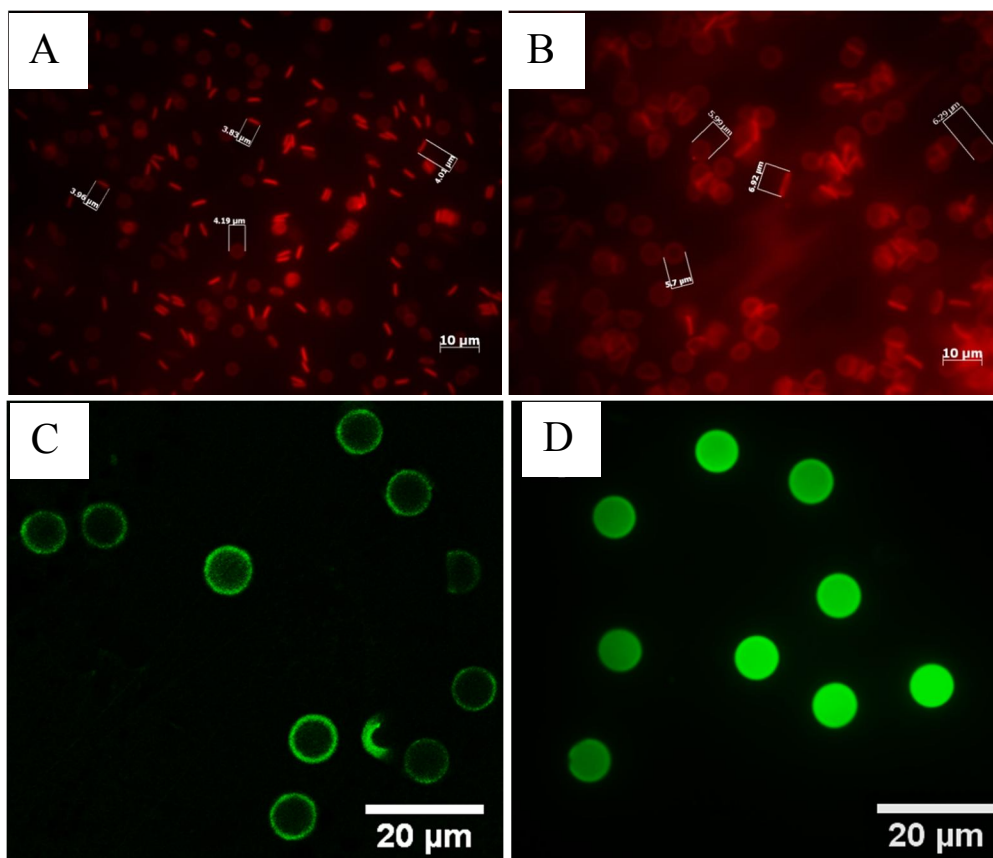


Figure 4.16 Effect of PEGylation on ADA crosslinked AEM-particles. Fluorescent image of acid-treated particle **A** after PEGylation with unpurified (A) and purified (B) mPEG_{5k}-NHS. Confocal microscopic image of model particles (7×7×3 μm cylinders) after reaction with (C) fluorescein-PEG_{2k}-NHS and (D) fluorescein-NHS.

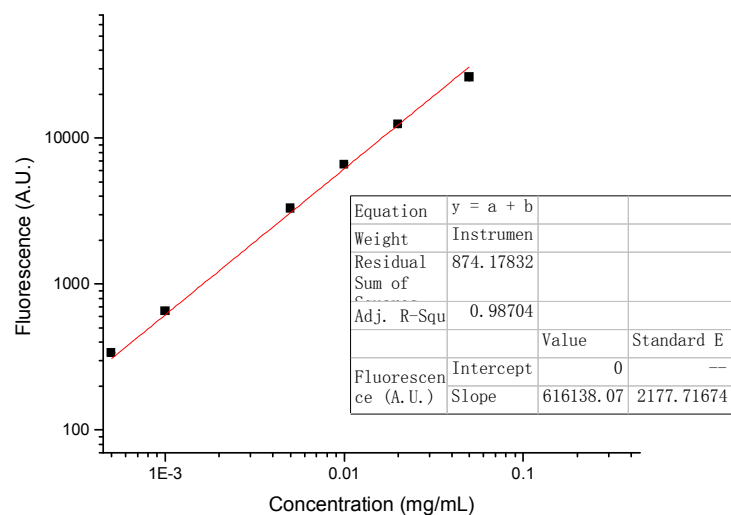


Figure 4.17 Standard curve for fluorescein-PEG_{2k}-NHS regarding fluorescence excited at 492 nm and emitted at 518 nm (3 readings averaged for each concentration). Starting from 1 mg dyeless particle A, the same numbers (5×10^{11}) of particle C and F were prepared respectively. Both C and F were reacted with 10 mg fluorescein-PEG_{2k}-NHS for 12 h followed by thorough, repeated washing/centrifugation circles. The obtained particle suspensions were re-suspended in PBS to obtain concentration of 1×10^{11} particles/mL for both particles. Then starting from this concentration, defined dilutions were made to fit into the linear range of the standard curve. Particle F reacted with mPEG_{2k}-NHS for 6 h (needed time to acquire near-neutral zeta-potential) was also measured for amine content using this method.

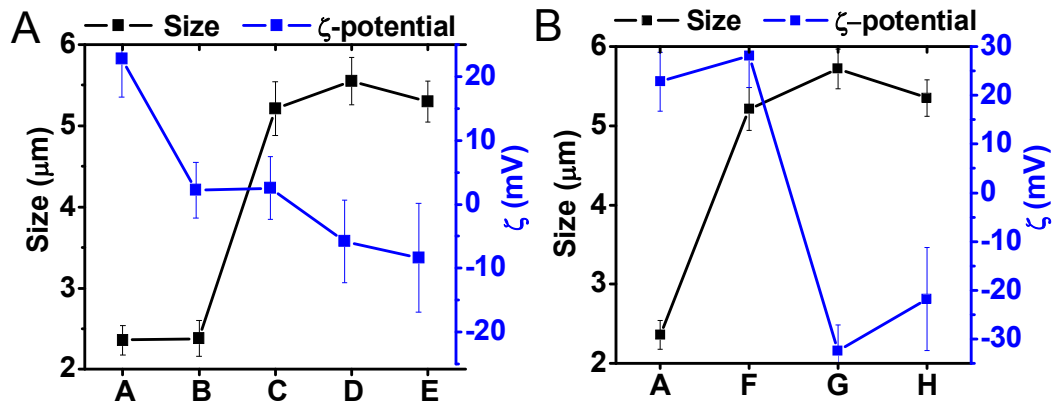


Figure 4.18 Size and ζ -potential change of particles synthesized following route of (A) particle A to particle E and (B) particle A to particle H.

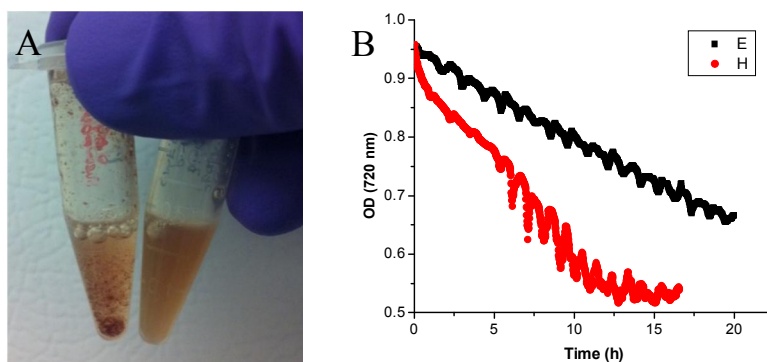


Figure 4.19 (A) The solutions of 4 mg Hb reacted with 1 mg particles (0.5 mL) of **G** (left) or **D** (right) for 6h. The aggregation for **G** could be avoided when conjugation was carried out at dilute concentrations (0.5 mg/mL particles). For all the *in vitro* and *in vivo* studies, the conjugation was carried out at low concentration for both **G** and **D** particles. (B) The optical density (720 nm to avoid Hb absorbance) change for hemoglobin loaded particles **E** and **H** dispersed in PBS containing 10% fetal bovine serum (900 μ L particle suspension was mixed with 100 μ L fetal bovine serum quickly in the cuvette before reading started). The optical density at 720 nm for the suspensions was read every 1 min over 15-20 h at 23 $^{\circ}$ C.

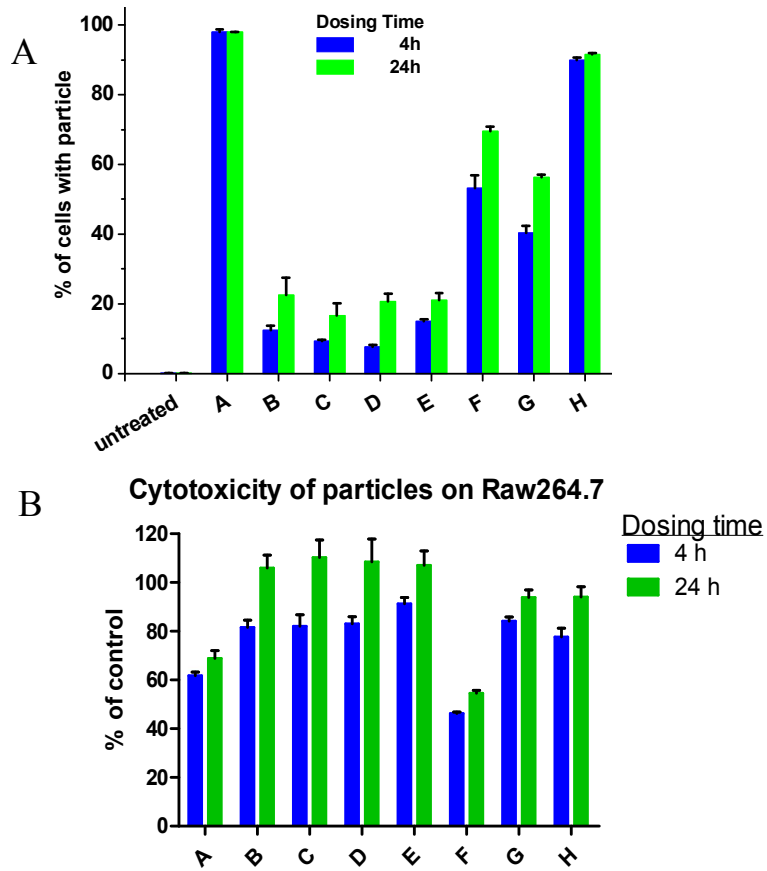


Figure 4.20 (A) Macrophage interaction with different particles. About 400 particles/cell dosed to a total of 10^5 Raw264.7 cells for each particle type. (B) Cytotoxicity of different particles to Raw264.7 cell line.

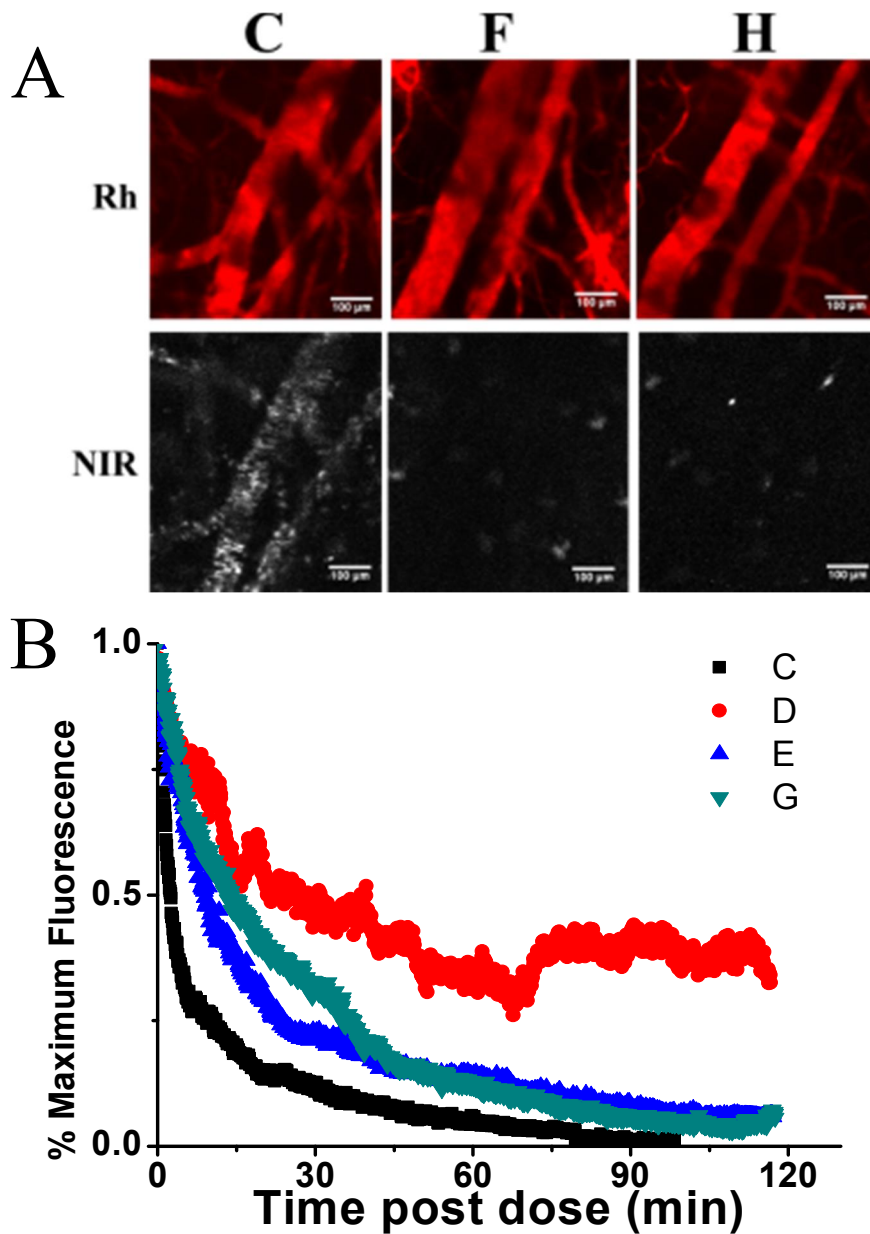


Figure 4.21 (A) Intravital microscopy images of mice earlobe blood vasculature imaged at the rhodamine (Rh) channel by injecting dextran_{70k}-rhodamine prior to dosing particles, and imaged at the near-IR (NIR) channel just 100 secs after dosing particles (C, F, H). (B) Decrease in fluorescence of area of interest within 2 h of imaging by IVM (averaged of n=3). For each particle type, 10^7 particles/g body weight were dosed.

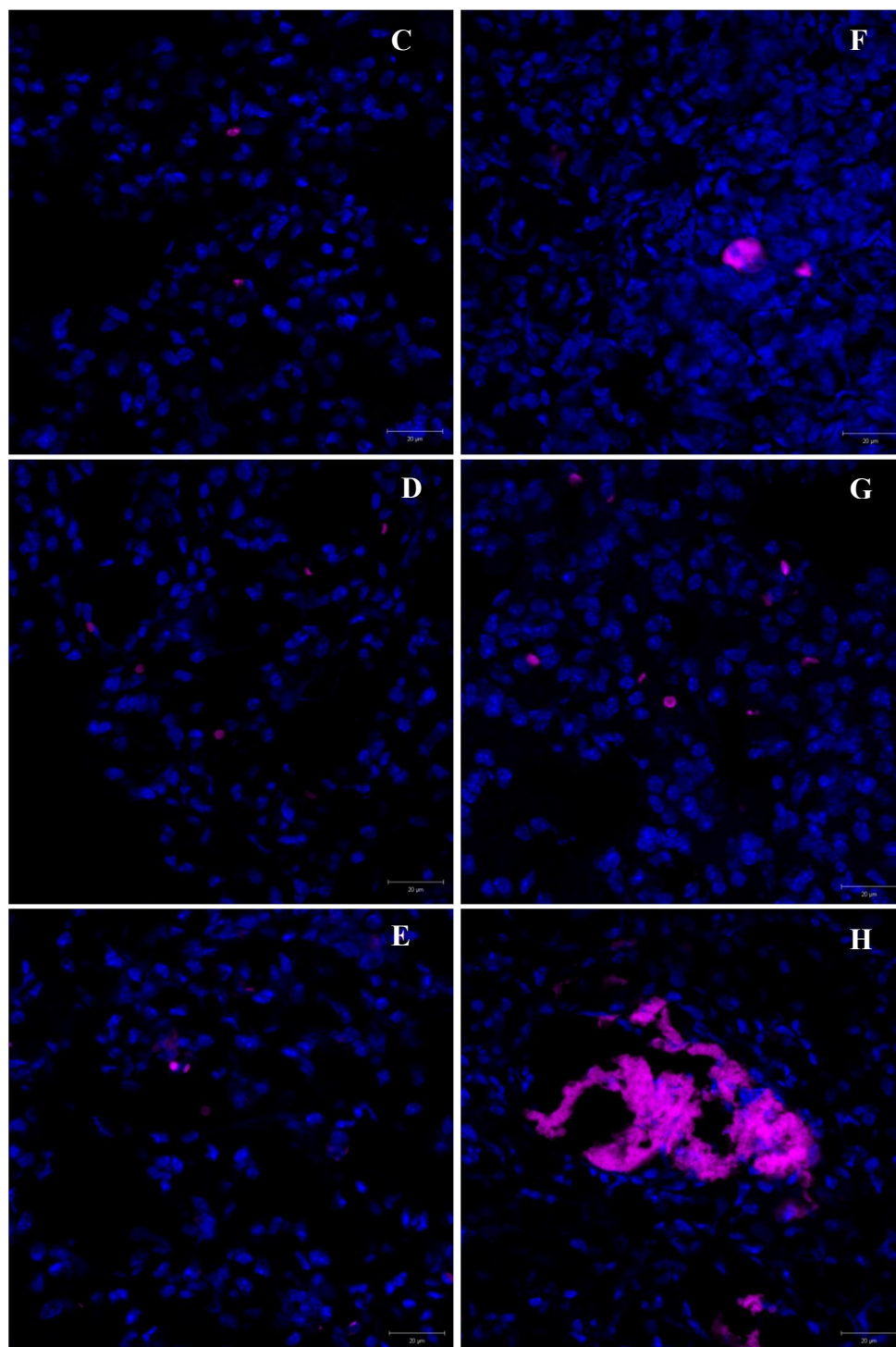


Figure 4.22 Fluorescent images of lung with nucleus stained by DAPI for mice injected with different particles (shown in purple from NIR dye) denoted on the right corner of each picture. All scale bars=20 μm .

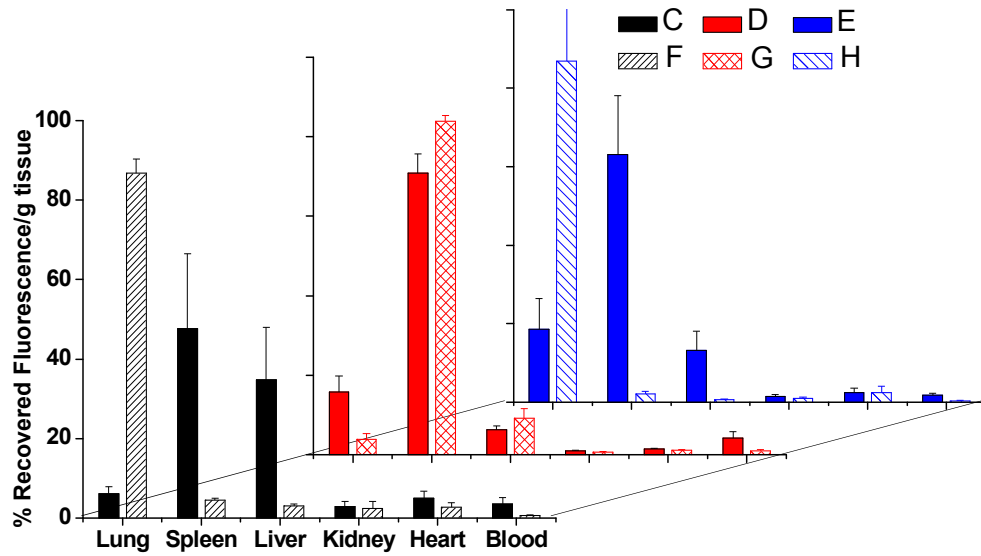


Figure 4.23 Biodistribution of the different particles into various tissues 2 h postdosing presented by percent fluorescence normalized for tissue weight, with n=3 for each case.

4.5 REFERENCES

- (1) Eylar, E. H.; Madoff, M. A.; Brody, O. V.; Oncley, J. L. *J. Bio. Chem.* **1962**, *237*, 1992-2000.
- (2) Jan, K.-M. *J. General Physiology* **1973**, *61*, 638-654.
- (3) Durocher, J.; Payne, R.; Conrad, M. *Blood* **1975**, *45*, 11-20.
- (4) Kahane, I.; Polliack, A.; Rachmilewitz, E. A.; Bayer, E. A.; Skutelsky, E. *Nature* **1978**, *271*, 674-675.
- (5) Gattegno, L.; Bladier, D.; Cornillot, P. *Carbohydrate Research* **1974**, *34*, 361-369.
- (6) Wood, B.; Gibson, D.; Tait, J. *Blood* **1996**, *88*, 1873-1880.
- (7) Li, S.-D.; Huang, L. *Mol. Pharm.* **2008**, *5*, 496-504.
- (8) Zhang, J.-S.; Liu, F.; Huang, L. *Adv. Drug Deliv. Rev.* **2005**, *57*, 689-98.
- (9) Mayer, A.; Vadon, M.; Rinner, B.; Novak, A.; Wintersteiger, R.; Fröhlich, E. *Toxicology* **2009**, *258*, 139-47.
- (10) Dobrovolskaia, M. A.; Clogston, J. D.; Neun, B. W.; Hall, J. B.; Patri, A. K.; McNeil, S. E. *Nano Lett.* **2008**, *8*, 2180-7.
- (11) Harris, J. M.; Chess, R. B. *Nat. Rev. Drug Discov.* **2003**, *2*, 214-21.
- (12) Veronese, F. M.; Pasut, G. *Drug discovery today* **2005**, *10*, 1451-8.
- (13) Perry, J. L.; Reuter, K. G.; Kai, M. P.; Herlihy, K. P.; Jones, S. W.; Luft, J. C.; Napier, M.; Bear, J. E.; DeSimone, J. M. *Nano Lett.* **2012**, *12*, 5304-10.
- (14) Cao, Z.; Zhang, L.; Jiang, S. *Langmuir* **2012**, *28*, 11625-32.
- (15) Cao, Z.; Jiang, S. *Nano Today* **2012**, *7*, 404-413.
- (16) Merkel, T. J.; Jones, S. W.; Herlihy, K. P.; Kersey, F. R.; Shields, A. R.; Napier, M.; Luft, J. C.; Wu, H.; Zamboni, W. C.; Wang, A. Z.; Bear, J. E.; DeSimone, J. M. *Proc. Natl. Acad. Sci.* **2011**, *108*, 586-91.
- (17) Cohen, J. a; Beaudette, T. T.; Cohen, J. L.; Broaders, K. E.; Bachelder, E. M.; Fréchet, J. M. J. *Adv. Mater.* **2010**, *22*, 3593-7.
- (18) Shenoi, R. a; Narayanannair, J. K.; Hamilton, J. L.; Lai, B. F. L.; Horte, S.; Kainthan, R. K.; Varghese, J. P.; Rajeev, K. G.; Manoharan, M.; Kizhakkedathu, J. N. *J. Am. Chem. Soc.* **2012**, *134*, 14945-57.

- (19) Wu, Y.; Chen, W.; Meng, F.; Wang, Z.; Cheng, R.; Deng, C.; Liu, H.; Zhong, Z. *J. Control. Release* **2012**, *164*, 338-45.
- (20) Sankaranarayanan, J.; Mahmoud, E. A.; Kim, G.; Morachis, J. M.; Almutairi, A. *ACS nano* **2010**, *4*, 5930-6.
- (21) Reese, C. B.; Saffhill, R.; Sulston, J. E. *J. Am. Chem. Soc.* **1967**, *89*, 3366-3368.
- (22) Palmieri, F.; Adams, J.; Long, B.; Heath, W.; Tsiartas, P.; Willson, C. G. *ACS Nano* **2007**, *1*, 307-12.
- (23) Valeur, E.; Bradley, M. *Chem. Soc. Rev.* **2009**, *38*, 606-31.
- (24) Han, S.-Y.; Kim, Y.-A. *Tetrahedron* **2004**, *60*, 2447-2467.
- (25) Roberts, M. J.; Bentley, M. D.; Harris, J. M. *Adv. Drug Deliv. Rev.* **2002**, *54*, 459-76.
- (26) Wilchek, M.; Miron, T. *Biochemistry* **1987**, *26*, 2155-61.
- (27) Smith, B. R.; Cheng, Z.; De, A.; Koh, A. L.; Sinclair, R.; Gambhir, S. S. *Nano Lett.* **2008**, *8*, 2599-606.
- (28) Hak, S.; Reitan, N. K.; Haraldseth, O.; Lange Davies, C. de *Angiogenesis* **2010**, *13*, 113-30.
- (29) Jones, S. W.; Roberts, R. A.; Robbins, G. R.; Perry, J. L.; Kai, M. P.; Chen, K.; Bo, T.; Napier, M. E.; Ting, J. P. Y.; Desimone, J. M.; Bear, J. E. *J. Clin. Invest.* **2013**, *123*, 3061-3073.
- (30) Merkel, T. J.; Chen, K.; Jones, S. W.; Napier, M. E.; Zamboni, W. E.; Desimone, J. M. *J. Control. Release* **2012**, *162*, 37-44.
- (31) Hu, C.-M. J.; Zhang, L.; Aryal, S.; Cheung, C.; Fang, R. H.; Zhang, L. *Proc. Natl. Acad. Sci.* **2011**, *108*, 10980-5.
- (32) Tabata, Y.; Ikada, Y. *Biomaterials* **1988**, *9*, 356-362.
- (33) He, C.; Hu, Y.; Yin, L.; Tang, C.; Yin, C. *Biomaterials* **2010**, *31*, 3657-66.
- (34) Xiong, Y.; Liu, Z. Z.; Georgieva, R.; Smuda, K.; Steffen, A.; Sendeski, M.; Voigt, A.; Patzak, A.; Bäumler, H. *ACS nano* **2013**.
- (35) Liao, J. C.; Hein, T. W.; Vaughn, M. W.; Huang, K. T.; Kuo, L. *Proc. Natl. Acad. Sci.* **1999**, *96*, 8757-61.
- (36) Lee, J.; Sohn, J. W.; Zhang, Y.; Leong, K. W.; Pisetsky, D.; Sullenger, B. A. *Proc. Natl. Acad. Sci.* **2011**, *108*, 14055-60.

- (37) Glasgow, B. J.; Marshall, G.; Gasymov, O. K.; Abduragimov, A. R.; Yusifov, T. N.; Knobler, C. M. *Invest. Ophthalmol. Vis. Sci.* **1999**, *40*, 3100-7.
- (38) Zlotnik, A.; Gurevich, B.; Tkachov, S.; Maoz, I.; Shapira, Y.; Teichberg, V. I. *Experimental Neurology* **2007**, *203*, 213-20.

CHAPTER 5: SUMMARY AND FUTURE DIRECTIONS

5.1 Summary

RBC, which can be regarded as a natural microparticle since it is anucleate (nucleus-free), can circulate for 120 days in blood. This exceptionally long circulation time for a particle of such a size, is guaranteed by the unique combination of such factors: shape, modulus and surface properties that are found in RBCs. To date, out of the many RBC substitutes in the form of Hb-loaded particles, there is not a single one that mimics the size of true RBCs, not only because of inadequate control over size and size distribution, but more importantly lack of concurrent tuning of modulus. The long-standing dogma that microparticles would be quickly removed from circulation because of filtration by the lung was only challenged recently from our study that sufficiently deformable particles with the size of RBC could navigate the lung to circulate for extended times.¹

PRINT, a precision micro-molding technique that can generate uniform particles with tight control over size, shape, modulus and surface properties, allowed for hydrogel particles that mimick the size, shape, modulus of RBCs. Mimicking the size of RBCs for the fabrication of oxygen carrier is not trivial. A major hurdle that is difficult to overcome for most oxygen carriers is vasoconstriction due to scavenging of NO by Hb in these carriers.² It is known that vasoconstriction is inversely proportional to the size of the carrier,³ making our RBC-sized oxygen carriers promising. It also seems to follow design rules that, for similarly deformable soft particles with a low modulus (6.5 kPa), RBC-sized particles could circulate longer than other particles with either larger or smaller sizes. Again, only through PRINT was such a study

possible as modulus could be firmly controlled by using identical formulation while size could be varied by using different molds. With the intention to extend circulation and avoid vasoconstriction, RBC-sized PRINT hydrogels seemed to be the best starting particles for fabricating Hb loaded oxygen carriers.

The highly swollen nature of PRINT hydrogels allowed for diffusion of Hb even into the interior of particles, thus a high loading could be obtained. We could achieve a suspension of particles with [Hb] = 5.2 g/dL so far. The conjugation was carried out under mild conditions so that the structure and function of Hb could be well maintained. Since the reacting handles were originally distant from each other because of high swelling of particles, extra crosslinking could be avoided after conjugation, resulting in sufficient deformability of the protein-laden particles. This conjugation method can be applied to other proteins, such as BSA. Nevertheless, the uniform distribution of Hb in the particles also caused a drawback regarding the surface properties of particles, as it is well-known that surface-bound proteins could accelerate aggregation and MPS clearance of particles.

Confined distribution of Hb within particles without surface exposure was obtained by designing a new type of PRINT hydrogel that had asymmetric distribution of functional groups. It is well accepted that charged particles would be cleared from circulation faster than neutral ones. Through the constricted PEGylation method, particles with neutral surface could be obtained with functional groups reserved to the interior. When Hb was conjugated to the particles, the protein would be exclusively installed in the interior. We investigated the *in vivo* behavior of three groups of particles where each group had the same interior characteristic but different surface properties, and found that particles with neutral surface had extended circulation than their charged counterparts. Most noteworthy is that surface-neutral particles

loaded with Hb managed to navigate the lung, while the control particles with Hb on the surface were rigorously filtered by the lung. Our results not only agreed with previous research regarding effect of particle surface on *in vivo* circulation, but also demonstrated that a non-dense layer of PEG on soft particles could achieve similar result as a dense layer of PEG did on solid particles.

In summary, when one mimics the size, shape, modulus of RBCs as well as the distribution pattern of Hb within the particles, a viable RBC substitute seems evident. By PRINT, we have prominent control over the carrier particles. With preservation of Hb structure and function, we expect to see the Hb loaded particles act as an efficient oxygen carrier with minimal vasoconstriction and efficient oxygen delivery capacity.

5.2 Future Directions

5.2.1 Effect of ζ -potential on PK and BioD of Soft Particles

The distribution map of RBC mimics can be completed by maintaining the size, shape, modulus of particles while varying the ζ -potential. Our study in Chapter 4 on particles with a neutral surface versus charged surfaces definitely indicates the importance of surface charge of particles on PK and biodistribution. It was also found that RBC mimics with ζ -potential of -32 mV were cleared faster than that with -18 mV of ζ -potential.

For true RBCs, there is a strict window of negative ζ -potential, out of which RBCs would be recognized by the MPS. To map out a window for ζ -potential that allows extended circulation of soft particles, future directions should consider the fabrication of the same-sized PRINT hydrogels with varied CEA amount in the formulation. However, as can be seen in **Figure 5.1**, particles with more CEA tend to swell more when made out of the same 2 μm mold. The modulus of particles with higher content of CEA may also be different (higher swelling does not necessarily mean lower modulus as it is possible that polymer chains can be so extended that

more stress is required for further deformation). Therefore, to control size, shape and modulus while varying ζ -potential may not be as easy as it seems to be.

An indirect way to fabricate such particles with the same size, shape, modulus but different ζ -potential may be possible. Starting from PRINT hydrogels containing a fixed content of AEM (say 40%), different amounts of mPEG-NHS can be added to the swollen particles to quench the amine groups to varying extents, generating particles with different positive surface charges. Since PEG attached to an amine can still act as “repelling group” similarly to the originally charged amine, size and probably modulus of the resultant particles may still be similar when mPEG-NHS with a suitable MW is chosen. Our estimation is low MW (around 500 Da) PEG may fulfill this purpose. Then the remaining amines in different particles can be converted to carboxyls by succinylation, generating soft particles with varying ζ -potential but a similar size and modulus.

IVM studies of the particles with the same size, shape and modulus but varied ζ -potential can possibly map out a suitable window for ζ -potential that allows extended circulation for soft particles.

5.2.2 Nerve Agent Scavenger

Conjugation of Hb to PRINT RBC-sized hydrogels is a facile method that can be applied to other therapeutically-relevant proteins. Because of the large size, the RBC mimics cannot be used for delivery of proteins into cells. The application should be limited to proteins that can take effect during circulation. For such proteins with limited circulation half-life, conjugation into the RBC mimics can greatly improve the therapeutic availability.

Of special interest is to load butyrylcholinesterase (BuChE) into the particles. Such particles can be used as bioscavenger to remove nerve agent in circulation over extended time

because BuChE is an efficient enzyme that can degrade phosphorous nerve agents. Using the CEA containing particles with a neutral surface, the circulation half-life of the scavenger may still be long enough even after BuChE loading since the loading ratio does not have to be as high as that of Hb in oxygen carriers. A compelling advantage of using PRINT hydrogel as the bioscavenger may arise from rapid diffusion of nerve agent into the swollen particles.

5.2.3 Nucleic Acid Scavenging

Free nucleic acid released from dying or dead cells may enter bloodstream and can be taken up by inflammatory cells and activate multiple nucleic acid-sensing toll-like receptors (TLRs). Over activation of these TLRs can cause a variety of inflammatory and autoimmune disease. Materials that can neutralize the proinflammatory effects of any nucleic acids regardless of its sequence, structure, or chemistry are highly sought after. Sullenger's group developed a simple method to use cationic polymers as molecular scavenger to soak up and neutralize the inflammatory nucleic acids.⁴ However, one obvious drawback of the cationic polymers is their limited half-life in circulation.

We had previously tested homogeneous cationic particles regarding nucleic acid binding capacity, and found that the particles could effectively bind DNA (**Figure 5**). However, the particles were also highly cytotoxic. The surface-neutral, interior cationic RBC mimics synthesized may fit this application very well as nucleic acid scavenger. After binding with nucleic acids in bloodstream, the particles may become stiff and removed in the spleen. A proof-of-concept experiment can be carried out by using the microfluidic device to test, after binding with varying amounts of DNA, if particles can still pass through or not.

5.2.4 Other Formulations for Soft Particles

So far, we have utilized synthetic polymers as the matrix for soft particles, especially photocurable acrylates. Even though very low amount of long-chain crosslinker was used to decrease the crosslinking density, chain transfer reaction cannot be completely avoided especially with the presence of hydroxyl groups in HEA or HP3A. To further decrease the modulus of hydrogels so that even higher loading of proteins like Hb can still retain sufficient deformability, new materials may have to be explored. PEG hydrogel can be a good candidate because of absence of side groups in PEG and the flexibility of the main chain. While crosslinking density may still be high when PEG-diacrylate is used to construct PEG hydrogel, adding PEG-dithiol to decrease the crosslinking density and elongate the main chain may generate even softer hydrogel. The thiol-ene chemistry has been widely used to construct PEG networks from PEG-dithiol and PEG-diene or PEG-diacrylate.⁵ While those constructed PEG hydrogels had been mostly prepared in bulk for tissue engineering purposes with elastic modulus that could be around 1 kPa,⁶ there has been no report of making such soft hydrogels in the micron size. It is possible for us to PRINT such particles in a manner similar to PRINT PLGA particles. PEG-dithiol and PEG-diacrylate with high MW are solids with melting point around 65 °C. We can thermally fill the mold with the PEGs followed by photocuring. To ensure sufficient mobility of PEG molecules in the mold, we may need to heat the mold during UV curing.

A completely new material, resilient-like-polypeptide (RLP) can also be used to fabricate protein-based soft hydrogel particles. Recombinant RLPs possess the favorable attributes of native resilin, which is the rubber-like protein found in specialized compartment of most arthropods with excellent mechanical properties including high resilience and low stiffness.⁷ Using RLP as matrix, PRINT particles with low modulus and high resilience may be obtained,

and used for *in vivo* applications because of the biocompatibility. The deformability of RLP-based microparticles may allow them to navigate small capillaries similarly to hydrogel particles, circulating for extended time.

5.2.5 Nanoparticle Loading

Generally speaking, nanoparticles are used to deliver therapeutics into tissues or cells, so there is no need to encapsulate nanoparticles in bigger carriers. However, there may be emerging areas that long circulating microgels like the RBC mimics discussed here can be used as mother-ship carriers for nanoparticles.

For nanoparticles that are supposed to stay and take effect in bloodstream without sequestration into specific tissues, the RBC mimics could help to extend their circulation time by trapping them inside. Here is an example. RBC membrane-coated PLGA nanoparticles prepared by Zhang's lab had been an intriguing construct for toxin scavenger *in vivo*.⁸ Most toxins are pore-forming on the membrane of RBCs and endothelial cells. By coating mouse's RBC membrane onto PLGA nanoparticles, the formed structure could efficiently bind toxins as decoy. Due to the nano-size of the PLGA particles, the total surface area of administered nanoparticles can be large enough to compete with RBCs so that toxins can be preferentially trapped by the nanoparticles. These RBC membrane-camouflaged PLGA nanoparticles could circulate a long time as they tested before.⁹ However, to make this technique really scalable, it is important to just use synthetic lipid membrane as coating to scavenge toxins. However, PLGA nanoparticles coated with synthetic lipid membrane cannot stay long enough in bloodstream. It will benefit greatly to load these nanoparticles in our RBC mimics to extend their circulation.

A possible method to load nanoparticles into the RBC mimics is to incubate the nanoparticles with RBC mimics in DI water, in which the RBCs can swell more due to lowered

ionic strength. Then adding suitable amount of 10X PBS to the solution to obtain 1X PBS can instantly shrink the RBC mimics, also tightening the pores of the hydrogels to entrap nanoparticles.

5.2.6 Hollow RBC Mimic

The RBC mimics discussed in this dissertation, though mimicked the size, shape and deformability of RBCs, are structurally quite different from true cells. The particles were structurally homogenous hydrogels, while RBCs are fluid-filled sacs contained by a complex membrane that has extreme flexibility. The two different structures may possibly behave differently in flow, despite sharing similar mechanical properties. To mimic the structure of true cells, a hollow particle with membrane structure is desired.

There have been enormous studies using layer-by-layer (LBL) technique to deposit polymers on sacrificial template particles in order to reproduce cell-like hollow capsules.^{10,11} Generally, polymer films are coated onto colloid particles by depositing alternating layers of oppositely charged polymers sequentially. Other complementary layers containing hydrogen-bonding polymers are also candidates for driving the assembly of polymer films onto particle surface. Crosslinking of the deposited polymer films is often needed to form a stable core-shell structure. Removal of the sacrificial core can generate hollow polymer capsules. Using LBL technique to coat polymers on spherical PLGA particles that had similar diameter as RBCs, Mitragotri's group managed to generate a hollow membrane structure that mimicked RBCs by dissolving the PLGA core.¹²

PRINT provides exciting opportunity to generate uniform particles that can be used as sacrificial template for synthesizing hollow membrane structures. PLGA PRINT particles can be used for this purpose. Other materials include polymers crosslinked by acid-labile monomers

such as ADA or silyl ether crosslinkers. While most hollow structures prepared by LBL method rely on spherical templates, we can explore the outcome when non-spherical particles are used. For example, disk-like particles can be used as template for constructing polymer membranes. Dissolving the sacrificial core may lead to highly collapsed polymer capsules that may deform more easily than capsules replicated from spherical particles.

5.3 Figures

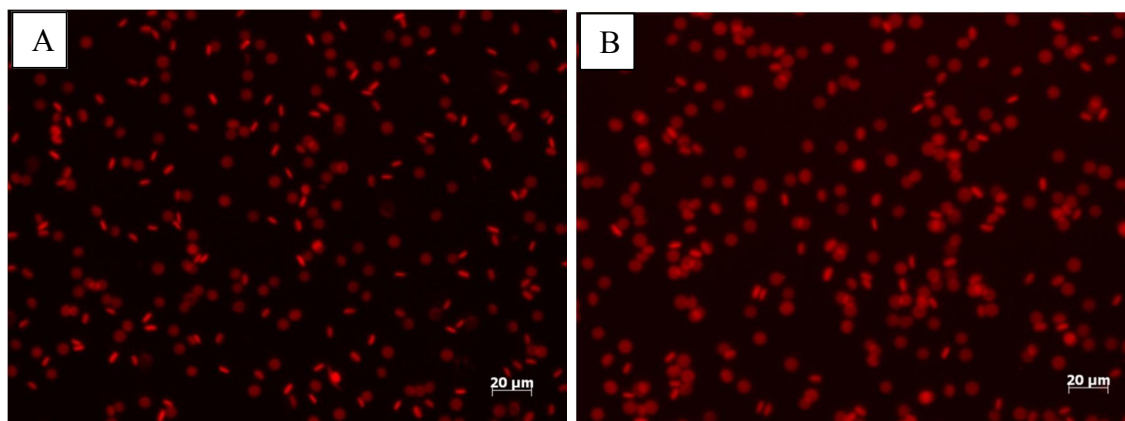


Figure 5.1 Fluorescent micrographs of HP3A particles with (A) 20 wt% and (B) 50wt% CEA. The size of the particles were 6.5 and 7.5 μm , and the zeta-potential were -23.5 and -29.9 mV respectively.

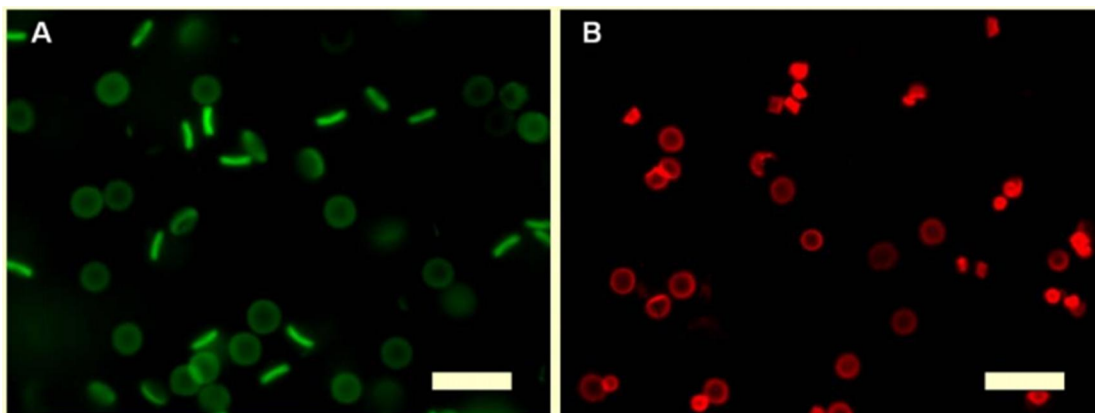


Figure 5.2 Cationic hydrogel particles. (A) Particles fluoresce in the green channel due to matrix bound fluorescein dye. (B) Fluorescence in the red channel from adsorbed Cy3 dye-conjugated DNA 20mer. Particles were incubated at 37 °C for one hour with 1 μ M DNA, then washed 3 times to remove unassociated DNA. Scale bars are 20 μ m.

5.4 REFERENCES

- (1) Merkel, T. J.; Jones, S. W.; Herlihy, K. P.; Kersey, F. R.; Shields, A. R.; Napier, M.; Luft, J. C.; Wu, H.; Zamboni, W. C.; Wang, A. Z.; Bear, J. E.; DeSimone, J. M. *Proc. Natl. Acad. Sci.* **2011**, *108*, 586-91.
- (2) Alayash, A. I. *Nature reviews. Drug discovery* **2004**, *3*, 152-9.
- (3) Xiong, Y.; Liu, Z. Z.; Georgieva, R.; Smuda, K.; Steffen, A.; Sendeski, M.; Voigt, A.; Patzak, A.; Bäuml, H. *ACS nano* **2013**.
- (4) Lee, J.; Sohn, J. W.; Zhang, Y.; Leong, K. W.; Pisetsky, D.; Sullenger, B. A. *Proc. Natl. Acad. Sci.* **2011**, *108*, 14055-60.
- (5) Hoyle, C. E.; Bowman, C. N. *Angew. Chem. Int. Ed.* **2010**, *49*, 1540-73.
- (6) Aimetti, A. A.; Machen, A. J.; Anseth, K. S. *Biomaterials* **2009**, *30*, 6048-54.
- (7) Li, L.; Tong, Z.; Jia, X.; Kiick, K. L. *Soft Matter* **2013**, *9*, 665-673.
- (8) Hu, C.-M. J.; Fang, R. H.; Copp, J.; Luk, B. T.; Zhang, L. *Nature Nanotech.* **2013**, *8*, 336-40.
- (9) Hu, C.-M. J.; Zhang, L.; Aryal, S.; Cheung, C.; Fang, R. H.; Zhang, L. *Proc. Natl. Acad. Sci.* **2011**, *108*, 10980-5.
- (10) Donath, E.; Sukhorukov, G. B.; Caruso, F.; Davis, S. A.; Möhwald, H. *Angew. Chem. Int. Ed.* **1998**, *37*, 2201-2205.
- (11) Caruso, F. *Chem. Eur. J.* **2000**, *6*, 413-9.
- (12) Doshi, N.; Zahr, A. S.; Bhaskar, S.; Lahann, J.; Mitragotri, S. *Proc. Natl. Acad. Sci.* **2009**, *106*, 21495-21499.